Tailoring supported olefin polymerisation catalysts using non-equilibrium plasmas

Godfrey, Simon Paul

TAILORING SUPPORTED OLEFIN POLYMERISATION CATALYSTS USING NON-EQUILIBRIUM PLASMAS

Ph.D. Thesis

by

Simon Paul Godfrey

University of Durham

Department of Chemistry

1999

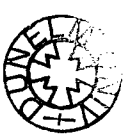

For Lynsey, Mum and Dad

STATEMENT OF COPYRIGHT

DECLARATION

The work described in this thesis was carried out in the Chemistry Department at the University of Durham between October 1996 and September 1999. It is the original work of the author except where otherwise acknowledged, and has not been submitted previously for a degree at this or any other University.

Solid state NMR (Chapters 2-6) was undertaken at the University of Durham Industrial Research Laboratories by Dr. D.C. Apperley. Inductively coupled plasma mass spectrometry (Chapters 2 and 4) and scanning electron microscopy (Chapter 6) was carried out in the Durham University Geology Department by Dr. C.J. Ottley and Dr. H.A. Armstrong. Polymer characterisation (Chapter 2) was performed under the supervision of Dr. I.R. Little at BP Amoco. The dibutylmagnesium/silica precursors (Chapter 5) were synthesised by Dr. I.R. Little and Dr. S.J. Dossett of BP Amoco. Elemental analysis (Chapters 5 and 6) was carried out in the Durham University Chemistry Department by L.W. Lauchen and J. Dostal. Imaging TOF-SIMS (Chapter 6) was undertaken by E.J. Kinmond and Dr. I.W. Fletcher at ICI Wilton.

ACKNOWLEDGEMENTS

I would like to thank my supervisor, Prof. J.P.S. Badyal, for his support and encouragement during the three years of my Ph.D. Many thanks also go to my colleagues past and present in lab 98.

Financial support for this work was provided by EPSRC and BP Amoco. Thanks go to Dr. I.R. Little and Dr. J.G. Speakman of BP Amoco for their input and help with catalyst testing.

I would also like to thank Crosfield Ltd. for providing the catalyst precursor and high surface area silica used in the work reported here.

Within the chemistry department there are many people without whom this work would not have been possible. Thanks go to: Neil and Jim in the mechanical workshop together with Kelvin from the electrical workshop for building the rotating plasma reactor. Ray, Gordon and Malcolm, the glassblowers, for their ability to repair all my bits of glassware. Barry and George of the electrical workshop for all the things they helped to fix.

Special thanks go to David Apperley at the University of Durham Industrial Research Labs, for running endless solid state NMR spectra and without whom analysis would have been very difficult.

Very special thanks go to Lynsey for putting up with me, especially during the last six months, it can't have been easy!

ABSTRACT

Supported olefin polymerisation catalysts are used to produce more than 20 million tonnes of polyethylene a year. In this thesis, the application of non-equilibrium plasmas to Phillips, Ziegler-Natta, and metallocene catalysts is described.

A Cr(acetate)/silica Phillips catalyst precursor was activated using either thermal, plasma, or combined activations. Oxygen plasma activation was found to completely oxidise the acetate ligands, but left a low chromium dispersion and high hydroxyl population on the support. This large hydroxyl population caused the resulting catalyst to display a low activity. Plasma dehydroxylation of the silica support was then studied with the aim of increasing the activity of the plasma activated catalyst. Non-isothermal CF_4 plasma treatment of mesoporous silica decreased the total hydroxyl population to a level comparable to a 773 K thermal treatment. These optimum conditions were then applied to the catalyst precursor, which in combination with oxygen plasma activation, produced an active polymerisation catalyst. Also, it has been found that combined thermal and plasma activations produce catalysts of lower activity than when solely calcined, but the resulting polymers have a narrower molecular weight distribution.

Next, it was shown that Zeigler-Natta catalyst supports can be prepared by CCl_4 plasma chlorination of a dibutylmagnesium/silica precursor. This approach offers the benefits of fast reaction times and less chemical waste compared to conventional solution phase chlorination.

Finally, the replacement of conventional inorganic supports by polymer analogues has been investigated. It has been shown that plasma fluorination can be used to passivate the internal pores of high surface area polystyrene beads, thereby providing an ideal inert high surface area medium for high activity metallocene catalysts.

Overall, this work has demonstrated how non-equilibrium plasmas can be highly effective at chemically modifying porous media.

CONTENTS

CHAPTER 1

AN INTRODUCTION TO ETHYLENE POLYMERISATION CATALYSTS, THEIR SUPPORTS, NON-EQUILIBRIUM PLASMAS AND ANALYTICAL TECHNIQUES

1.1 Polyethylene

There are three major types of polyethylene, each characterised by a varying degree of chain branching. The three grades are known as low density polyethylene (LDPE), high density polyethylene (HDPE) and linear low density polyethylene (LLDPE).[1] A comparison of their properties is shown in Table 1.1.[1,2]

Property	LDPE	HDPE	LLDPE
Melting point (K)	383	> 403	393-403
Density (g cm^{-3})	0.92	0.94-0.97	0.92-0.94
Film tensile strength (MPa)	24	43	37

Table 1.1: Characteristics of the different grades of polyethylene.[1,2]

1.1.1 Low Density Polyethylene (LDPE)

High molecular weight polyethylene was first produced by accident in 1933, during an investigation into the reaction of ethylene and benzaldehyde at high pressure.[3] The polymer prepared using a high pressure, radical-initiated polymerisation process, is highly branched with approximately 60 branch points every 1000 carbon atoms.[1] This results in a low degree of crystallinity and a correspondingly low density. Such polymers have good film-forming properties and are used commercially for packaging and cable coatings.[1]

1.1.2 High Density Polyethylene (HDPE)

This class of polyethylene is obtained using either Ziegler-Natta or Phillips catalysts, and is structurally regular, possessing few branch points (less than 7 per 1000 carbon atoms).[2] As a consequence, the polymer chains can pack efficiently, resulting in a highly crystalline, high density material.[1] High density polyethylene is used for manufacturing items such as bottles and crates.[1]

1.1.3 Linear Low Density Polyethylene (LLDPE)

Linear low density polyethylene possess properties between LDPE and HDPE. It is a copolymer of ethylene and another alpha olefin, such as hex-1-ene, added to provide a controlled number of short chain branches. This branching reduces the crystallinity and density to between that of LDPE and HDPE, making it suitable for film blowing.[1]

1.2 Alkene Polymerisation Catalysts

World production of polyolefins in 1995 was estimated at 53.6 million tons (twice the figure for 1983) and is expected to increase by a further 50% over the next ten years.[4] The two groups of catalysts responsible for the production of most high density polyethylene are Ziegler-Natta and Phillips catalysts.[5] Both these catalysts produce a range of polymer products with well defined properties dependent upon the catalyst used and the conditions employed.

1.2.1 Ziegler-Natta Catalysts

Ziegler-Natta catalysts comprise mixtures of a group IA to IIIA base metal alkyl promoter and a group IVB to VIIIB metal salt, although not all possible combinations are active for polymerisation.[6,7] The promoter or co-catalyst creates the active species, thought to be a cationic metal salt, by alkylation, ligand abstraction and counter-ion complexation, Figure 1.1.[8] Ziegler-Natta catalysts may be further classified into conventional and single site catalysts, which are described in more detail below.

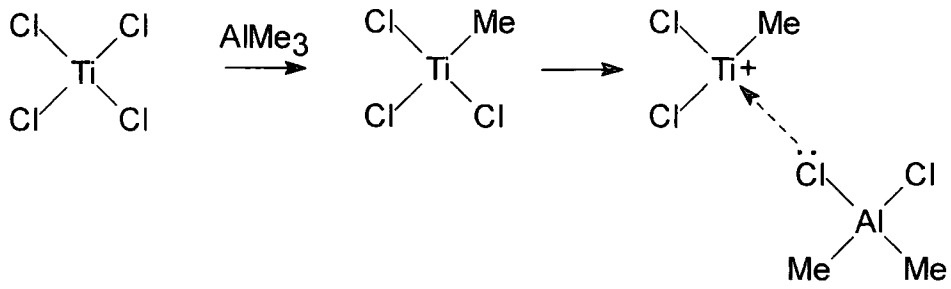

Figure 1.1: Activation of a Ziegler-Natta catalyst.[8]

1.2.1.1 Conventional Heterogeneous Ziegler-Natta Catalysts

The first generation Ziegler-Natta catalysts consisted of ball-milled $TiCl_3$ activated using a trialkylaluminium co-catalyst. Only 1% of the titanium in such catalysts produced active polymerisation centres.[6] An improvement of several orders of magnitude in activity was achieved by supporting the catalyst on magnesium chloride. Magnesium chloride is activated by ball-milling which reduces particle size, and also generates the surface defects required to produce an active catalyst when combined with $TiCl_4$ and a co-catalyst.[9,10] Although higher in activity, such catalysts produce a wide range of polymer products and the addition of a third component, to selectively poison some sites, is required to reduce the molecular weight distribution. Using silica as a support is advantageous as ball-milling is not required. A controlled silanol population can be reacted with a magnesium alkyl, upon which (after chlorination) the catalyst is built.[11,12]

Inorganic impurities originating from the support can have a detrimental effect on polymer properties, causing problems with processing as well as aesthetic defects. Polymeric supports have been used to create catalysts capable of producing polymers with reduced levels of inorganic impurities.[13,14]

1.2.1.2 Single Site Ziegler-Natta Catalysts

Unlike conventional Ziegler-Natta catalysts, single site catalysts can produce polymers with very narrow molecular weight distributions.[15] Current research in the area of polyolefin catalysts is focused on single site catalysts.

Soon after the discovery of Ziegler-Natta catalysts, metallocenes were used in conjunction with aluminium alkyls for the polymerisation of olefins. These catalysts were initially only used for mechanistic studies due to poor activity. Kaminsky accidentally discovered a dramatic improvement in activity when water contaminated an NMR tube and reacted with trimethylaluminium to form methylaluminoxane (MAO). Catalysts such as $(Cp)_2ZrMe_2$ with a large excess of MAO ([Al]:[metallocene] up to 15000:1) can produce polyethylene activities greater than 25 x 10^6 (gPE) $(gZr)^{-1}$ h^{-1}.[7] Despite the improvement in activity the main advantage of metallocene catalysts is their ability to control polymer properties by changing the ligand environment.[15]

Homogeneous metallocene catalysts are not suitable for producing polyolefins on an industrial scale. If they are to be used as drop-in catalysts in existing gas phase or slurry plants, metallocenes require heterogenation.[15]

Differing approaches have been used to fix metallocenes on to supports; the simplest approach, and one of the most widely used, involves impregnating the active catalyst directly on to the support. A mixture of metallocene and co-catalyst is prepared in solution and impregnated on to the support.[16,17,18] An MAO type surface can be created on silica, either by reacting the surface silanols with trimethylaluminium to produce MAO *in situ* on the surface or by reacting MAO directly with the hydroxyls.[19,20,21,22] By altering the silica pre-treatment, the hydroxyl distribution and hence MAO properties can be tailored. Such supports, when reacted with the metallocene and further co-catalyst, produce catalysts with similar polymer products to corresponding homogeneous systems.[15] Fixing the catalyst site on to the support requires careful control of the surface chemistry. To retain the single site characteristics of the catalyst, functional groups are first produced on the silica surface, on to which the catalyst ligands are subsequently tethered.[23,24,25,26] Alternatively,

functionalised poly(styrene-*co*-divinylbenzene) can be used as a support material.[27,28,29,30]

1.2.2 Phillips Catalysts

The Phillips catalyst has been the subject of extensive research since its discovery by Hogan and Banks in the early 1950s.[31] The catalyst is prepared by impregnating or dry blending a porous oxide support with a chromium compound. Instead of the original CrO_3 catalysts, trivalent chromium precursors are commonly used because of the carcinogenic nature of Cr(VI). After drying, the catalyst is activated by heating to 573-1273 K in a stream of dry air or oxygen.[32,33] During calcination, the chromium precursor is esterified as mono, di or polychromate species on to the support.[32] Polymerisation of ethylene is catalysed after activation at approximately 573 K, but a high activity is not seen until 773 K. The activity then continues to increase with activation temperature until the support sinters.[32] During calcination at higher temperatures the hydroxyl population decreases as neighbouring silanols undergo condensation.[34] It has been suggested that hydroxyls either coordinate to the active site[32] or that silanol condensation causes a subtle structural change, which in turn affects polymerisation activity.[35]

After calcination the catalyst is cooled before being contacted with ethylene at temperatures between 333-383 K (the temperature depends on the process used, and the polymer properties required). On exposure to ethylene the chromium is reduced to form the active polymerisation centre. Despite many investigations, the oxidation state is not unambiguously known: oxidation states between Cr(II) and Cr(VI) have been proposed.[35,32] Reduction of chromium by ethylene results in an induction period before polymerisation occurs;[32] this can be eliminated by pre-reduction using carbon monoxide at 573-623 K.[32] The polymer produced is almost identical to that produced by an ethylene reduced catalyst.[32]

Alternatively the catalyst precursor can be activated using a low temperature non-equilibrium plasma.[36,37] It has been reported that plasma activation does not produce ethylene polymerisation activities comparable to that obtained for thermally activated catalysts.[36]

1.3 Catalyst Supports

The accessibility of a catalyst surface to reacting gases is of importance in the selection of a solid material which is to function as an active catalyst for heterogeneous gas reactions.[38] For a given catalyst, the greater the amount of surface available to the reacting gas the better the conversion to products. A catalyst support may either increase the surface area available for adsorption and reaction or increase the activity per unit surface area.[38]

1.3.1 Silicas

Silica comprises a large class of products with the general formula SiO_2. Although silica occurs naturally, e.g. as quartz, most of the silica used for chemical applications is of synthetic origin, and can be produced as fibres, sheets, sols, gels and powders depending on the required use.[34,39,40,41] By changing the method of silica preparation, the surface area, particle size and pore structure can be controlled.

Sol gel silicas are made by condensing $Si(OH)_4$ molecules to form a siloxane network. A silica *sol* is formed by mixing a silicate salt (generally sodium silicate) with an acid.[41] Stable particles of colloidal size are formed by condensation, which grow into small three dimensional networks. As condensation proceeds, the viscosity of the medium increases. When an elastic stress can be supported the *sol* has condensed to form a *gel*.[41] When formed the *gel* is classed as a *hydrogel*, and the structure is controlled by the temperature, pH, solvent and starting materials.

Ageing or drying the *hydrogel* results in a loss of the pore-filling liquid to produce an *xerogel*, whose porosity and surface area are dependent on ageing and drying conditions.[41]

Silica may also be formed by a high temperature process, using a flame, arc or thermal plasma. One of the largest sources of silica is obtained by burning $SiCl_4$ with a mixture of hydrogen and oxygen.[41] In the flame the following reactions take place:

$$2H_2 + O_2 \rightarrow 2H_2O$$
$$SiCl_4 + 2H_2O \rightarrow SiO_2 + 4HCl$$
$$2H_2 + O_2 + SiCl_4 \rightarrow SiO_2 + 4HCl$$

In this way "*fumed*" silicas are formed, which are marketed by Degussa under the brand, *Aerosil®*.

A summary of the properties of different silicas is made in Table 1.2.[41]

	Preparation	
Characteristic	**Sol-Gel**	**Fumed**
BET surface area / m^2g^{-1}	250-1000	50-600
Mean pore size / nm	2-20	non porous until ca, 300 m^2g^{-1}
Pore distribution	narrow	-

Table 1.2: Physical properties of different silicas.[41]

1.3.1.1 Surface Chemistry of Silicas

Silica is made up of interlinked SiO_4 tetrahedra. At the surface, the structure terminates in either a siloxane group (O_3Si-O-SiO_3) with oxygen on the surface, or silanol (or hydroxyl) groups (O_3Si-OH). Silanols can be further divided into *isolated*, when the surface silicon has three bonds into the bulk and the fourth bond attached to a single hydroxyl and *vicinal* (or hydrogen bonded), when two hydroxyl groups are attached to different silicon atoms close enough to hydrogen bond. A third type, *geminal* occurs when two hydroxyls are attached to one silicon atom, Figure 1.2.

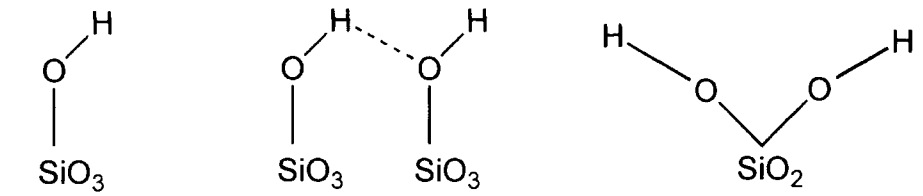

Figure 1.2: The different types of hydroxyl.[41]

Amorphous silica is highly disordered, and has an irregular arrangement of isolated and hydrogen bonded hydroxyl groups.[41]

On heating silica two processes occur; dehydration and dehydroxylation. Dehydration refers to the loss of the layer of physisorbed water, hydrogen bonded to the surface hydroxyls.[34] This can be achieved either by vacuum drying or heating the silica to 473 K.[34] Vacuum drying has no effect on the surface hydroxyls,[42] whereas heating to 473 K will cause some hydroxyls to undergo condensation.[34] During dehydroxylation silanols condense to form siloxane bridges. This process has been extensively studied.[34,39,40,41] In the temperature range 473-673 K mostly vicinal hydroxyls condense, whereas heating above 673 K is required to condense isolated hydroxyls. The silanol condensation mechanism is shown in Figure 1.3.

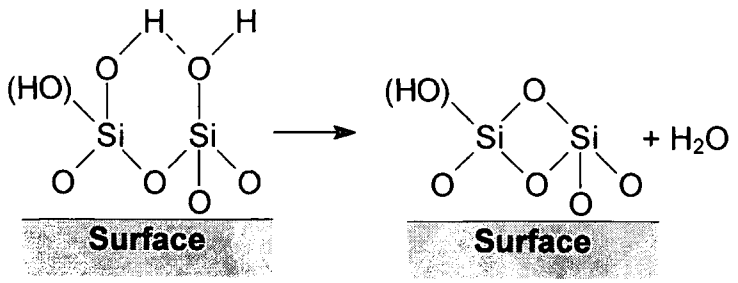

Figure 1.3: The silanol condensation mechanism.[43] (the reaction may be considered with or without the geminal hydroxyls in parenthesis).

If a geminal hydroxyl is present, then an isolated hydroxyl remains after condensation.[43] Beyond 1100 K, sintering commences[32] prior to the total loss of surface hydroxyls.[41]

1.3.2 Polymer Supports

There is growing interest in the use of polymers as potential supports for metallocene catalysts,[27,28,29,30,44] as they offer several advantages over metal oxide supports. Polymer supports may be hydrophobic, catalytically inert and possess a wide range of physical properties.[45]

Beads with a gel-like pore structure ("microporous") have been frequently studied as possible catalyst supports.[45] Uniformity of bead size can be achieved by the inclusion of a water soluble surfactant which stabilises the emulsion of organic monomers in the aqueous reaction medium. Typically, 80% styrene and 20% divinylbenzene (added to provide cross linking) is used during polymerisation.[45] Macroporous beads can be prepared from a mixture of styrene, divinylbenzene and a porogen, which controls the porosity and is subsequently extracted to leave the porous polymer.

Porous polymer beads can be made with a wide range of physical properties. Perfectly spherical beads can be produced within a very narrow size distribution, making them suitable for use in fluidized bed reactors.[46,47,48] Depending on the preparation conditions the void fraction can be as high as 0.99,[49] and the pore size from microporous to macroporous.[45] The disadvantages of polymer supports include low thermal stability and their fragility - many polymers cannot be used in stirred reactors without being pulverised.

1.3.2.1 Surface Chemistry of Polymer Supports

Unlike inorganic oxides, polymeric supports may be relatively chemically inert. Direct fluorination, which also results in improved heat stability, has been used to further achieve this.[44,50] An alternative approach to modify the surface chemistry is to add a small amount of a functionalised styrene during the polymerisation. This produces a dispersion of functional groups throughout the support.[27]

1.4 Plasmas

In 1879, Crooks suggested that such gases, consisting of neutrals, electrons, radicals, ions, metastables and electromagnetic radiation, could be regarded as the fourth state of matter. It was not until 1929 that Langmuir first coined the word "*plasma*" to describe such a gas.[51] A plasma can be defined as "*a quasi-neutral gas of charged and neutral particles which exhibit collective behaviour*".[52] Estimates have suggested that up to 99% of the universe consists of plasmas, in the form of stella interiors and atmospheres, and gaseous nebula.[52] On earth they are less common, and are seen naturally in the form of lightning and the Aurora.[52]

1.4.1 Types of Plasma

Plasmas can be described by their electron density, n_e, in the range of 1 to 10^{20} cm^{-3} and electron temperature, T_e, which can vary between 10^{-2} and 10^5 eV. The temperatures of the electrons, T_e, ions, T_i, neutrals, T_n, and radiation, T_r, are not necessarily equivalent. Several different types of plasma are shown in Figure 1.4.

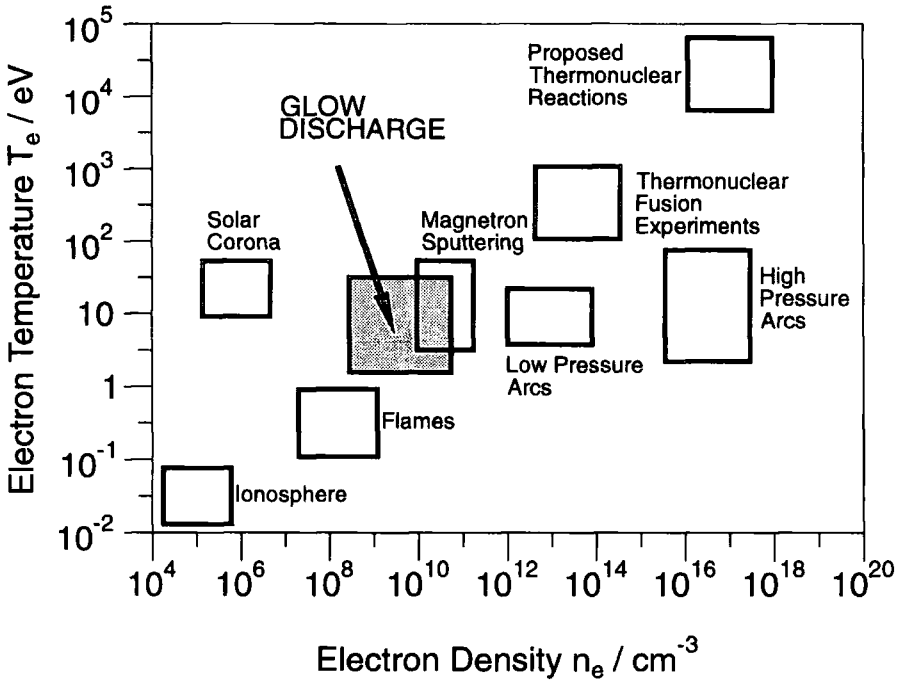

Figure 1.4: Different types of plasma as categorised by their electron density and electron temperature.[53]

Plasmas can be classified into several categories:

- Plasmas in complete thermodynamic equilibrium, i.e. with all plasma temperatures equal. These exist only in stars or during a nuclear explosion; and cannot be generated under controlled laboratory conditions.

- Plasmas in local thermodynamic equilibrium where all of the temperatures, except the radiation temperature are equal. These are classed as thermal or equilibrium plasmas, and are described in more detail in Section 1.4.1.1.

- Plasmas not in any local thermodynamic equilibrium are classed as cold or non-equilibrium plasmas. These are described in more detail in Section 1.4.1.2.

1.4.1.1 Equilibrium ("Thermal") Plasmas

At high pressures there is an increase in the number of collisions between electrons and heavy particles. As a result the two systems approach thermodynamic equilibrium, with $T_e \approx T_g$. Examples of such thermal plasmas are electric arcs or plasma jets, where the temperature of the gas can reach 20,000 - 30,000 K. Thermal plasmas are used for deposition of coatings by the plasma spraying process, in extraction metallurgy, for reduction or smelting of ores and as ionisation sources for inductively coupled plasma mass spectrometry.[53,54,55]

1.4.1.2 Non-Equilibrium ("Cold") Plasmas or Glow Discharges

In low pressure discharges, thermodynamic equilibrium between electrons and heavier particles is not reached, even at a local scale. Such non-equilibrium plasmas have electron temperatures much higher than that of the heavy particles. Whilst the electron temperature can reach 10^4-10^5 K (1-10 eV), the overall temperature of the gas, T_g, can be as low as room temperature.[53] As a consequence non-equilibrium plasmas can induce physical alteration and chemical reactions within a gas at relatively low temperatures.[53]

The simplest form of glow discharge apparatus, is that in which a dc potential is applied across metal electrodes sealed into opposite ends of a glass tube containing a gas at low pressure, Figure 1.5.[53,56]

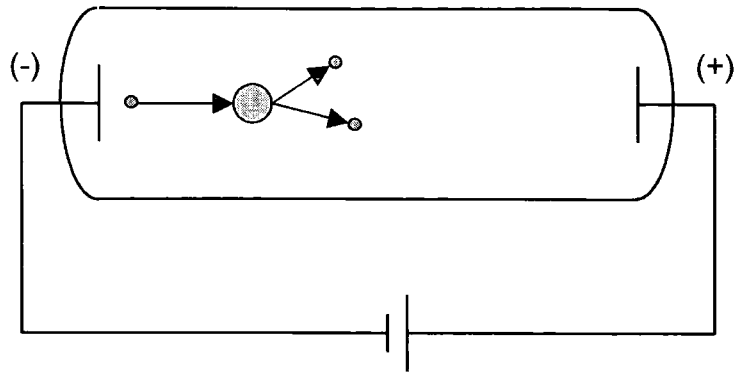

Figure 1.5: Schematic representation of the dc glow discharge apparatus with an ionisation process occurring.[53]

There are always a small number of free electrons present in a gas as a result of ionisation by naturally occurring radioactivity or cosmic rays.[53] These are accelerated as the voltage applied to the discharge tube is increased. If the energy of the electrons is insufficient to cause excitation or ionisation of atoms or molecules, the collisions will be elastic. Very little of the electron's kinetic energy is lost during these elastic collisions. As a result the electron continues to accelerate until it has sufficient energy to cause excitation or ionisation. Further electrons produced by ionisation processes are in turn accelerated by the electric field to produce a cascade of ionisation events.

In order to sustain a dc discharge, electrically conductive electrodes have to be inserted inside the reactor, in direct contact with the plasma. Contamination of the process can be avoided by having the electrodes outside the reactor, as in an ac system.

When an alternating field is applied between the electrodes, each act alternatively as cathode and anode. Once the breakdown potential is surpassed on each half cycle, a temporary dc discharge is obtained, which is extinguished as the voltage drops below the breakdown voltage.[53] As the frequency of the electric field increases, the time taken for the positive ions to move between electrodes becomes longer than one half cycle. As a result the discharge is partially retained between the two cycles.

Two different methods of producing an rf plasma with external electrodes are shown in Figure 1.6.

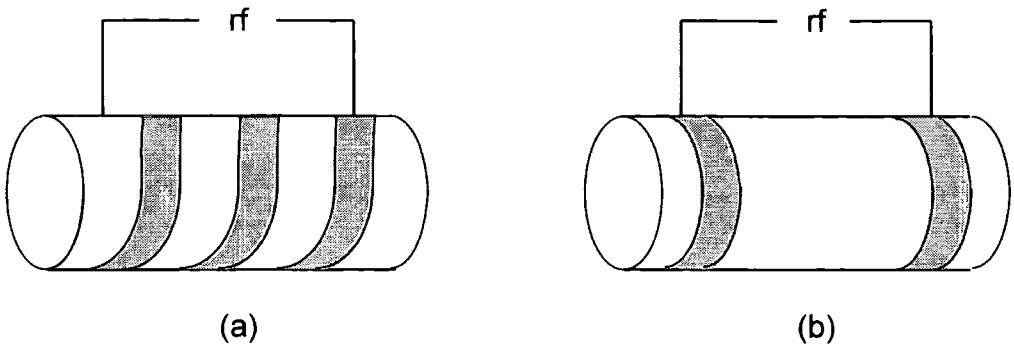

Figure 1.6: Schematic representation of two rf discharge configurations: (a) inductively coupled, a coil connected to the power supply through a matching unit is wound around the reactor and (b) capacitively coupled, the rf power is transferred through a matching unit to two separate electrodes mounted outside the reactor.[53]

The main advantage of rf over dc discharges is that the electrodes can be either internal or external. External electrodes are desirable when the discharge gas is corrosive or to prevent contamination of the plasma from the electrode material.

1.4.2 Plasma Theory

As a result of a plasma being conductive, it can respond to local changes in potential. The distance over which a small potential can perturb a plasma is known as self shielding or the Debye length, λ_D, Equation 1.1,[57]

$$\lambda_D = \left(\frac{kT_e\varepsilon_0}{n_e e^2}\right)^{\frac{1}{2}} \qquad \textbf{Equation 1.1}$$

where ε_0 is the permittivity of free space, k Boltzmann's constant, n_e electron density, T_e electron temperature and e the electronic charge.

For a particular point charge in the plasma, the sum of the individual interactions need only be considered for the charged particles within a radius of 1 or 2 Debye lengths. Outside this sphere the net interaction is zero.[52] A plasma must be quasi-neutral, and as a result, the dimensions of the plasma chamber must be much larger than λ_D. This enables local concentrations of

charge to be shielded out, within distances which are short compared to the chamber.[52,58] For a glow discharge the value of λ_D varies between 2 μm and 7 mm; depending on the electron density, n_e, and electron temperature, T_e.[53]

1.4.2.1 Electron Energy Distribution Function

A Maxwellian electron energy distribution may be assumed if: the velocity distribution of electrons in a plasma is isotropic; inelastic collisions act only to perturb the isotropy and the effect of the electric field is negligible.[53] However a Maxwellian distribution also assumes that $T_e = T_g$, which does not hold for a non-equilibrium plasma. If instead it is assumed that $T_e >> T_g$, the field frequency is lower than the collision frequency, and the collision frequency is independent of the electron energy, then the distribution of the electrons in a non-equilibrium plasma is better approximated by a Druyvesteyn distribution.[53] Although both distributions contain a high energy tail, the Druyvesteyn distribution predicts a larger number of electrons with energy higher than the median Mawellian energy, Figure 1.7. These higher energy electrons have a significant influence on the reactions in the plasma.

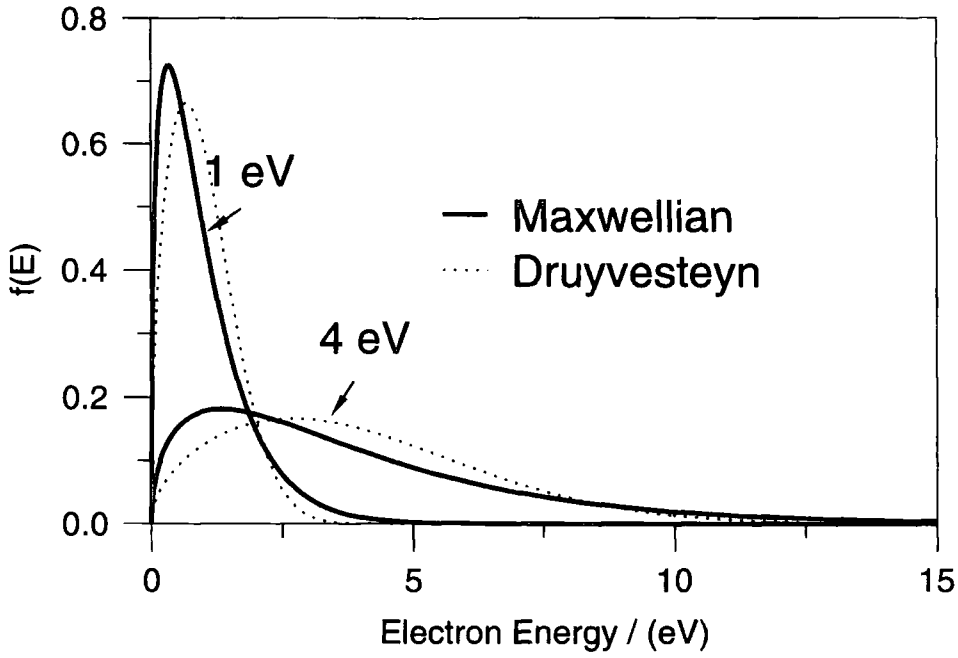

Figure 1.7: Comparison of electron energy distribution models.[53]

1.4.2.2 Plasma Potential

The electron and ion densities of a non-equilibrium plasma are, on average, equal. Electrons however, have a much larger flux due to the electron temperature being far greater than the ion temperature. A higher flux causes more electrons to reach the edges of the plasma than ions, causing a negative charge to develop at the chamber walls. The plasma will therefore develop a net positive charge in relation to the walls.[59] As the walls develop a negative charge, electrons are repelled and ions attracted, until a steady state is reached. The average potential of the bulk plasma is called the plasma potential (V_p), and will be positive with respect to the wall or floating potential (V_f).[59]

1.4.2.3 Plasma Sheath

The repulsion of electrons by the negatively charged walls results in the formation of an adjacent region of low electron density. This positively charged

volume is known as the sheath.[59] As the characteristic glow associated with a discharge is caused by the relaxation of atoms or molecules excited by electron impact,[59] the number of excited atoms or molecules, and therefore the intensity of the glow decreases across the sheath. The sheath is also sometimes referred to as the dark space because of the lower luminosity.

1.4.3 Treating Powders with Plasmas

In order to plasma treat powders there must be physical contact between the plasma and powder. In a deep bed of powder only the surface layer will be treated, while the bulk will remain unaffected. In order to successfully treat a powder, either a very thin layer spread across the reactor can be modified, or alternatively, the powder can be agitated to bring all of the powder into contact with the plasma. Treating a thin layer is impractical as only a small quantity can be modified.

There are several different approaches used to agitate powders. The most simple approach is to agitate the powder at regular intervals by physically shaking the reactor.[60] Fluidized bed reactors have also been used,[46,47,48] although careful control of the gas flow is required to stop pneumatic transportation of the powder from the reactor. Alternatively, when the reactor is designed with baffles along the walls, the powder can be agitated homogeneously by rotating the whole plasma reactor.[37]

1.5 Analytical Techniques

The catalyst activation processes and the resulting materials were analysed using various techniques. These are described in the order in which they appear in the experimental chapters. Plasmas are generally thought to modify the surface region of a substrate, and are therefore typically analysed using surface sensitive techniques, e.g. X-ray photoelectron spectroscopy. The substrates investigated in this thesis are all porous, and as such have required a combination of surface sensitive and bulk techniques.

1.5.1 Mass Spectrometry

Mass spectrometry involves the separation and detection of ions according to their mass-to-charge ratio. Ionisation is commonly performed by bombarding the sample with a perpendicular beam of electrons.[61] Once the ions are formed, they pass through a mass analyser which separates them on the basis of their mass-to-charge ratio.

1.5.1.1 The Quadrupole Mass Spectrometer

As the gas enters the spectrometer it is ionised by a perpendicular electron beam, emitted from a hot filament.[61,62] The positive ions are then accelerated by electrostatic forces between a series of slits, and focused into the quadrupole analyser,[61] which consists of four parallel electrically-conducting rods, with hyperbolic cylindrical surfaces. A combination of dc and rf electric fields is applied to the rods, with opposite pairs in the quadrupole connected to a potential given by Equation 1.2,[63]

$$P(t) = \pm\left[U + V\cos\left(2\pi ft\right)\right] \qquad \textbf{Equation 1.2}$$

where U is the dc voltage and V the peak rf amplitude of frequency f.[63] A potential of opposite sign is applied to the perpendicular pair of electrodes, shown schematically in Figure 1.8.

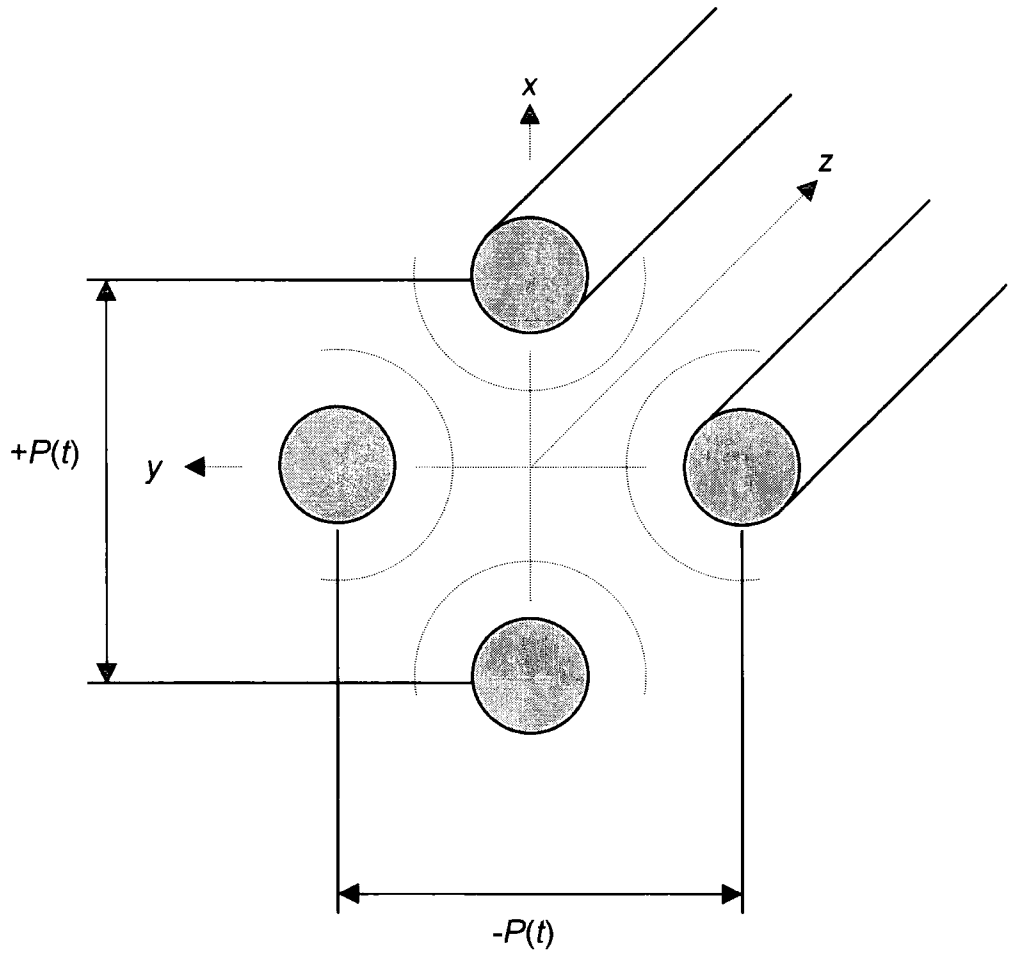

Figure 1.8: Schematic representation of a quadrupole mass analyser.[64]

An ion entering the assembly with a constant velocity in the *z* direction will acquire oscillations in the *x* and *y* directions due to perpendicular dc and rf fields. For a set dc and rf peak voltage, only ions of a given mass-to-charge ratio will have stable trajectories and emerge for detection at the opposite end of the analyser. Other mass-to-charge ratios will have unstable oscillations and will move away from the *z* axis before reaching the analyser.

After passing through the mass analyser, ions are most commonly detected using a standard electron multiplier. These are secondary electron multipliers, containing a series of dynodes. Ions are accelerated on to the surface of the first dynode. The impact releases several electrons, resulting in a cascade process. This is amplified to yield a measurable current which is taken as a signal and fed into a PC based data system.

1.5.2 Optical Emission Spectroscopy

Optical emission spectroscopy (OES) is a widely used, non-intrusive technique for the analysis of low pressure gas discharges.[65] The technique is based on measuring the intensity and wavelength of radiation emitted by excited plasma species. A simplified scheme of the excitation-radiation process is shown in Figure 1.9.[65]

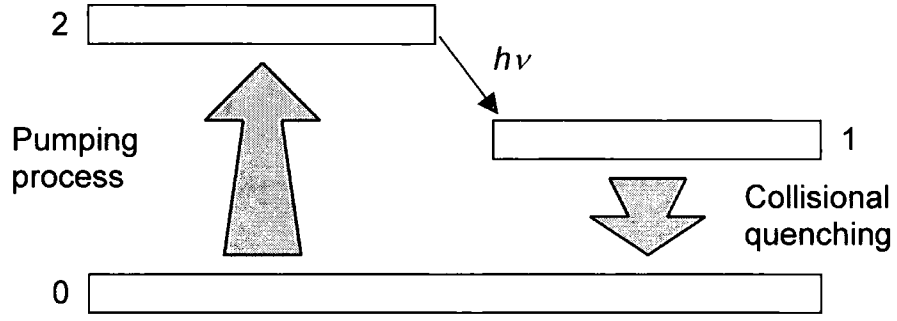

Figure 1.9: The pumping process required for OES.[65]

In a low pressure discharge direct electron impact most often causes the "pumping" into the emitting levels.[65] The emission intensity depends on the population in the excited state 2, n_2. In the glow discharge the majority of the species remain in the ground state 0, n_0. The relationship between n_0 and n_2 depends on the electron density, n_e, electron energy distribution function and excitation cross section. As a consequence, only a complicated combination of experiments and calculations can roughly track concentrations of ground state species by means of OES.

The experimental arrangement used for the work presented in this thesis consists of a 100 μm SiO_2 fibre optic cable, pointed towards the plasma reactor. After dispersion on a diffraction grating, the light from the cable is collected on a charged coupling device (CCD) which a PC then converts into a characteristic intensity versus wavelength spectrum, Figure 1.10.

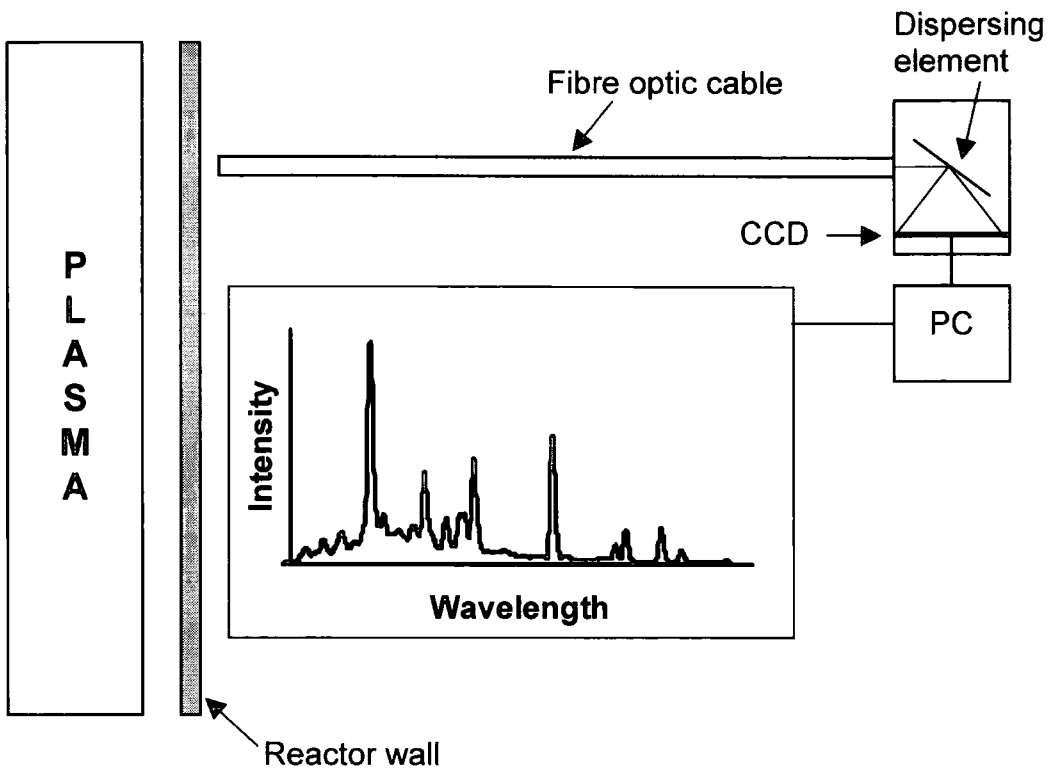

Figure 1.10: Schematic of the OES experimental arrangement.

1.5.3 Nuclear Magnetic Resonance Spectroscopy

When a magnetic nucleus is placed in a magnetic field, it adopts one of a small number of allowed orientations of different energy. A proton (Spin I=1/2) has two permitted orientations separated by energy, ΔE, which is dependent on the strength of the interaction between the nucleus and field, the nuclear magnetic moment and the strength of the magnetic field, Figure 1.11.[66]

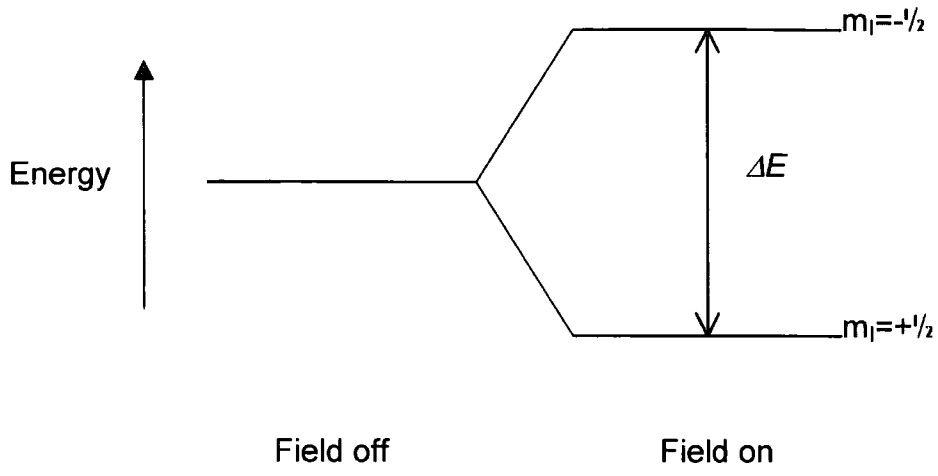

Figure 1.11: Energy levels of a hydrogen nucleus in a magnetic field.[67]

The energy separation ΔE, may be measured by applying radiation of frequency ν. Provided $\Delta E = h\nu$, this causes nuclei to "flip" from the lower to higher energy state. For a given magnetic field strength, the energy gap ΔE is determined principally by the nuclei observed, as every nuclide has a characteristic magnetic moment.[66] The resonance frequency also depends on the chemical environment of the nucleus, an effect known as the chemical shift.[68]

1.5.3.1 Chemical Shift

Not all protons (or other nuclei) have identical resonant frequencies, ν depends on the position of the nucleus in the molecule.

Chemical shifts arise because the field, B, experienced by a nucleus in an atom or molecule differs slightly from the external field, B_o. The external field B_o causes the electrons to circulate within their atomic orbitals, inducing a small magnetic field, B^I in the opposite direction to B_o. The nucleus is thus shielded from the external field by its surrounding electrons, Equation 1.3,[68]

$$B = B_o - B^I$$
$$= B_o(1-\sigma) \qquad \textbf{Equation 1.3}$$

where σ is the shielding constant.

Both the size and sign of the shielding constant are determined by the electronic structure of the molecule in the vicinity of the nucleus, and σ is therefore characteristic of the chemical environment.

1.5.3.2 Experimental Requirements

There are three experimental requirements for an NMR experiment.[66] First, a strong static magnetic field, to split the energy levels. Secondly a source of rf radiation to excite nuclei to the higher energy state, and finally a method for detecting the signal. The magnetic field is most commonly provided by a super-conducting solenoid. This consists of a coil of resistance-free alloy supporting a persistent current. A short, intense burst of rf is applied to the sample to set the nuclear moments precessing around the static field direction. A crucial feature of pulsed NMR is the ability to excite uniformly and simultaneously all nuclei within a range of chemical shifts. A typical range of ^{1}H resonance frequencies is 4 kHz which will excite all protons in the sample irrespective of their resonance frequency.[66] The oscillating magnetisation is detected as a function of time after the pulse and is known as the free induction decay (FID). The FID is the sum of the individual oscillating nuclei, each with a characteristic offset frequency due to its chemical shift. A Fourier transform is then performed to convert the FID to the frequency domain.

1.5.3.3 NMR of Solids

High resolution NMR spectroscopy in solution has become one of the most powerful techniques for the elucidation and investigation of chemical structure. In contrast, NMR spectra of solid systems typically show a very broad absorption with chemical shifts and spin-spin coupling obscured.[68]

The aim of "high resolution" solid state NMR is to remove or average the solid state interactions in order to obtain chemical information. The interaction of nuclear spins in the solid state varies markedly from that in solution. These interactions are dependent on the orientation of the nuclear spin vector to the magnetic field, and the random distribution of these orientations in solids gives rise to the severe spectral broadening.

1.5.3.4 Causes of Line Broadening in the Solid State

1.5.3.4.1 Dipolar Interactions

For most systems containing spin 1/2 nuclei, dipolar interactions are the most dominant line broadening interaction.[69] For a particular nuclei, pairwise interactions will occur between a single nucleus and all of its neighbours, Equation 1.4,[69]

$$\Delta v \propto \frac{1}{r^3}\left(1-3\cos^2\theta\right) \qquad \textbf{Equation 1.4}$$

where Δv is the peak separation, r the distance between the nuclei and θ the angle between the internuclear vector and the magnetic field. For a polycrystalline material, Equation 1.4, must be averaged over all possible angles θ, due to the random distribution of polycrystallites. For proton-proton interactions, dipolar line broadening can range up to $\approx$ 80 kHz and carbon-proton up to $\approx$ 40 kHz in the carbon spectrum.[68]

1.5.3.4.2 Chemical Shift Anisotropy

The chemical shift is caused by the modification of the applied magnetic field experienced at the nucleus by the surrounding electrons. The orientation dependence of the chemical shift for a given nuclei in an axially symmetric environment is given in Equation 1.5,[69]

$$\sigma(\theta) = \sigma_a + \frac{(3\cos^3\theta - 1)(\sigma_{\parallel} - \sigma_{\perp})}{3} \qquad \textbf{Equation 1.5}$$

where $\sigma_{\parallel}$ and $\sigma_{\perp}$ are shielding constants at $\theta = 0$ and 90° respectively, and σ_a is the isotropic average of $\sigma(\theta)$.

The averaging of the interactions over all possible random orientations in a polycrystalline sample produces line broadening in the range 0-250 ppm for ^{13}C and 0-15 ppm for ^{1}H NMR.[68]

1.5.3.5 Line Narrowing Techniques

1.5.3.5.1 Dipolar Interactions - Proton Decoupling

In "abundant" spin systems, e.g. protons, there is a high density of nuclei of high isotopic abundance, and dipolar interactions are dominant (other terms being negligible). As a consequence, the proton NMR spectra of solids generally show only a broad, featureless absorption.[69]

A less complicated situation exists for "dilute" spin systems, where there is only a low concentration of the nucleus being observed. This may be due to a low isotopic abundance of a particular nucleus, or simply from the low concentration of a particular nucleus in the sample. The heteronuclear H-X dipolar interactions remain large, but can be removed by decoupling at the proton resonance frequency. Homonuclear X-X dipolar interactions either do not exist or are very small.

1.5.3.5.2 Chemical Shift Anisotropy - Magic Angle Spinning

After removal of the heteronuclear and homonuclear dipolar interactions, the major remaining cause of broadening for spin 1/2 nuclei is chemical shift anisotropy.

The chemical shift anisotropy may be averaged to the isotropic value by the technique of magic angle spinning (MAS). The sample is mechanically spun around the axis at an angle β to the magnetic field at frequencies comparable to the frequency of the shift anisotropy, Figure 1.12. Spinning the sample modifies the chemical shift anisotropy by a factor of the form $(3\cos^2\beta - 1)$. If β is set at 54.74°, the "magic angle", the chemical shift anisotropy then becomes zero.[66]

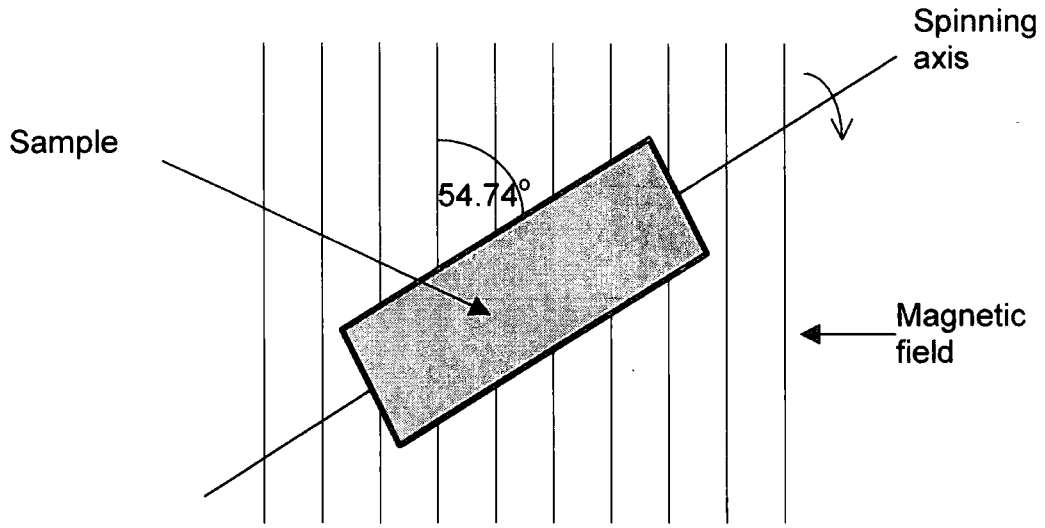

Figure 1.12: The magic angle spinning experiment.[67]

1.5.4 Infrared Spectroscopy

Infrared (IR) radiation refers to the electromagnetic spectrum between the visible and microwave regions.[70] In IR spectroscopy, the vibrational excitation is achieved by radiating the sample with a broad source of radiation in the infrared region, generally between 4000-200 cm^{-1} (2.5-50 μm).[71] The molecules are excited to a higher vibrational state by directly absorbing the infrared radiation. Within a bond, two types of vibration are possible: (i) stretching or (ii) bending. As a rule, less energy is required to bend a bond than to stretch it, therefore bending vibrations are observed at lower wavenumbers than stretching modes.[70] In order for a transition to be infrared active there must be a change in the dipole moment of the excited group. Totally symmetrical transitions are IR inactive because there is no change in dipole moment during motion.

Attenuated total reflectance Fourier transform infrared spectroscopy (ATR-FTIR) can be used to obtain spectra of opaque materials. The sample is placed on top of a crystal (e.g. KRS-5, silver chloride or diamond), which is transparent in the IR region. The refractive index of the sample has to be much less than that of the crystal. Internal reflectance occurs at the interface, due to the difference in refractive indices between the optically more dense crystal and

more rare sample, for angles of incidence, Θ_i, greater than the critical angle, Θ_c, Equation 1.6,

$$\Theta_c = \sin^{-1}\left(\frac{n_1}{n_2}\right) \qquad \textbf{Equation 1.6}$$

where n_2 and n_1 are the refractive indices of the sample and the crystal respectively. The beam is not completely reflected at the interface but propagates a short distance (a few microns into the surface), shown in Figure 1.13.

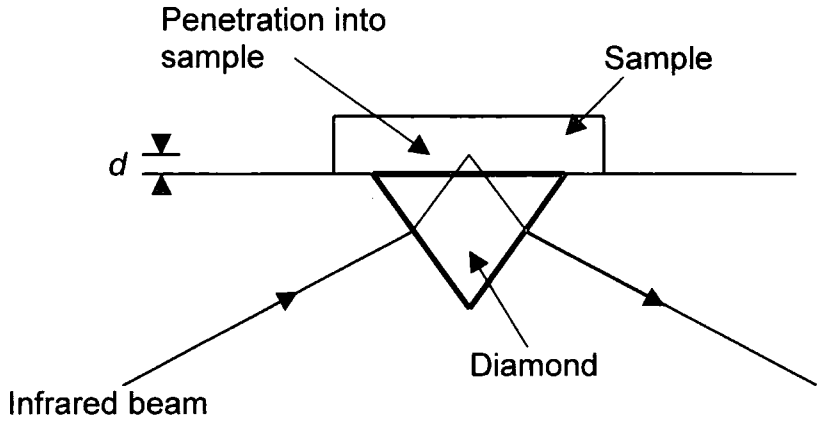

Figure 1.13: Reflection at the interface between the ATR crystal and the sample.[72]

The IR beam can interact with the groups in the surface region and is attenuated, resulting in an absorption spectrum of the sample. The depth of penetration, *d*, into the sample is dependent on wavelength, and is about 20 μm for infrared radiation,[73] Equation 1.7,[74]

$$d = \frac{\lambda}{2\pi n_1\left[\sin^2\theta - \left(\frac{n_1}{n_2}\right)^2\right]^{\frac{1}{2}}} \qquad \textbf{Equation 1.7}$$

where λ is the wavelength of radiation.

1.5.5 Surface Area by Gas Sorption Experiments

1.5.5.1 Adsorption Forces

Molecules and atoms can attach to surfaces in two ways: physisorption (physical adsorption) or chemisorption (chemical adsorption).[75] In physisorption, only weak van der Waals interactions exist between the molecule or atom and the surface. These are insufficient to lead to bond breaking and the molecule retains its identity. Distortion may however occur due to the presence of the surface. In chemisorption a chemical bond is formed between the molecule and the surface.

1.5.5.2 The Adsorption Isotherm

Physisorption occurs whenever a gas or vapour (the adsorbate) is brought into contact with a solid surface (the adsorbent). All solids attract an adsorbed layer of gas molecules, to a varying degree, which depends upon the temperature and pressure of the adsorbate. At a given temperature, the relationship between the amount of gas adsorbed (V_{ads}) and the pressure of the gas is known as the adsorption isotherm. Examples are shown in Figure 1.14. The surface area of the sample can be determined by measuring the point at which monolayer coverage occurs. Information on the pore structure of the adsorbent can also be obtained by analysing the shape of the isotherm.

1.5.5.2.1 Classification of Adsorption Isotherms

Nitrogen adsorption isotherms are generally obtained using volumetric methods; the amount of adsorbed gas is plotted against the differential pressure (p/p_o). Although there are many types of adsorption isotherm, the majority fall within the five classes shown in Figure 1.14.[76]

Type 1 isotherms are characteristic of microporous materials. Adsorption takes place in narrow pores by the process of micropore filling,[77] with the final amount adsorbed related to the micropore volume. Examples include porous carbons and zeolites.

Type 2 are characteristic of unrestricted monolayer-multilayer adsorption on macroporous or non-porous solids. The point B, at the beginning of the linear section, provides a measure of the monolayer capacity.

Type 3 are convex over the entire isotherm and are uncommon; the most well known examples are found with water vapour on carbon or other non polar materials. In such cases, the adsorbent-adsorbate interactions are relatively weak.

Type 4 are obtained with mesoporous solids. If point B is well defined it can again provide an indication of monolayer coverage. The hysteresis loop is associated with the secondary process of capillary condensation which results in the complete filling of the mesopores at a pressure less than the saturation pressure of the adsorbent.

Type 5 isotherms are uncommon. They are related to type 3 in that adsorbent-adsorbate interactions are weak, but pore filling also takes place leading to a limited uptake at high p/p_o.

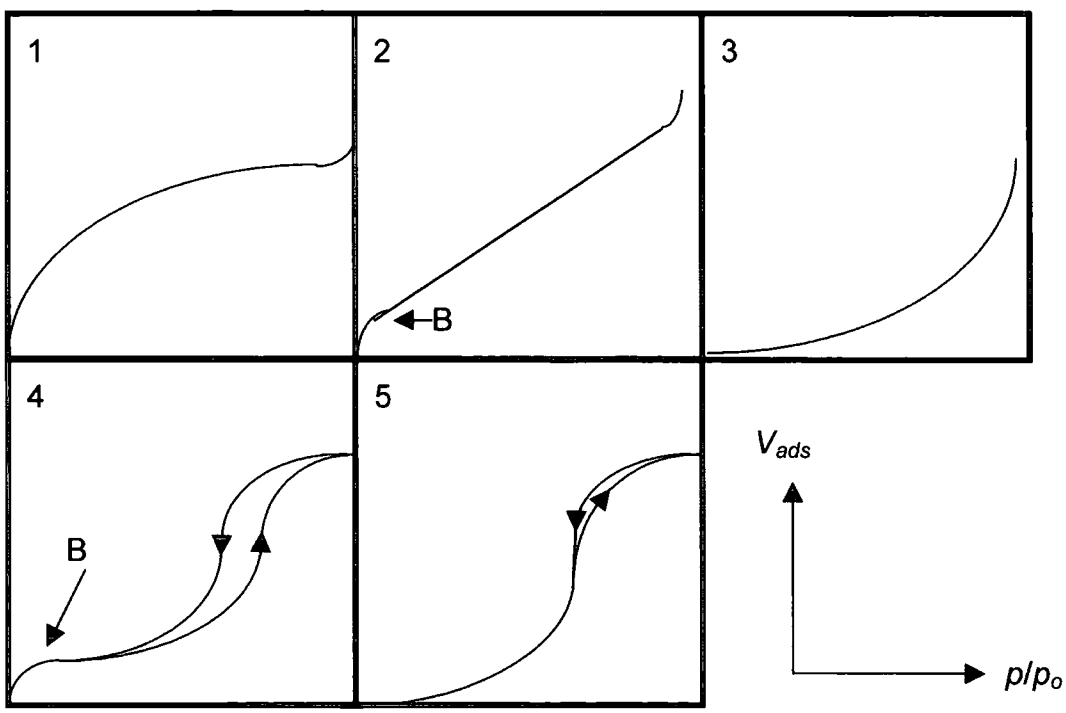

Figure 1.14: The five classes of adsorption isotherm.[76]

1.5.5.3 Surface Area Measurement

The Langmuir model of adsorption is based on the assumption that every surface site is equivalent and that the ability of a particle to bind is independent of other sites.[75] The dynamic equilibrium is

$$A(gas) + M(surface) \underset{k_d}{\overset{k_a}{\rightleftharpoons}} AM$$

where k_a and k_d are rate constants for adsorption and desorption respectively. The rate of change of surface coverage due to adsorption is proportional to the pressure p of A and the number of vacant sites $N(1-\theta)$, where N is the total number of sites and θ is the fractional coverage. The rate of change of desorption is proportional to the number of adsorbed species, $N\theta$. The Langmuir isotherm is given by Equation 1.8.

$$\theta = \frac{Kp}{1+Kp} \qquad \textbf{Equation 1.8}$$

where $K = (k_a/k_d)$

The Brunauer, Emmett and Teller[78] (BET) method for surface area determination extends the Langmuir model to multilayer adsorption and has been adopted by various official bodies as standard procedure.

The BET equation assumes that adsorption of the first layer takes place on an array of surface sites of uniform energy, with a characteristic heat of adsorption ΔH_1. Molecules in the first layer act as sites for subsequent multilayer adsorption, which in the simplest case approaches infinite thickness as the pressure, p, approaches saturation pressure, p_o. It is assumed that for all layers subsequent to the first the heat of adsorption is equal to the heat of condensation for the liquid state ΔH_L.[78]

The BET equation is defined in Equation 1.9,

$$\frac{p}{n(p_o - p)} = \frac{1}{n_m c} + \frac{(c-1)}{n_m}\left(\frac{p}{p_o}\right) \qquad \textbf{Equation 1.9}$$

where p is the adsorbate pressure, p_o the adsorbate saturation pressure, n_m the monolayer capacity, n the amount of condensed adsorbate and $c \approx \exp[(\Delta H_L - \Delta H_1)/RT]$.[78] A plot of $p/n(p_o-p)$ versus p/p_o, gives a linear relationship with intercept $1/n_m c$ and slope $(c-1)/n_m$. The range of linearity of the BET plot is restricted, usually within the range of $0.05 < p/p_0 < 0.30$, but in some cases the linear plot may not extend above $p/p_0 = 0.1$.

To calculate the surface area, A_{BET}, from the value n_m requires knowledge of the average area, A_m, occupied by the adsorbate molecule, Equation 1.10,

$$A_{BET} = n_m N_A A_m \qquad \textbf{Equation 1.10}$$

where N_A is Avogadro's constant. This assumes that the area of the adsorbate molecule is constant on all surfaces.

1.5.5.4 Classification of Pore Size

Pores are classed into three groups according to their size. The precise limits of these groups are arbitrary and should not be treated as strict boundary conditions, Table 1.3.[17]

Pore type	Pore Diameter x / nm
Micro	$x < 2$
Meso	$2 < x < 50$
Macro	$x > 50$

Table 1.3: The classification of pore size.[17]

A solid containing micropores will be subject to preferential filling of the pores as an alternative to monolayer-multilayer adsorption.[79] Micropore filling may be considered as a primary process because of its dependence on the overlap of the adsorbent-adsorbate interactions in very narrow pores. However capillary condensation in mesopores only occurs after an adsorbed layer has

formed. It is therefore a secondary process, occurring when the vapour is close to the saturation pressure.

1.5.5.5 Experimental Arrangement

A schematic diagram of the gas sorption apparatus is shown in Figure 1.15. The sample under investigation is loaded into the sample cell and outgassed at 473 K for 16 hours *in situ* to remove physisorbed water prior to analysis. By pressurising the volume V_a with helium, opening the sample cell to helium and measuring the equilibrium pressure, the volume occupied by the sample can be computed, assuming no physisorption occurs at room temperature. Following this, the sample cell is evacuated and cooled to liquid nitrogen temperature (77 K). In a similar manner to the calculation of the sample volume, a known quantity of nitrogen can be exposed to the sample and the amount of nitrogen adsorbed on to the sample calculated.

In a complete experiment, different initial pressures of nitrogen are used to obtain different equilibrium pressures, p, which are then used to calculate the BET surface area.

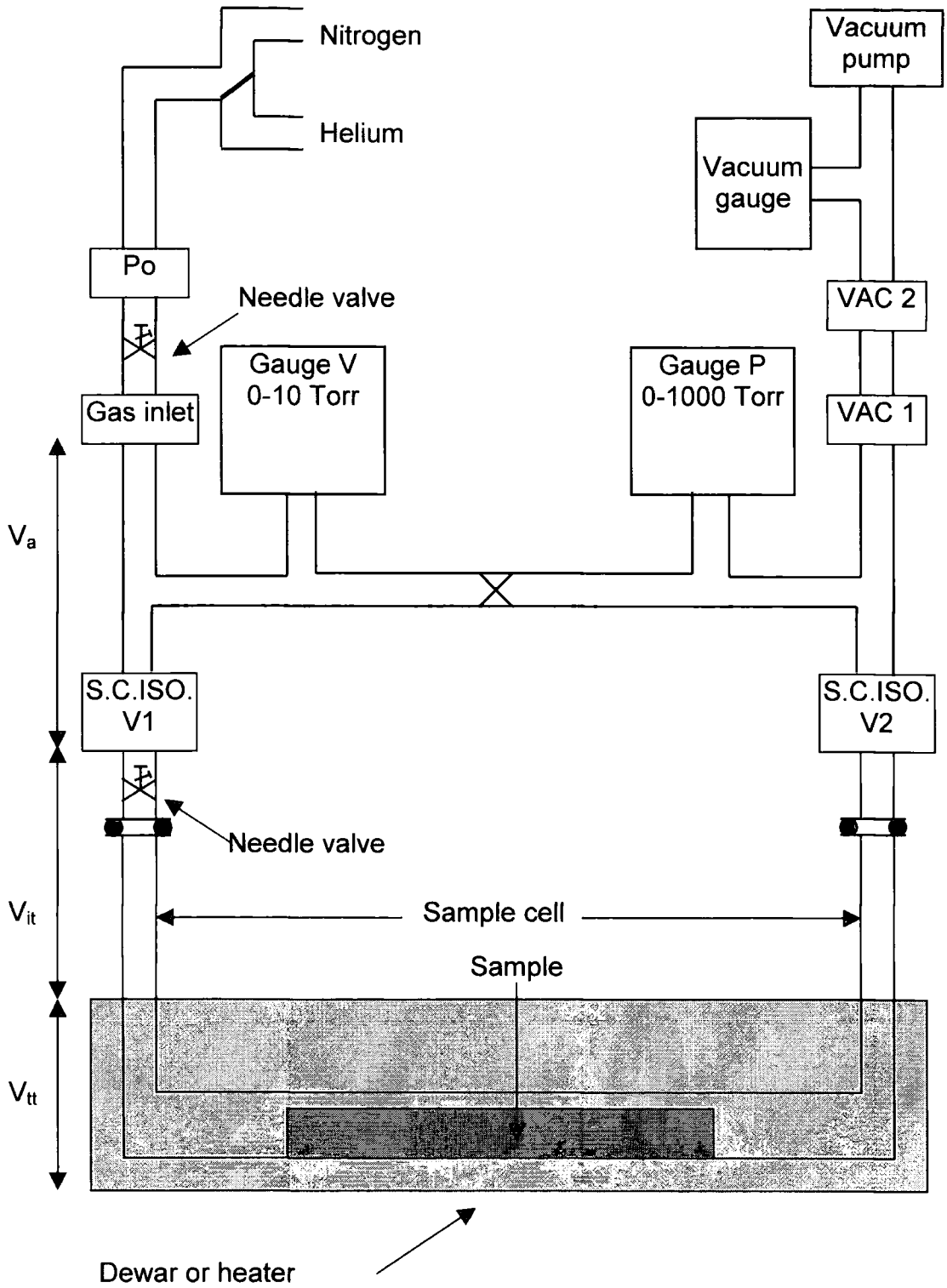

Figure 1.15: Schematic of the sorptometer.[80]

1.5.6 X-Ray Photoelectron Spectroscopy

Photoelectron spectroscopy involves the ejection of electrons (photoelectrons) from atoms or molecules following bombardment by photons.[73] Bombardment of the surface with photons of tuneable frequency does not produce any photoelectrons until a threshold frequency is reached.[73] At this frequency, ν_t, the photon energy is just sufficient to overcome the work function ϕ of the surface, Equation 1.11.

$$h\nu_t = \phi \qquad \textbf{Equation 1.11}$$

At higher frequencies the excess energy of the photons is converted into kinetic energy of the photoelectrons, Equation 1.12.

$$h\nu = \phi + \frac{1}{2}m_e v^2 \qquad \textbf{Equation 1.12}$$

where m_e and v are the electron mass and velocity.

For an atom or molecule in the gas phase the orbitals can be separated into core and valence orbitals, Figure 1.16. The valence electrons have higher orbital energies than the core electrons. Far ultraviolet radiation only has sufficient energy to probe valence electrons and is used in ultraviolet photoelectron spectroscopy (UPS). A source of low energy (soft) X-rays may be used to eject core electrons, and the technique is often referred to as X-ray photoelectron spectroscopy (XPS). The creation of a core hole by the photoelectron process leads to the possibility of recombination by an Auger process. An electron in a valence orbital relaxes to fill the photoelectron hole and the excess energy is lost when another valence electron is ejected.

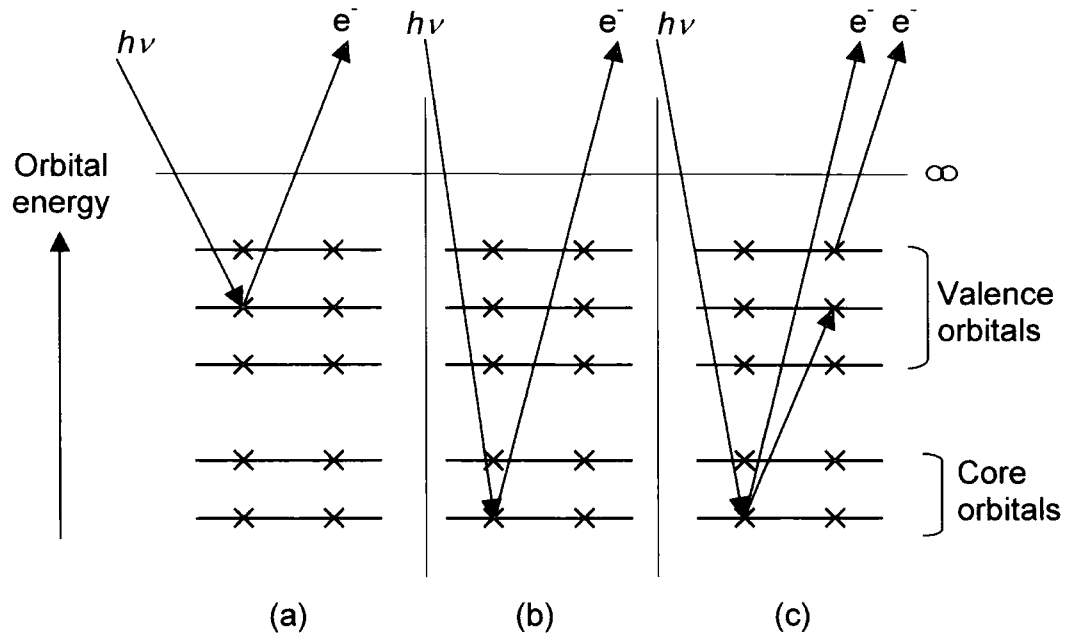

Figure 1.16: Photoelectron processes; (a) ultraviolet, (b) X-ray and (c) the Auger process.[73]

In photoelectron methods, the surface sensitivity is not dependent upon the penetration depth of the incident radiation (10^2-10^3 nm),[81] but upon the probability of the photoelectron escaping without further loss of energy. Inelastic scattering disperses the kinetic energy of the emitted electrons produced in the subsurface. Only electrons from the surface region can escape without losing energy, Figure 1.17. The mean free path passes through a minimum of about 3 nm. Photoelectron spectroscopy is therefore a surface sensitive technique, only detecting electrons from the first few monolayers of the sample.[81]

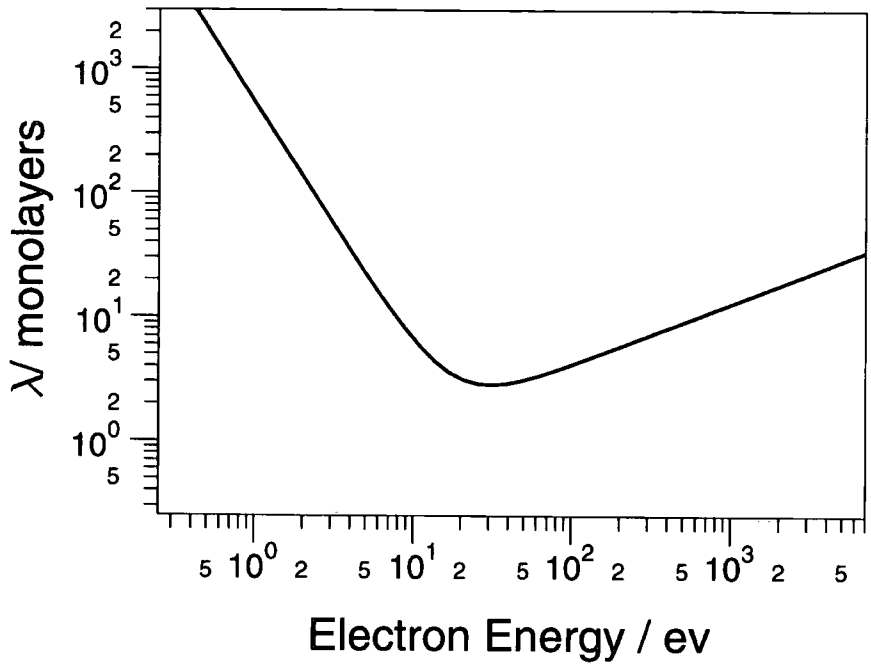

Figure 1.17: The dependence of emitted electron energy on the attenuation length λ.[81]

1.5.6.1 Experimental Arrangement

A schematic diagram of an XPS spectrometer is shown in Figure 1.18.

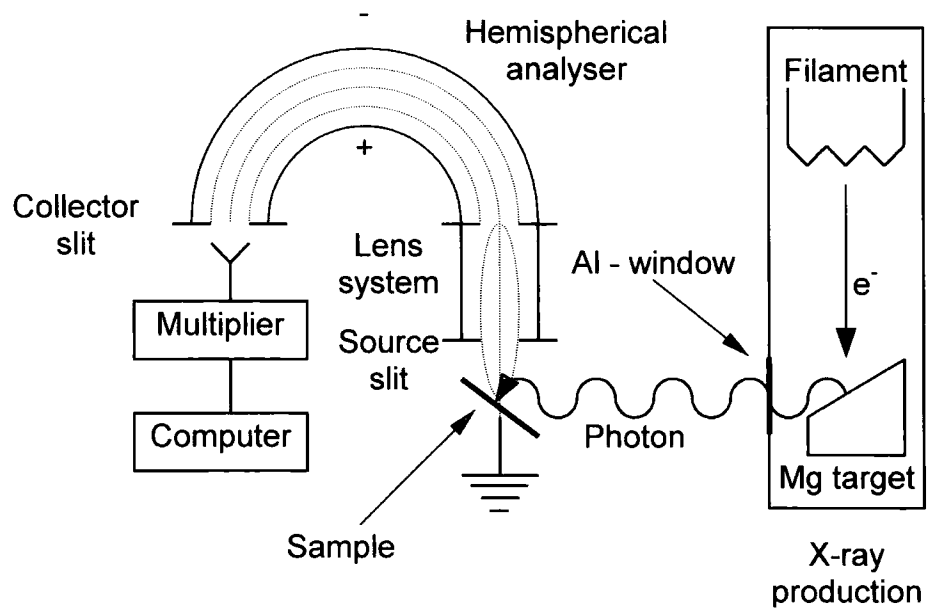

Figure 1.18: Schematic of an XPS spectrometer.

The K_α X-rays are produced by electron bombardment of either an aluminium (1486.6 eV) or magnesium (1253.6 eV) surface. *Bremsstrahlung* background radiation is removed from the characteristic X-ray lines on passing through the aluminium window.[82]

X-rays bombard the sample surface and the emitted electrons are collected, retarded and analysed as a function of their kinetic energy. Concentric hemispherical analysers (CHA) are made of two concentric hemispheres, held at opposite potentials. Only electrons of a specific kinetic energy will be able to pass through and on to the detector.[82] The electron leaving the analyser slit is detected using a solid state multiplier, i.e. a channeltron.

XPS spectra can be recorded by scanning the potential applied to the retarding lens while keeping the potential difference between the hemispheres constant (fixed analyser transmission or FAT mode), or by scanning the

potential across the CHA at a fixed retarding potential (fixed retard ratio of FRR mode).[82]

1.5.7 Inductively Coupled Plasma Mass Spectrometry

A sequence of processes leads to an inductively coupled plasma mass spectrometry (ICP-MS) signal. The sample is typically introduced as an aerosol, vaporised and then converted into atoms and ions in the ICP. The ions are then transported from the ICP to a quadrupole mass spectrometer.[54] A schematic of the experimental arrangement is shown in Figure 1.19.[55]

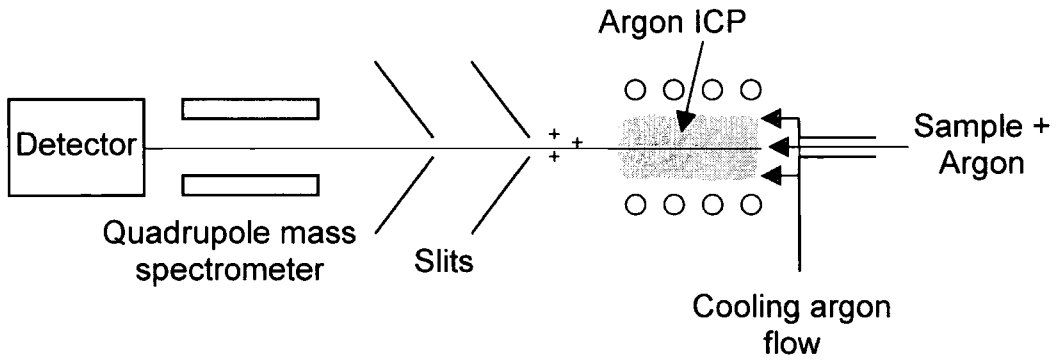

Figure 1.19: Schematic of an ICP-MS.

The quadrupole mass spectrometer signal is calibrated using a series of known standards for the elements under study, before the sample being investigated is analysed.

1.5.8 Diffuse Reflectance Spectroscopy

Diffuse reflectance has been widely used for UV/vis and IR analysis of solids and particulates, due to the minimal sample preparation required.[83]

Two processes can occur when a ray of light arrives at the surface of a particulate medium, Figure 1.20.[83] There is a random arrangement of crystal faces at the interface so that there will be a range of angles of incidence with the crystal faces. Some rays (R_1) will arrive at such an angle that they will be

reflected from the surface. This gives rise to a specular or surface reflectance component which does not undergo an absorption interaction with the sample. Another ray (R_2), on the other hand, may arrive at such an angle that it is not reflected but refracted and enters a crystallite. It may then emerge or become internally reflected a number of times, and in general, will undergo reflection and refraction through many crystallites before emerging from the solid.[83] The angle of emergence for this ray is dependent on the path taken and can assume any value. Such rays, having passed through the sample, have undergone interaction with the sample and contain spectral information.[83]

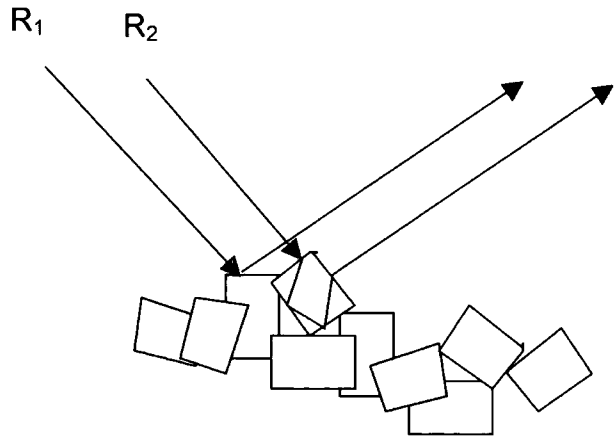

Figure 1.20: Diffuse reflectance. Ray R_1 is specularly reflected whereas R_2 enters the sample and is diffusely reflected.[83]

Due to the random orientation of particulates, there will be a distribution of the angles of specularly reflected rays. Thus diffuse and specular reflection are always mixed and cannot be spatially resolved. The energy arriving at the detector is therefore the sum of the reflected and refracted radiation from the sample.[83]

Experimentally the relative reflection from a sample is measured with respect to a reference sample.

1.5.9 Secondary Ion Mass Spectrometry

Secondary ion mass spectrometry (SIMS) is used to study atomic or molecular particles which are emitted (via a process know as sputtering) when a surface is bombarded by energetic primary particles. The secondary ions which are detected may be emitted from the surface in the ionised state or they may be initially emitted as neutrals and then ionised before analysis.[84]

There are two main components in the SIMS experiment - the primary particle beam and the mass spectrometer. The primary particle beam can be produced by either ion, atom or liquid metal ion sources. Secondary ions are then analysed using either a quadrupole, magnetic sector or time of flight mass spectrometer.[84]

When a high flux of primary ions is directed at the surface a high yield of secondary ions is produced. This leads to sample erosion and is classed as *Dynamic SIMS*. When a very low primary beam density is used the secondary ions are emitted from areas not previously damaged, therefore the lifetime of the surface monolayer is in excess of the time of analysis. This is described as *Static SIMS*.[84]

Where there is a need to produce a chemical map of the surface, a highly focused primary particle beam is used. The beam is rastered over the sample and the secondary ions generated from each point are collected to form a chemical map of the surface.[84]

1.6 References

[1] H. Ulrich, *Introduction to Industrial Polymers*, Hauser, Munich, 1982.

[2] J.M.G. Cowie, *Polymers: Chemistry and Physics of Modern Materials*, 2nd ed., Blackie, Glasgow, 1991.

[3] D.C. Miles and J.H. Briston, *Polymer Technology*, 1st ed., Temple, London, 1965.

[4] M. Bochmann, *J. Chem. Soc., Dalton Trans.*, **1996**, *3*, 255.

[5] R.F. Jordan, *J. Chem. Ed.*, **1988**, *65*, 285.

[6] J. Boor, *Ziegler-Natta Catalysts and Polymerizations*, Academic Press, London, 1979.

[7] P.J.T. Tait. In *Comprehensive Polymer Science*, G. Allen and J.C. Bevington, Eds., Pergaman Press, Oxford, 1989, Vol. 4, Chapter 1.

[8] J.P. Candin. In *Catalysis and Chemical Processes*, R.E. Pearce and W.R. Patterson, Eds., Blackie, Glasgow, 1981, Chapter 10.

[9] J.C.J. Bart, *J. Mater. Sci.*, **1993**, *28*, 278.

[10] E. Magni and G.A. Somorjai, *Surf. Sci.*, **1996**, *345*, 1.

[11] B.H. Johnson, U.S. Patent 4,707,530, 1987.

[12] F. Milani, L. Luciani and A. Labianio, U.S. Patent 5,348,925, 1994.

[13] L. Sun, C.C. Hsu and D.W. Bacon, *J. Polym. Sci., Polym. Chem. Ed.*, **1994**, *32*, 2127.

[14] D.A. Kritskia, A.D. Pomogatio, A.N. Pomonavev and F.S. Dyashkouskh, *J. Appl. Polym. Sci.*, **1980**, *25*, 349.

[15] W. Kaminsky, *J. Chem. Soc., Dalton Trans.*, **1998**, 1413.

[16] T.J. Burkhardt, M. Murata and W.B. Brandley, U.S. Patent 5,554,704, 1996.

[17] H.C. Welburn, U.S. Patent 4,808,561, 1989.

[18] M. Kaminaka and K. Soga, *Macromol. Chem., Rapid Commun.*, **1991**, *12*, 367.

[19] M. Chang, U.S. Patent 5,629,253, 1997.

[20] M. Chang, U.S. Patent 4,912,075, 1990.

[21] T.E. Nowlin, F.Y. Lo, R.S. Shinomoto and P.P. Shirokar, U.S. Patent 5,332,706, 1994.

[22] S. Shin and D. Lee, *Macromol. Symp.*, **1995**, *97*, 195.

[23] K. Soga, *Macromol. Symp.*, **1995**, *89*, 249.

[24] T. Uozumi, T. Toneri, K. Soga and T. Shiono, *Macromol. Rapid Commun.*, **1997**, *18*, 9.

[25] E.I. Iiskola, S. Timonen, T.T. Pakkanen, O. Harkki, P. Lehmus and J.V. Seppela, *Macromolcules*, **1997**, *30*, 2859.

[26] K. Patsidis, B. Peifer, S.J. Palackal, H.G. Alt, M.B. Welch, R.L. Geerts, D.R. Fahey and H.R. Deck, U.S. Patent 5,466,766, 1995.

[27] T. Kitagawa, T. Uozumi, K. Soga and T. Takata, *Polymer*, **1997**, *38*, 615.

[28] S.B. Roscoe, J.M.J. Frechet, J.F. Walker and A.J. Dias, *Science*, **1998**, *280*, 270.

[29] A.G.M. Barrett and Y.R. de Miguel, *Chem. Commun.*, **1998**, 2079.

[30] M.C.W. Chan, K.C. Chew, C.I. Dalby, V.C. Gibson, A. Kohlmann, I.R. Little and W. Reed, *Chem. Commun.*, **1998**, 1673.

[31] J.P. Hogan and R.L. Banks, U.S. Patent 2,825,721, 1958.

[32] M.P. McDaniel, *Adv. Catal.*, **1985**, *33*, 47.

[33] A. Clark, *Catal. Rev.*, **1969**, *3*, 145.

[34] R.K. Iler, *Chemistry of Silica*, John Wiley and Sons, New York, 1979, Chapter 6.

[35] C.E. Marsden, *Plast., Rubber Compos. Proces. Appl.*, **1994**, *21*, 193.

[36] B. Horvath, U.S. Patent 3,485,771, 1966.

[37] V.J. Ruddick and J.P.S. Badyal, *J. Phys. Chem., B*, **1997**, *101*, 9240.

[38] J.M. Thomas and W.J. Thomas, *Introduction to the Principles of Heterogeneous Catalysis*, Academic Press, London, 1967, Chapter 4.

[39] L.T. Zhuralev, *Langmuir*, **1987**, *3*, 316.

[40] L.T. Zhuralev and A.V. Kiselev, *Russ. J. Phys. Chem. (Eng. Transl.)*, **1965**, *39*, 236.

[41] E.F. Vansant, P. van der Voort and K.C. Vrancken, *Stud. Surf. Sci. Catal.*, **1995**, *93*.

[42] G. Ghiottit, E. Gavvore, C. Montera and F. Boccuzzi, *J. Phys. Chem.*, **1979**, *83*, 2863.

[43] J.P. Gallas, J.C. Lavalley, A. Burneau and O. Berres, *Langmuir*, **1991**, *7*, 1235.

[44] J.J. Wu, L. Fu and K.T. Chung, *Appl. Catal.*, **1991**, *72*, 71.

[45] J. Lieto, D. Milstein, R.L. Albright, J.V. Minkiewicz and B.C. Gates, *CHEMTECH*, **1983**, *13*, 46.

[46] S.H. Park and S.D. Kim, *Polymer Bull.*, **1994**, *33*, 249.

[47] N. Inagaki, S. Tasker and H. Abe, *J. Appl. Polym. Sci.*, **1992**, *46*, 595.

[48] N. Inagaki, S. Tasker and K. Ishii, *J. Appl. Polym. Sci.*, **1995**, *48*, 1433.

[49] N.R. Cameron, D.C. Sherrington, I. Ando and H. Kurosu, *J. Mater. Chem.*, **1996**, *6*, 719.

[50] J.D. Hewes, S. Curren and E.A. Leone, *J. Appl. Polym. Sci.*, **1994**, *53*, 291.

[51] I. Langmuir, *Phys. Rev.*, **1929**, *33*, 954.

[52] F.F. Chen, *Introduction to Plasma Physics*, Plenum Press, New York and London, 1974, Chapter 1.

[53] A. Grill, *Cold Plasmas in Materials Technology*, IEEE press, New Jersey, 1994.

[54] J.W. Olesik, J.A. Kinzer and M.P. Dziewatoski. In *Plasma Source Mass Spectrometry. Developments and Applications*, G. Holland and S.D. Tanner, Eds., Royal Society of Chemistry, Bodmin, 1997, Chapter 1.

[55] K.E. Jarvis, A.L. Gray and R.S. Houk, *Handbook of Inductively Coupled Plasma Mass Spectrometry*, Blackie, Glasgow, 1992, Chapter 1.

[56] F.K. McTaggart, *Plasma Chemistry in Electrical Discharges*, Elsevier, Amsterdam, 1967.

[57] S.M. Rossnagel, *Thin Film Processes II*, Academic Press, London, 1991.

[58] A.T. Bell, *Techniques and Applications of Plasma Chemistry*, J.R. Hollham and A.T. Bell, Eds., John Wiley and Sons, New York, 1974, Chapter 1.

[59] B. Chapman, *Glow Discharge Processes*, John Wiley and Sons, New York, 1980.

[60] B.E. Scruggs and K. Gleason, *J. Phys. Chem.*, **1993**, *97*, 9187.

[61] R.M. Silverstein, G.C. Bassler, T.C. Morrill, *Spectrometric Identification of Organic Compounds*, 5th ed., John Wiley and Sons, Singapore, 1991, Chapter 2.

[62] D.H. Williams and I. Flemming, *Spectroscopic Methods in Organic Chemistry*, 5th ed., McGraw Hill Publishing Company, Maidenhead, 1995, Chapter 4.

[63] H.E. Duckworth, R.C. Barber and V.S. Venkatasubramanian, *Mass Spectroscopy*, 2nd ed., Cambridge University Press, Cambridge, 1990.

[64] E. Constantin, A. Schnell, *Mass Spectrometry*, Ellis Horwood, Chichester, 1990.

[65] R. d'Agostino, F. Cramarossa, F. Fracassi and F. Illuzzi. In *Plasma Deposition, Treatment, and Etching of Polymers*, R. d'Agostino, Ed., Academic Press, San Diego, 1990, Chapter 2.

[66] P.J. Hore, *Nuclear Magnetic Resonance*, Oxford University Press, New York, 1995.

[67] P.W. Atkins, *Physical Chemistry*, 4th ed., Oxford University Press, Oxford, 1990, Chapter 18.

[68] J.W. Akitt, *NMR and Chemistry. An Introduction to Modern NMR Spectroscopy*, 3rd ed., Chapman and Hall, London, 1992, Chapter 10.

[69] M.E.A. Cudby and D.J. Williamson, *Perspectives in Modern Chemical Spectroscopy*, D.L. Andrews, Ed., Springe-Verlay, Berlin, 1990, Chapter 7.

[70] R.M. Silverstein, G.C. Bassler, T.C. Morrill, *Spectrometric Identification of Organic Compounds*, 5th ed., Wiley, Singapore, 1991, Chapter 3.

[71] D. Lin-Vien, N.B. Colthup, W.G. Fateley and J.G. Grasselli, *The Handbook of Infrared and Raman Characteristic Frequencies of Organic Materials*, Academic Press, London, 1991.

[72] H.A. Wills, V.J.I. Zichy. In *Polymer Surfaces*, D.T. Clark and W.J. Feast, Eds., John Wiley and Sons, Chichester, 1978, Chapter 15.

[73] J.M. Hollas, *Modern Spectroscopy,* 2nd ed., John Wiley and Sons, Chichester, 1993.

[74] J. Comyn. In *Handbook of Adhesion*, D.E. Packham, Ed., Longman Group UK Ltd, Harlow, 1992. p 251.

[75] P.W. Atkins, *Physical Chemistry*, 4th ed., Oxford University Press, Oxford, 1990, Chapter 29.

[76] S. Brunauer, L.S. Deming, W.E. Deming and E. Teller, *J. Am. Chem. Soc.*, **1940**, *62*, 1723.

[77] K.S.W. Sing. In *Characterisation of Catalysts*, J.M. Thomas and R.M. Lambert, Eds., John Wiley and Sons, 1980, Chapter 2.

[78] S. Brunauer, P.H. Emmett and E. Teller, *J. Am .Chem. Soc.*, **1938**, *60*, 309.

[79] K.S.W. Sing. In *Characterisation of Catalysts*, J.M. Thomas and R.M. Lambert, Eds., John Wiley and Sons, 1980, Chapter 4.

[80] Porous Materials Inc, *PMI Automated BET Sorpotometer Instruction Manual*, 1990.

[81] D. Briggs and M.P. Seah, *Practical Surface Analysis, Volume 1 - Auger and X-ray Photoelectron Spectroscopy*, 2nd ed., John Wiley and Sons, Chichester, 1983.

[82] E. Desimoni and P.G. Zamborini. In *Surface Characterisation of Advanced Polymers*, L. Sabbatini and P.G. Zamborini, Eds., VCH Publishers, New York, 1993, Chapter 1.

[83] P.S. Belton and R.H. Wilson. In *Perspectives in Modern Chemical Spectroscopy*, D.L. Andrews, Ed., Springe-Verlay, Berlin, 1990, Chapter 3.

[84] D. Briggs, A. Brown and J.C. Vickerman, *Handbook of Static Secondary Ion Mass Spectrometry*, John Wiley and Sons, Chichester, 1989.

CHAPTER 2

PLASMA ACTIVATION OF THE PHILLIPS Cr(ACETATE)/SiO_2 POLYMERISATION CATALYST PRECURSOR. PART 1: PLASMA VERSUS THERMAL ACTIVATION

2.1 Introduction

In the early 1950s, Hogan and Banks discovered that chromium oxide supported on silica or other carriers could polymerise olefins to yield high molecular weight polymers.[1] Today this catalyst accounts for approximately 40% of the global high density polyethylene production.[2] This is due to the variety of polymer properties which can be obtained by either altering the catalyst activation conditions or adding promoters such as alumina, titania or fluoride species.[3]

Conventionally, the supported chromium precursor is activated by heating to 573-1273 K in either dry air or oxygen for several hours.[3,4] During activation, the chromium precursor is esterified (at temperatures up to 573 K) as mono, di or polychromate species on to the support.[3,5] Heating to higher temperatures causes silanol condensation of hydroxyls on the support.[6] Following cooling to 333-383 K, the catalyst is contacted with ethylene. This is followed by an induction period, where the supported hexavalent chromium species are reduced,[3,7] in conjunction with methanal evolution,[8] before polymerisation occurs.[9] This reduction process causes the characteristic accelerating activity profile observed with Phillips catalysts.[3] Alternatively, the induction period can be removed by pre-reducing the activated catalyst by exposing to carbon monoxide at 573-623 K.[3] The temperature of activation effects the catalyst activity. After calcination at 573 K, when the chromium has been oxidised and anchored to the support, the Phillips catalyst begins to polymerise ethylene.[5] However, a respectable activity is not reached until calcination above 773 K. The activity and melt index continue to increase with activation temperature up to the point at which sintering of the support occurs

at around 1250 K.[3] There are thought to be no changes to either the chromium species or the physical properties of the support until sintering occurs,[3,10] - only a reduction in hydroxyl population. It has been suggested that the residual hydroxyls interfere with the active sites through coordination to the chromium.[11,12,13] The polymers produced using Phillips catalysts typically have a broad molecular weight distribution (MWD) due to the diversity of active sites on the support.[3]

Alternatively, a non-equilibrium ("cold") plasma may be used to activate the catalyst.[14,15] A low activity was obtained using a CrO_3/SiO_2 precursor,[15] whereas no polymerisation data have been presented for a Cr(acetate)/SiO_2 precursor.[14] However, such a low temperature plasma process is highly desirable, due to the increased speed of activation, and the low energy consumption required compared to conventional thermal treatment. Furthermore, a plasma process would allow continuous catalyst activation rather than batch processing, thereby speeding up production and allowing greater flexibility over the type of polymer produced.

In this study, the polymerisation activity and polymer properties of a Cr(acetate)/SiO_2 Phillips catalyst precursor are investigated after either a thermal, plasma or a combined activation. The characteristics of the catalyst are then compared using temperature programmed desorption (TPD), optical emission spectroscopy (OES), inductively coupled plasma mass spectrometry (ICP-MS), UV/vis diffuse reflectance, CO reduction and ^1H solid state NMR.

2.2 Experimental

The catalyst precursor was prepared by impregnating silica (EP10X, Crosfield Ltd, particle size $\approx$ 100 μm) with an aqueous solution of basic chromium(III) acetate (EP30X, Crosfield Ltd, Cr 1 wt.% after calcination).

Conventional thermal calcination was performed in a catalytic microreactor using oxygen and nitrogen carrier gases (Air Products 99.995%, BOC 99.998% respectively, dried through activated 3A molecular sieve (Aldrich) to give H_2O < 1.0 ppm_v) at a flow rate of 1.5 $dm^3\ h^{-1}$. 1 g of catalyst precursor was loaded into a quartz microreactor tube and heated under a flow of O_2 at 1 K min^{-1} up to 1053 K using a Eurotherm temperature controller. The

furnace was held at this high temperature under O_2 for a further 5 h prior to cooling at 5 K min^{-1}. At 873 K the carrier gas was switched to N_2 and the cooling continued. A Vacuum Generators SX 200 quadrupole mass spectrometer, connected via a heated fine capillary tube to the microreactor outlet, was used to monitor the composition of the gases within the exhaust during activation.

Plasma activation was carried out in a 13.56 MHz rotating plasma reactor designed to enable the treatment of powder samples, and allow subsequent analysis without exposure to air, Figure 2.1. The reactor was continuously pumped by a 33 dm^3 h^{-1} Edwards E2M2 Fomblin rotary pump via a liquid air cold trap to yield a base pressure of 2 x 10^{-2} mbar (with a leak rate better than 3.5 x 10^{-8} mol s^{-1}).[16] Prior to each experiment, the reactor chamber was cleaned with detergent, rinsed with isopropyl alcohol, dried in an oven, and then cleaned *in situ* using a 0.3 mbar air plasma at 30 W. 1 g of catalyst precursor was then loaded into the reactor and evacuated down to base pressure before O_2 was introduced to the reactor at a pressure of 0.3 mbar (equivalent to a flow rate of 2 x 10^{-6} mol s^{-1}) via a fine needle valve. At this stage rotation of the reactor commenced and a 70 W plasma was ignited. After 45 min, agitation of the catalyst particles was stopped, the rf power supply switched off, and the reactor evacuated to its original base pressure, prior to bringing up to an atmosphere of O_2. An Ocean Optics Inc. SD 1000 Fibre Optic Spectrometer was used for optical emission spectroscopy (OES), giving a real-time diagnostic of the discharge during activation. In particular, the intensity of the hydrogen (H_α 656.3 nm),[17] carbon monoxide (CO $B^1\Sigma$-$A^1\Pi$ 483.0 nm)[17] and atomic oxygen (O $3s^5S$-$3p^5P$ 775.5 nm)[18] emission lines were studied.

All sample transfers for analysis were carried out under an atmosphere of dry nitrogen (H_2O < 1.0 ppm_v).

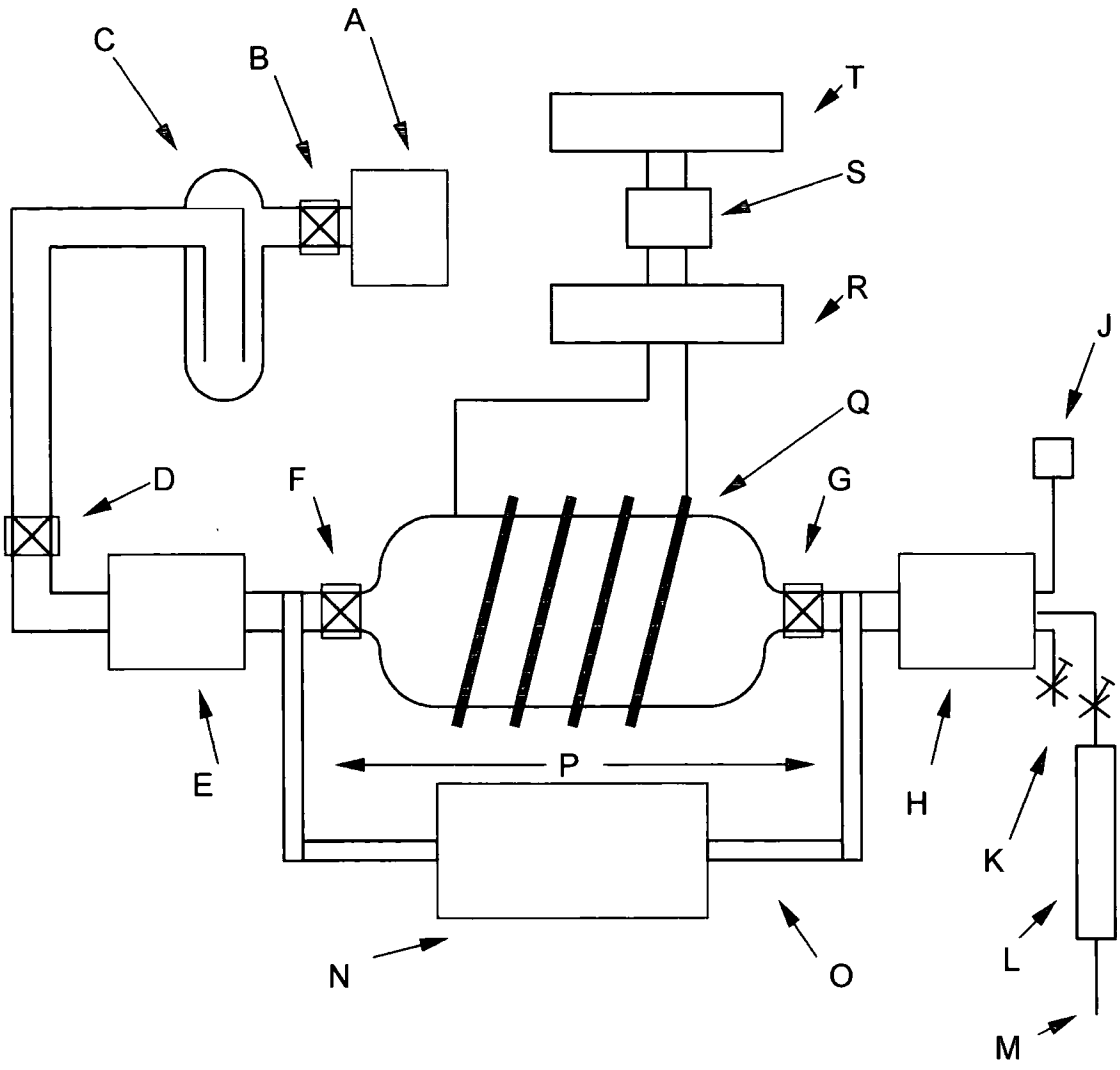

Figure 2.1: Schematic of rotating plasma reactor for treating powder samples; A, rotary pump, B, Young's tap, C, cold trap, D, Young's tap, E, rotary seal unit, F, Young's tap, G, Young's tap, H, rotary seal unit, J, Pirani vacuum gauge, K, air feed via leak valve, L, 3A molecular sieve column, M, oxygen gas feed via leak valve, N, stepper motor, O, drive shaft, P, drive belts, Q, copper coils, R, matching unit, S, SWR meter and T, rf generator.

Inductively coupled plasma mass spectrometry (ICP-MS) was used to quantify the total chromium content of the activated catalysts. The activated catalysts were digested in a hydrofluoric acid (48%) / nitric acid (70%) mixture (4:1) at 413 K for 48 h. Hydrofluoric acid and silicon tetrafluoride were then removed by evaporation, and the resultant solid dissolved in nitric acid before dilution in water. Analysis was then performed using a Perkin Elmer SCIEX Elan 6000 ICP-MS, after calibration with standard solutions.

UV/vis diffuse reflectance was performed on a PYE UNICAM SP8-150 UV/vis spectrophotometer fitted with an integrating spheroid accessory. Spectra were obtained using a 2 nm bandwidth and a scan speed of 1 nm s^{-1}. The output was collected on a chart recorder and then manually digitised.

Carbon monoxide reduction isotherms of the activated catalyst were collected in the microreactor. After thermal activation the catalysts were cooled in the microreactor under nitrogen to 623 K. Plasma activated catalysts were transferred under N_2 from the plasma reactor to a clean quartz reactor (pre-baked *in situ* at 473 K under N_2), and then heated at 1 K min^{-1} under flowing N_2 to 623 K using a Eurotherm temperature controller. Carbon monoxide (BOC 99.9%, dried as before) reduction was then performed using a flow rate of 6.0 dm^3 h^{-1}. The amount of CO_2 produced was quantified by integration of the mass 44 intensity measured using quadrupole mass spectrometry.

Quantification of the total hydroxyl population on the support was obtained using solid state ^1H NMR performed on a Varian Unity Plus 300 MHz spectrometer. Activated catalysts were transferred into 5 mm o.d. silicon nitride rotors with push-on caps in a nitrogen atmosphere glove box. Static solid echo NMR experiments,[19] acquired 32 transients using a 90° pulse - 15 μs delay - 90° pulse, 5 s recycle delay, and a 1000 kHz spectral width. The background signal of the rotor was removed from each set of data. The measured integral between 100 and -100 kHz was divided by the weight of silica to yield the number of protons per unit mass, subsequently referred to as the "*Proton Number*". ^1H magic angle spinning NMR experiments were used to compare the proportion of isolated and hydrogen bonded hydroxyls. 32 transients were acquired using a 90° pulse, 5 s recycle delay, 100 kHz spectral width, and a magic angle spinning speed of 4-8 kHz. Again, the background signal of the empty rotor was subtracted from each spectrum. The hydroxyl distribution was obtained by deconvolving the spectra into isolated and hydrogen bonded hydroxyl environments at 1.7 and 3.0 ppm respectively.[20,21,22]

A slurry polymerisation reactor was used to test catalyst activities. A 2.5 litre stainless steel reactor fitted with a system of mechanical agitation was first heated to 90 °C using a water filled heating jacket. 1.2 litres of degassed solvent (a C6 alkane cut comprised principally of hexane) were introduced into the reactor before 2 g of silica coated with triethlyaluminium at a level of 1 mmol g^{-1} were added as a poison scavenger. The reactor contents were then

agitated at 300 rpm for several minutes before 0.12-0.18 g of catalyst was introduced. Hydrogen (1 bar gauge) was then introduced to the reactor and finally 7 bar of ethylene. Ethylene was automatically fed to maintain a constant reactor pressure during polymerisation. The reaction was terminated by cooling the reactor to ambient temperature, venting off the ethylene and purging with nitrogen. Polymerisation products were then removed from the reactor, dried, and their properties investigated using high load melt index (HLMI) and gel permeation chromatography (GPC).

2.3 Results

2.3.1 Polymerisation Data

Polymerisation activities of all the catalysts showed a typical Phillips catalyst profile, Figure 2.2. The activity of the catalysts decreased in the order: thermal > thermal + plasma > plasma + thermal > plasma, with the thermally activated catalyst showing little induction time before the onset of polymerisation. The maximum production of polymer during polymerisation was limited to 300 g to prevent reactor fowling. Therefore the final activity of the thermally activated catalyst is probably greater than that measured. The properties of each of the resulting polymers are summarised in Table 2.1. The high molecular weight of the polymers in this study can be attributed to the relatively low polymerisation temperature employed.[3] A narrower molecular weight distribution was obtained for each of the polymers produced using a combined catalyst activation compared with that produced when solely thermal calcined.

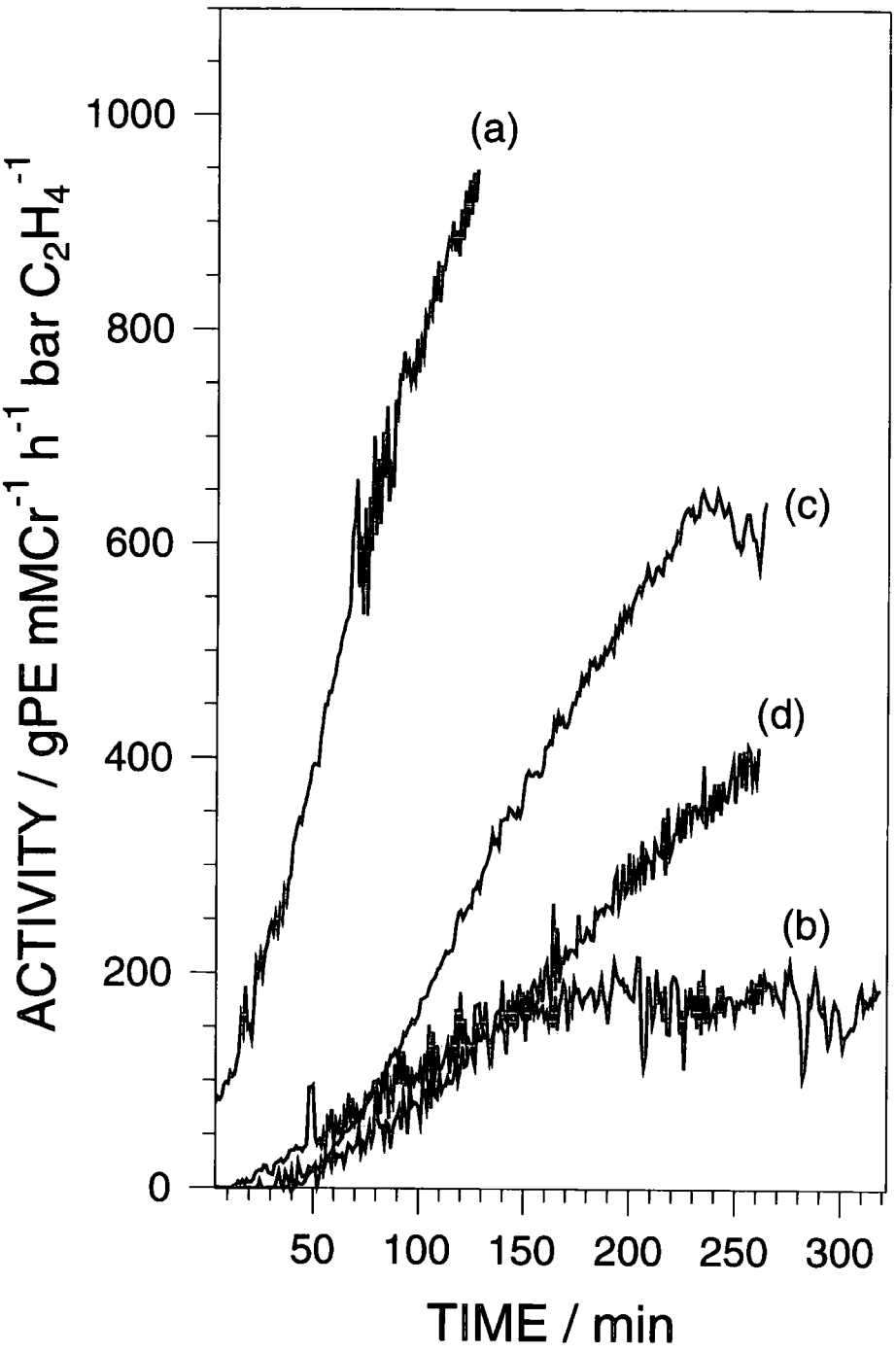

Figure 2.2: Polymerisation activity of catalyst activated: (a) thermally; (b) plasma; (c) thermal then plasma; and (d) plasma then thermal.

Activation conditions	High load melt index	GPC data x 10^3			
		M_n	M_w	M_{pk}	M_w/M_n
Thermal	0.29	24	564	244	24
Plasma	0.43	22	445	236	20
Thermal then plasma	0.21	29	376	253	13
Plasma then thermal	0.27	27	351	242	13

Table 2.1: Melt index and GPC analysis of the polymers.

2.3.2 Catalyst Analysis

Temperature programmed activation of the catalyst precursor showed a typical sharp peak due to the loss of physisorbed water at approximately 350 K,[23] and a broad peak due to silanol condensation at higher temperatures (≈ 720 K), Figure 2.3.[6,24] Acetate decomposition at ≈ 560 K produced water, carbon monoxide and carbon dioxide.[23] No peaks associated with acetate decomposition were observed after plasma activation, only the broad silanol condensation feature, Figure 2.4. This verified that plasma activation results in the total breakdown of the supported Cr(acetate) precursor.[14]

Optical emission spectroscopy (OES) was used to monitor the evolution of different species during plasma activation. Following an initial rise, there was a rapid reduction in the amount of hydrogen and carbon monoxide, with a corresponding rise in the intensity of atomic oxygen during activation, Figure 2.5. This is consistent with the oxidation of acetate groups by excited oxygen species generated in the plasma and the loss of hydroxyls from the silica support.[14] During subsequent plasma activation of a previously thermally activated catalyst, only atomic oxygen was detected, indicating that no further species were evolved from the catalyst, Figure 2.6.

Inductively coupled plasma mass spectrometry showed that all of the catalysts had the same chromium loading after activation, Table 2.2.

Prior to activation, the UV/vis diffuse reflectance spectrum showed strong absorbance features associated with the chromium acetate precursor at 420 and 600 nm,[10] Figure 2.7. After all activations the chromium was observed

as a chromate Cr(VI) species, which is characterised by an absorbance maximum at 470 nm.[25,26]

The chromium oxidation state was further investigated using carbon monoxide reduction which is reported to quantitatively reduce Cr(VI) to Cr(II) centres with 98% efficiency.[27] Both thermal and thermal then plasma activated catalysts generated the same quantity of CO_2, Table 2.2. However a reduction of 17% in the amount of CO_2 evolved was found for plasma and plasma then thermally activated catalysts.

The total hydroxyl population and relative distribution of hydrogen bonded and isolated hydroxyls on the silica support was measured using solid state ^1H NMR. After each activation sequence involving a high temperature thermal calcination, the resulting total hydroxyl population was very low, and comprised isolated hydroxyls (at 1.7 ppm),[20,21,22] Table 2.3 and Figure 2.8. This is consistent with high temperature activation of silica, where extensive silanol condensation of hydroxyls occurs.[6] However, after plasma activation, a total hydroxyl population 800% greater than the thermally calcined catalyst remained. The distribution also differed, and contained both hydrogen bonded and isolated hydroxyls (at 3.0 and 1.7 ppm respectively).

Activation	Cr / wt.%	CO_2 area
Thermal	0.84 ± 0.02	109 ± 3
Plasma	0.87 ± 0.02	91 ± 3
Thermal then Plasma	0.87 ± 0.02	108 ± 2
Plasma then Thermal	0.85 ± 0.02	91 ± 4

Table 2.2: Chromium elemental analysis and CO reduction areas.

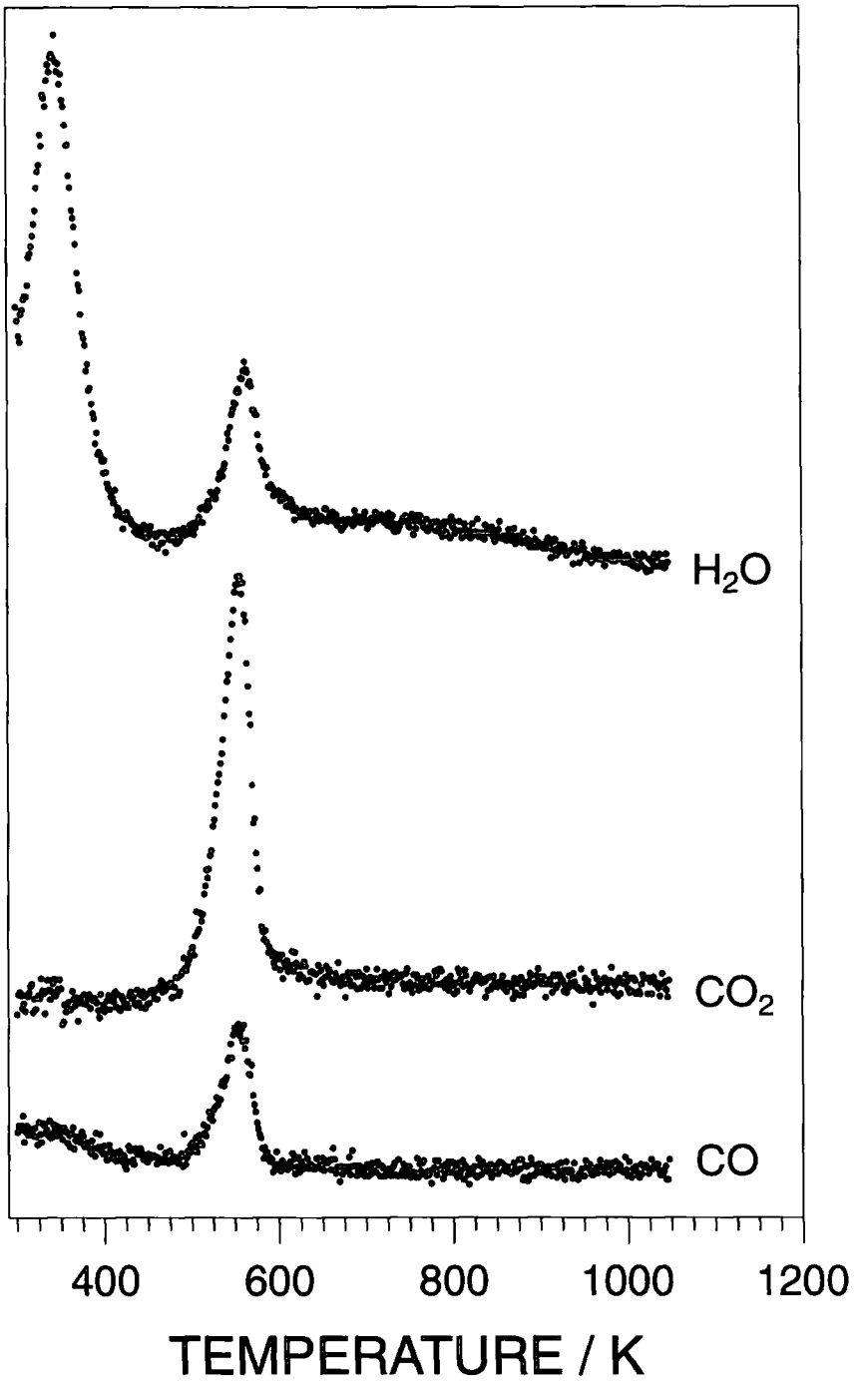

Figure 2.3: Temperature programmed activation profiles for the catalyst precursor under flowing oxygen.

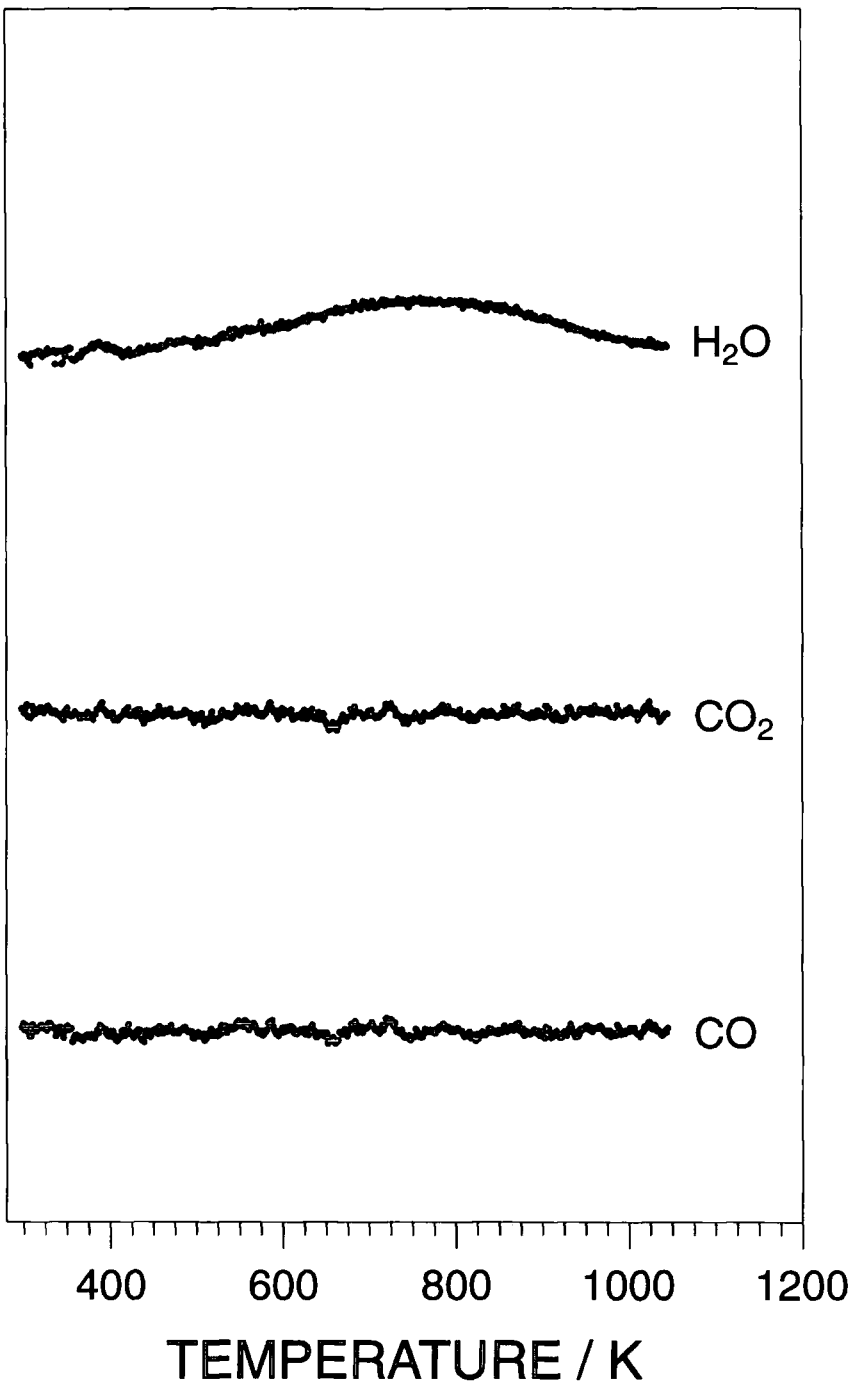

Figure 2.4: Temperature programmed activation profiles for the plasma activated catalyst under flowing oxygen.

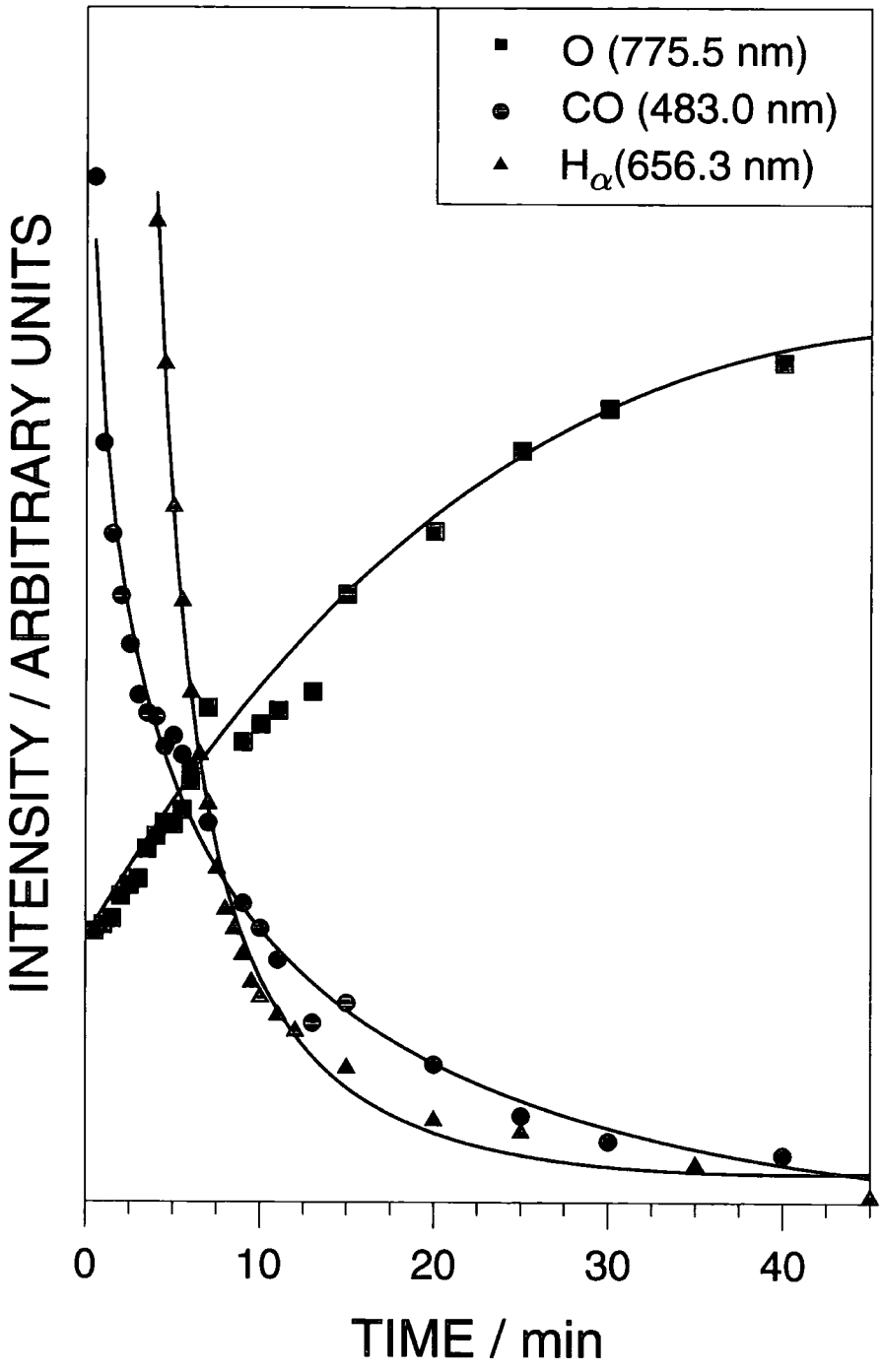

Figure 2.5: Time dependence of H_α (656.3 nm), CO (483.0 nm $B^1\Sigma$-$A^1\Pi$) and O (775.5 nm $3s^5S$-$3p^5P$) intensity during plasma activation of the catalyst precursor.

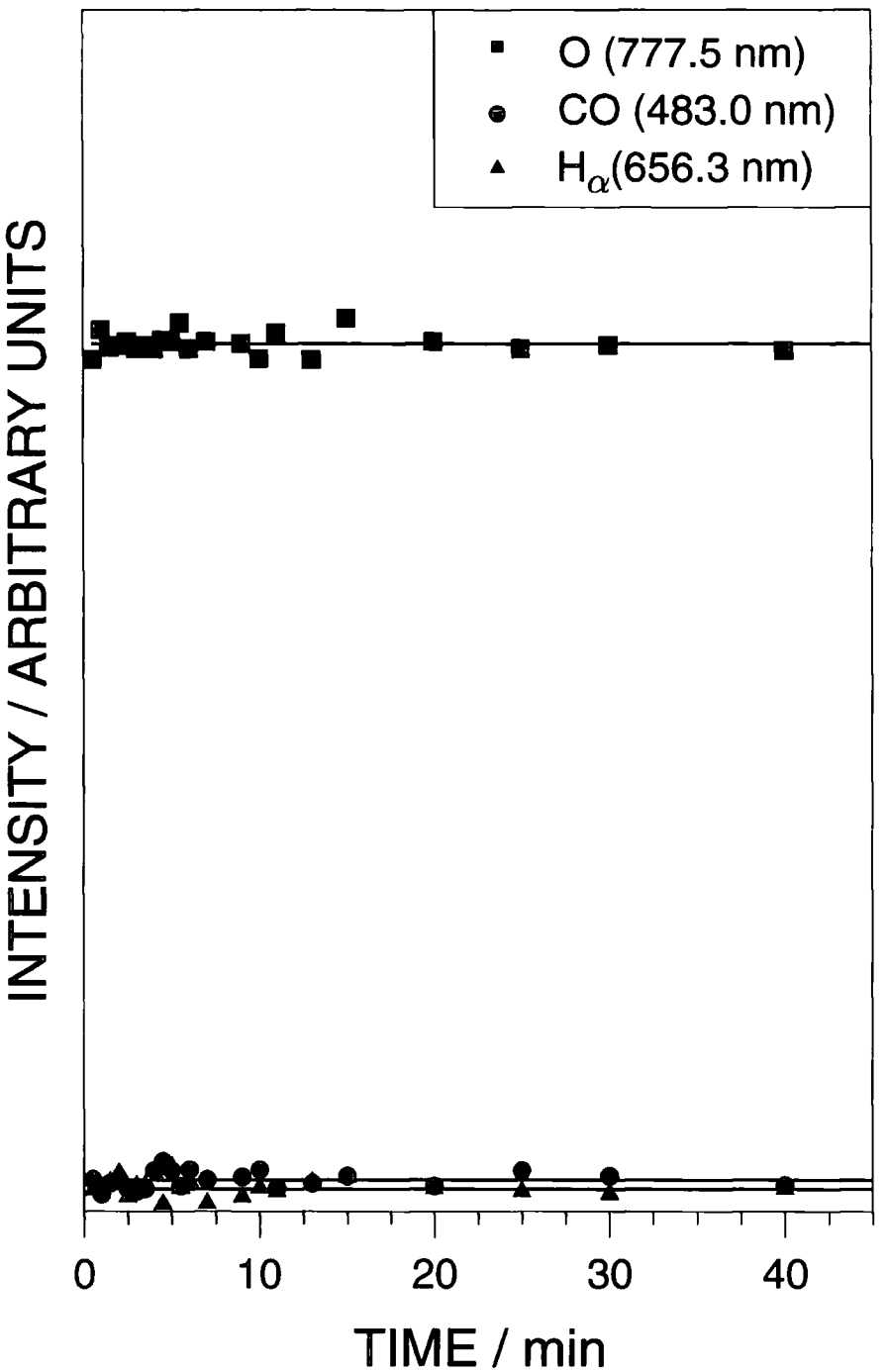

Figure 2.6: Time dependence of H_α (656.3 nm), CO (483.0 nm $B^1\Sigma$-$A^1\Pi$) and O (775.5 nm $3s^5S$-$3p^5P$) intensity during plasma activation of thermally calcined catalyst.

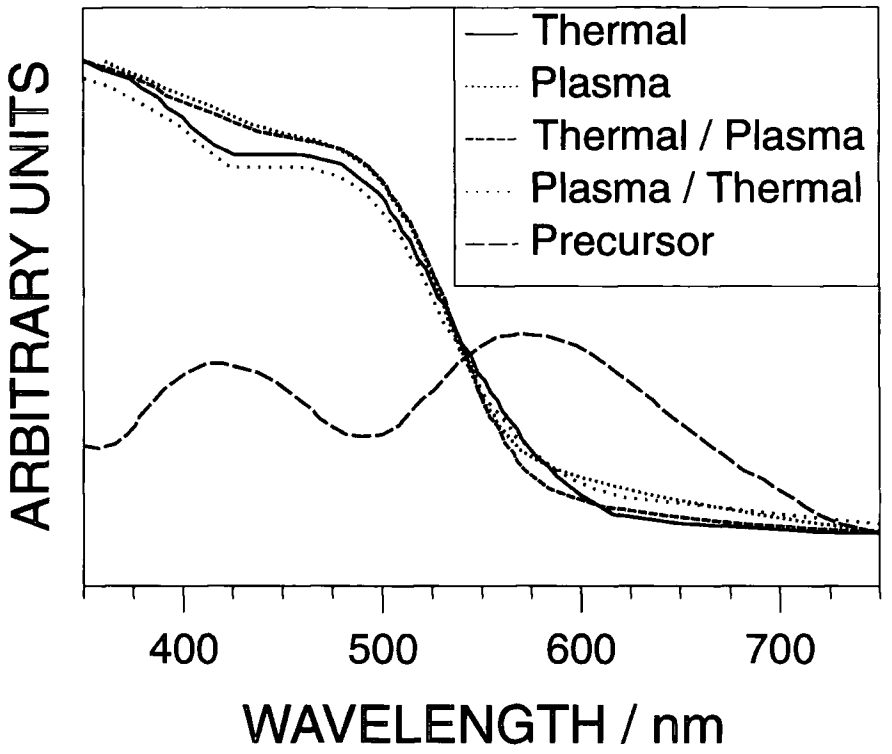

Figure 2.7: UV/vis diffuse reflectance spectra of the catalysts.

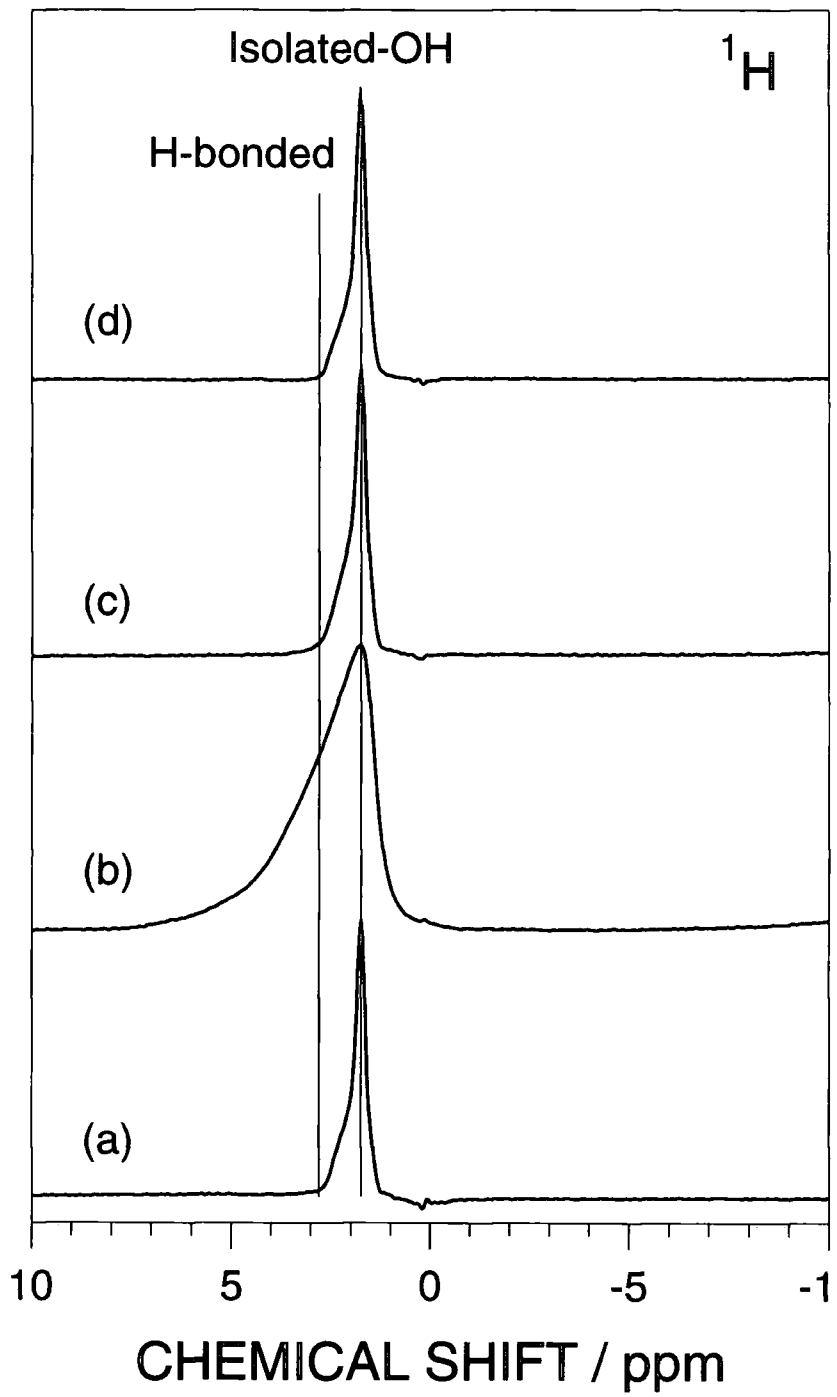

Figure 2.8: 299.945 MHz ^{1}H MAS NMR spectra (90° pulse, 5 s relaxation decay) of catalyst activated: (a) thermally; (b) plasma; (c) thermal then plasma; and (d) plasma then thermal.

Activation	"Proton Number"	Percentage	
		Hydrogen bonded	Isolated
Thermal	0.03 ± 0.01	2 ± 2	98 ± 2
Plasma	0.28 ± 0.02	62 ± 3	38 ± 3
Thermal then plasma	0.03 ± 0.01	3 ± 3	97 ± 3
Plasma then thermal	0.03 ± 0.01	2 ± 2	98 ± 2

Table 2.3: Solid state ^{1}H NMR data for the activated catalysts.

2.4 Discussion

2.4.1 Thermal Versus Plasma Activation

In the present study, the thermally activated catalyst is characterised by a low total hydroxyl population comprised of isolated hydroxyls, and with chromium present as a chromate, which is consistent with previous studies.[10,23] The activity of the catalyst was comparable with other studies, and produced a high molecular weight polymer with a broad MWD.[3,28]

The excitation of oxygen to the plasma state can enhance its chemical reactivity. Application of an electric field causes free electrons to gain energy, which is subsequently lost via electron-neutral or electron-ion collisions.[29] A wide range of reactants are generated by these processes, including neutral ground-state (e.g., O, O_2, O_3), metastables species (e.g., $O_2(a^1\Delta_g)$) and positively charged (e.g., O^+, O_2^+, O_3^+, O_4^+) and negatively charged ions (e.g., O^-, O_2^-, O_3^-, O_4^-) alongside electrons and electromagnetic radiation.[30,31] Atomic oxygen is the predominant reactive species.[31]

It can be calculated using the perfect gas equation that at the operating plasma pressure of 0.3 mbar, on average, there will be less than one atom/molecule within each pore.[32] The support pores are much smaller in size (between 2 and 50 nm) than the plasma Debye length (2 μm < λ_D < 7 mm).[33] Therefore plasma ignition within the pores is unlikely. Penetration of excited plasma species (electrons, ions and metastables) together with electromagnetic radiation are more probable causes of chemical modification

within the pores. The negative charge associated with the plasma sheath region adjacent to a particle surface will cause incident electrons to be retarded as they approach the catalyst surface;[29] hence electron bombardment is unlikely to be important. Ion and short-lived metastables will predominantly interact with the near surface region due to rapid loss of kinetic energy during collisions with pore walls.[34,35] This leaves long-lived neutrals and photochemistry able to initiate chemical reactions within the pores. Some atomic oxygen species can be expected to penetrate into the particle,[36] although atomic oxygen will undergo surface recombination processes:[37,38]

$$O + O\ (surface) \rightarrow O_2$$

Direct photo-excitation of molecular oxygen within the pores is an alternative source of atomic species. Plasma UV radiation in the 240-250 nm range (O_2 $A^3\Sigma^+_u$ - $X^3\Pi^-_g$ transition)[17] is longer in wavelength compared to the silica absorption threshold at 160 nm,[39] and therefore will penetrate throughout the particle to produce excited and ground state atomic oxygen within the pores:

$$O_2(X^3\Sigma_g^-) \rightarrow O_2(X^3\Sigma_u^+) \qquad 250 < \lambda < 300\ nm$$

$$O_2(X^3\Sigma_g^-) \rightarrow O(^3P) + O(^3P) \qquad \lambda < 242\ nm$$

Plasma activation was observed to completely oxidise the Cr(acetate) precursor, confirming the penetration of excited oxygen (in the presence of UV radiation) throughout the catalyst particles.[14]

The observed reduction in CO_2 evolution after O_2 plasma treatment could be due to the presence of some chromia (Cr_2O_3) after activation or a dispersion of Cr(VI) which can only be subsequently reduced to Cr(III).[25] The presence of chromia after activation can be eliminated as 17% Cr_2O_3 on the catalyst would produce a feature at 600 nm in the UV/vis spectra, Figure 2.7. A more likely explanation therefore is that after plasma activation all chromium is present as Cr(VI), but dispersed differently to the thermally activated catalyst. Chromium oxide conglomerates can only be reduced to Cr(III),[25] hence accounting for the reduction in carbon dioxide evolution. It can therefore be assumed that after plasma activation, Cr(VI) clusters are present on the surface.

In summary, plasma activation causes the total decomposition of the Cr(acetate) precursor throughout the support, but produces a catalyst with a high hydroxyl population (equivalent to only a 373 K thermal treatment[40]) composed of isolated and hydrogen bonded hydroxyls and a low chromium

dispersion. The observed low activity of the plasma activated catalyst is therefore explained by the large hydroxyl population and low chromium dispersion.[11,12,13]

2.4.2 Thermal Versus Combined Activations

All catalyst activations involving a high temperature treatment, have supports with an equally low hydroxyl population. If hydroxyl interference with active sites was the major factor contributing to a low activity after plasma activation, a combined treatment would be expected to raise polymerisation activity to that of a thermally calcined catalyst.

Thermal treatment followed by plasma activation produced catalysts with the same characteristics as that obtained after high temperature calcination, i.e. a low hydroxyl population and dispersed Cr(VI) centres. In contrast, the catalyst that was plasma treated then thermally calcined had a lower chromium dispersion. Both combined activations produced catalysts with lower activities than that obtained after thermal calcination, the catalyst with decreased chromium dispersion having the lower activity. This suggests that plasma treatment interferes with some chromium sites, preventing them from becoming active on contacting with ethylene. The loss of active sites appears to be specific, as the polymer produced using either combined treatments had a narrower MWD. The cause of the catalyst deactivation and resulting change in MWD is not clear at a molecular level, but cannot be attributed to oxygen poisoning of the catalyst during activation. Although this would reduce the activity of the catalyst, it would also broaden the MWD.[41,42,43]

2.5 Conclusions

Plasma activation of the Phillips Cr(acetate)/SiO_2 precursor produces a catalyst which is characterised by a high hydroxyl population and a low chromium dispersion. These characteristics cause the resulting catalyst to have a low polymerisation activity.

Using combined thermal and plasma treatments has the advantage of reducing the hydroxyl population, and hence increasing the polymerisation

activity compared to solely plasma activated catalysts. The polymers have a reduced MWD in comparison to those produced using a catalyst which has been solely thermally activated.

2.6 References

[1] J.P. Hogan and R.L. Banks, U.S. Patent 2,825,721, 1958.

[2] M.P. McDaniel, *Ind. Eng. Chem. Res.*, **1988**, *27*, 1559.

[3] M.P. McDaniel, *Adv. Catal.*, **1985**, *33*, 47.

[4] A. Clark, *Catal. Rev.*, **1969**, *3*, 145.

[5] B. Fubini, G. Ghiotti, L. Stradella, E. Garrone and C. Morterra, *J. Catal.*, **1980**, *66*, 200.

[6] R.K. Iler, *Chemistry of Silica*, John Wiley and Sons, New York, 1979, Chapter 6.

[7] C.E. Marsden. *Plast., Rubber Comps. Process. Appl.*, **1994**, *21*, 193.

[8] L.M. Baker and W.L. Carrick, *J. Org. Chem.*, **1968**, *33*, 616.

[9] V.J. Ruddick and J.P.S. Badyal, *Langmuir*, **1997**, *13*, 469.

[10] M.P. McDaniel, *J. Catal.*, **1982**, *76*, 37.

[11] M. Nishimura and T.M. Thomas, *Catal. Letts.*, **1993**, *21*, 149.

[12] D.L. Myers and J.H. Lunsford, *J. Catal.*, **1985**, *92*, 260.

[13] M.P. McDaniel and M.B. Welch, *J. Catal.*, **1983**, *82*, 98.

[14] V.J. Ruddick and J.P.S. Badyal, *J. Phys. Chem., B*, **1997**, *101*, 9240.

[15] B. Horvath, U.S. Patent 3,485,771, 1966.

[16] C.D. Ehrlich and J.A. Basford, *J. Vac. Sci. Technol., A*, **1992**, *10*, 1.

[17] R.W.B. Pearse and A.G. Gaydon, *The Identification of Molecular Spectra*, 4th ed., John Wiley and Sons, New York, 1976.

[18] R. d'Agostino, F. Cramarossa, F. Fracassi and F. Illuzzi. In *Plasma Deposition, Treatment, and Etching of Polymers*, R. d'Agostino, Ed., Academic Press, San Diego, 1990, Chapter 2.

[19] P. Mansfield, *Phys. Rev. A: At., Mol., Opt. Phys.*, **1965**, *137*, 961.

[20] C.E. Bronnimann, R.C. Ziegler and G.E. Maciel, *J. Am. Chem. Soc.*, **1988**, *110*, 2023.

[21] S. Haukka, E.L. Lakomaa and A. Root, *J. Phys. Chem.*, **1993**, *97*, 5085.

[22] C.H.C. Liu and G.E. Maciel, *J. Am. Chem. Soc.*, **1996**, *118*, 5103.

[23] V.J. Ruddick, P.W. Dyer, G. Bell, V.C. Gibson and J.P.S. Badyal, *J. Phys. Chem.*, **1996**, *100*, 11062.

[24] J.P. Gallas, J.C. Lavalley, A. Burneau and O. Barres, *Langmuir*, **1991**, *7*, 1235.

[25] C. Groeneveld, P.P.M.M. Wittgen, A.M. van Kesbergen, P.L.M. Miestron, C.E. Nuijten and G.C.A. Schuit, *J. Catal.*, **1979**, *59*, 153.

[26] M.P. McDaniel, *J. Catal.*, **1982**, *76*, 17.

[27] H.-L. Krauss and H. Stach, *Inorg. Nucl. Chem. Lett.*, **1968**, *4*, 393.

[28] M.P. McDaniel, C.H. Leigh and S.M. Wharry, *J. Catal.*, **1989**, *120*, 170.

[29] B.N. Chapman, *Glow Discharge Processes*, John Wiley and Sons, New York, 1980.

[30] Y. Ichikawa, R.L.C. Wu and T. Kanede, *J Appl. Phys.*, **1990**, *67*, 108.

[31] M. Shibata, M. Nakana and T. Makabe, *J. Appl. Phys.*, **1995**, *77*, 6181.

[32] P.W. Atkins, *Physical Chemistry*, 4th ed., Oxford University Press, Oxford, 1990, Chapter 1.

[33] A. Grill, *Cold Plasmas in Materials Technology*, IEEE press, New Jersey, 1994.

[34] T. Yasuda, T. Okuno, M. Miyama and H. Yasuda, *J. Polym. Sci., Polym. Chem. Ed.*, **1994**, *32*, 1829.

[35] E.V. Karoulina and Y.A. Lebedev, *J. Phys. D: Appl. Phys.*, **1992**, *25*, 401.

[36] S.L. Koontz, U.S. Patent 5,798,261, 1998.

[37] M. Shibata, N. Nakano and T. Makabe, *J. Appl. Phys.*, **1995**, 77, 6181.

[38] G.A. Melin and R.J. Maddix, *Trans. Faraday Soc.*, **1971**, *67*, 198.

[39] A. Hollander, J.E. Klemberg-Sapieha and M.R. Wertheimer, *J. Polym. Sci., Polym. Chem. Ed.*, **1995**, *33*, 2013.

[40] S.P. Godfey, Ph.D. Thesis, Durham University, England, 1999, Chapter 3.

[41] H.W. Mayhew, R.J. French and L.J. Rekers, U.S. Patent 4,540,755, 1985.

[42] R.L. Batchelor and G.E. Kellam, U.S. Patent 5,473,072, 1995.

[43] M.P. DcDaniel and S.J. Martin, *J. Phys. Chem.*, **1991**, *95*, 3289.

CHAPTER 3

PLASMA DEHYDROXYLATION OF HIGH SURFACE AREA SILICA

3.1 Introduction

High surface area silica powders find a wide range of applications (e.g. as desiccants, additives in paints, inks, pharmaceuticals, and cosmetics).[1] Control of the silica surface hydroxyl density can have a profound impact upon performance, e.g. in catalysis and chromatography.[1] Prior to any treatment, the surface contains a large hydroxyl population[1] together with physisorbed water.[2] Traditionally, thermal and chemical methods have been predominantly employed for changing the surface chemistry of silica. In the former case, heating to approximately 473 K causes loss of physisorbed water; whilst higher temperatures are necessary for silanols (Si-OH) to undergo condensation to form siloxanes (Si-O-Si), Scheme 3.1.[3]

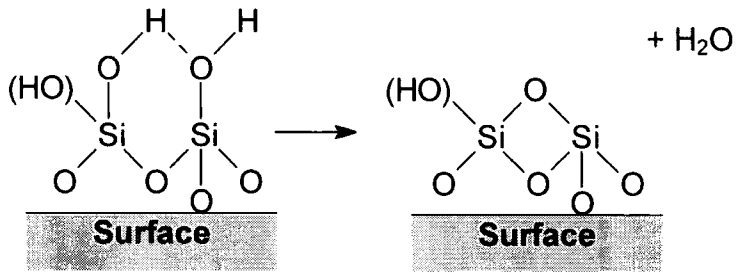

Scheme 3.1: Silanol condensation mechanism[3] (the reaction may be considered with or without the geminal hydroxyls in parenthesis).

Above 1100 K,[1] there is total loss of surface hydroxyls, however this is accompanied by sintering[4] and loss of surface area. On the other hand, wet chemical modification of silica surfaces typically comprises reaction of hydroxyls with silanes,[1] e.g. hexamethyldisilazane converts hydroxyls to siloxanes according to the following reaction:

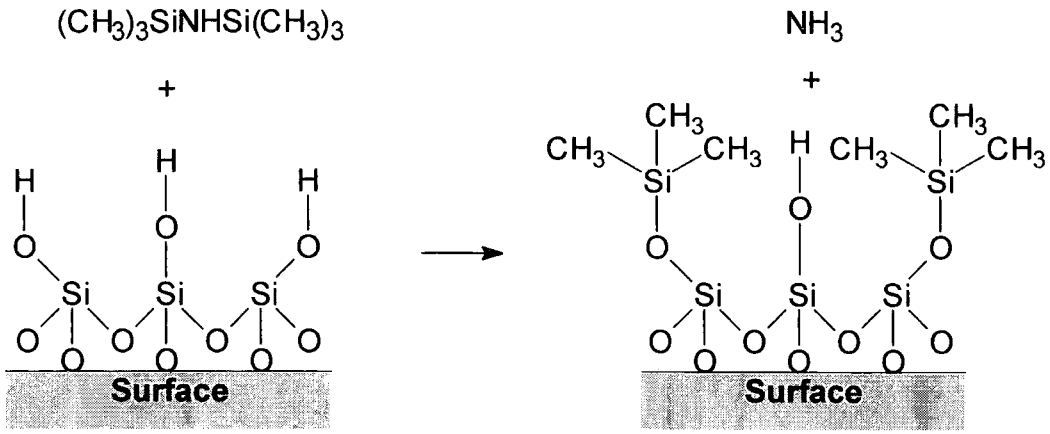

Scheme 3.2: Silane reaction.

However the complete elimination of hydroxyls is impracticable due to the steric hindrance of trimethylsilyl groups blocking accessibility to neighbouring surface hydroxyls.[5]

In order to overcome the drawbacks associated with conventional methods (large energy input, long treatment times, chemical waste, etc.) an alternative approach has been investigated using low temperature ("cold") plasmas. Such partially ionised electrical discharges consist of ions, electrons, neutrals, and electromagnetic radiation, where the electron temperature ($T_e \approx$ 10,000 K) is much greater than the bulk gas temperature ($T_g \approx$ 300 K).[6] Therefore, although the overall temperature of the system is close to ambient, the electrons possess sufficient energy to cause rupture and excitation of chemical bonds. It is this attribute which makes non-equilibrium plasmas so attractive for material processing. Current areas of application include: aerospace, automotives, microelectronics, optical coatings, packaging, lighting, and waste destruction.[7] For instance, plasma treatment of planar non-porous silica surfaces (where plasma penetration into the subsurface is not an issue) is well established:[8] oxygen plasmas can efficiently remove surface hydroxyls, whilst water plasmas are able to promote rehydroxylation. However, the use of non-isothermal electrical discharges to dehydroxylate the internal pores of high surface area silica particles has not been previously demonstrated.

3.2 Experimental

For comparison, conventional thermal dehydroxylation of silica was carried out in a nitrogen atmosphere (BOC 99.998%, dried through activated 3A molecular sieve (Aldrich) to give less than 1.0 ppm_v H_2O) at a flow rate of 3.0 dm^3 h^{-1}. Typically, 1 g of silica (EP10X, Crosfield Ltd, particle size $\approx$ 100 μm) was loaded into a quartz microreactor and heated at 1 K min^{-1} to temperatures between 373-1073 K using a Eurotherm controller. The temperature was then kept constant for 5 h, prior to cooling at 5 K min^{-1} back to 298 K. The composition of gases leaving the furnace was sampled in real time via a heated fine capillary tube connected to a computer controlled Vacuum Generators SX 200 quadrupole mass spectrometer.

An inductively coupled 13.56 MHz rotating plasma reactor, described earlier in Chapter 2, was used to treat the powdered silica. Prior to each experiment, the reactor was cleaned with detergent, rinsed with isopropyl alcohol, dried in an oven, and then cleaned *in situ* using a 0.3 mbar air plasma at 30 W. 1 g of silica was then loaded into the reactor and evacuated down to base pressure. At this stage, the silica was effectively vacuum dry. Argon (BOC 99.998%), helium (BOC 99.999%), oxygen (Air Products 99.995%), or carbon tetrafluoride gas (Air Products 99.7%) were then introduced into the plasma chamber via a fine leak valve. Rotation of the reactor then commenced and the glow discharge was ignited. Upon completion of plasma treatment, agitation of the particles was stopped, the rf power supply was switched off, and the chamber evacuated back to its original base pressure, prior to bringing up to an atmosphere of nitrogen. Each sample was then stored in a dry nitrogen atmosphere (H_2O < 1.0 ppm_v), awaiting analysis.

An Ocean Optics Inc. SD 1000 Fibre Optic Spectrometer was used for real time optical emission spectroscopy (OES) diagnostics of the electrical discharge during dehydroxylation. In particular, the intensity of the hydrogen (H_α 656.3 nm)[9] emission line characteristic of water loss was tracked.

Quantification of the proton signal intensity was obtained using solid state ^1H NMR performed on a Varian Unity Plus 300 MHz spectrometer. Silica samples were transferred into 5 mm o.d. silicon nitride rotors with push-on caps in a nitrogen atmosphere glove box. Static solid echo NMR experiments,[10] acquired 32 transients using a 90° pulse - 15 μs delay - 90° pulse, 5 s recycle

delay, and a 1000 kHz spectral width. The background signal of the rotor was removed from each set of data. The measured integral between 100 and -100 kHz was divided by the weight of silica in the sample rotor to yield the number of protons per unit mass, subsequently referred to as the "*Proton Number*". ^{1}H magic angle spinning NMR experiments were used to compare the proportion of isolated and hydrogen bonded hydroxyls. 32 transients were acquired using a 90° pulse, 5 s recycle delay, 100 kHz spectral width, and a magic angle spinning speed of 4-8 kHz. Again, the background signal of the empty rotor was subtracted from each spectrum. The hydroxyl distribution was then calculated by deconvolving the spectra into isolated and hydrogen bonded hydroxyl environments at 1.7 and 3.0 ppm respectively.[11,12,13]

Nitrogen gas sorption measurements at 77 K were carried out using a PMI sorptometer. 7 data points between $0.04 < p/p_o < 0.25$ were collected following *in situ* degassing of each silica sample at 473 K for 16 hours. The gradient of the BET graph over the selected p/p_o range was always found to be constant within experimental error.[14]

3.3 Results

3.3.1 Conventional Thermal Dehydroxylation

Temperature programmed desorption spectra of untreated silica display the loss of physisorbed water as a sharp peak at ≈ 350 K, and a broad water peak due to silanol condensation at higher temperatures (≈ 720 K),[2,15] Figure 3.1.

Static solid echo NMR experiments were used to follow the changes in the hydroxyl density at the silica surface during thermal dehydroxylation, Table 1. Also ^{1}H MAS NMR was used to compare the relative proportion of isolated versus hydrogen bonded hydroxyls. As-received silica exhibits a broad resonance around 3 ppm attributable to the overlap of physisorbed water (3.3 ppm), hydrogen bonded hydroxyls (3.0 ppm), and a small number of isolated hydroxyls (1.7 ppm),[11,12,13,16] Figure 3.2. Loss of physisorbed water at 373 K causes the main peak at 3.0 ppm to diminish at the expense of the 1.7 ppm component, (a small amount of physisorbed water remains at this temperature[2]). Peak deconvolution of the NMR spectra into hydrogen bonded and isolated hydroxyl chemical environments was carried out for samples

heated above 473 K (at which point all physisorbed water is lost[2]), Table 3.1, and Figure 3.3. Higher temperatures gave rise to the loss of hydrogen bonded and isolated silanols, until eventually only a small number of isolated hydroxyl groups are left behind at around 1073 K. In summary, raising the temperature reduces the hydroxyl density at the silica surface, whilst the relative proportion of isolated hydroxyls increases, Figure 3.3. This is in good agreement with related spectroscopic and chemical investigations.[1,17,18,19]

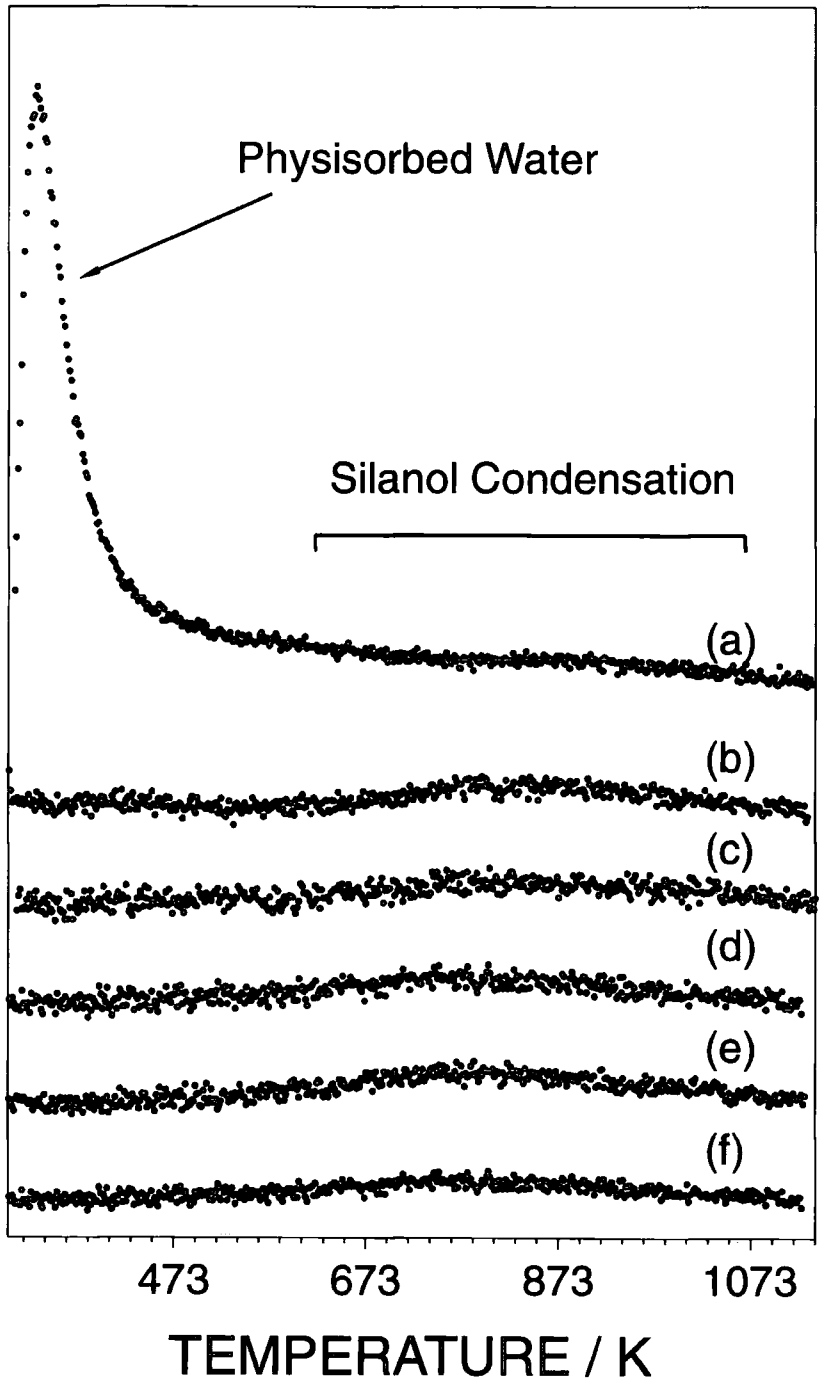

Figure 3.1: Temperature programmed desorption of silica: (a) no prior treatment; (b) vacuum dried; (c) argon plasma treated; (d) helium plasma treated; (e) oxygen plasma treated; and (f) carbon tetrafluoride plasma treated.

Silica treatment	"Proton Number"			Percentage		Ratio of hydrogen bonded to isolated hydroxyls
	Total	Hydrogen bonded	Isolated	Hydrogen bonded	Isolated	
Untreated [a]	0.75 ± 0.01	-	-	-	-	-
373 K [a]	0.29 ± 0.01	-	-	-	-	-
473 K	0.27 ± 0.01	0.20 ± 0.01	0.07 ± 0.01	74 ± 2	26 ± 2	2.9 ± 0.2
573 K	0.24 ± 0.01	0.15 ± 0.01	0.09 ± 0.01	61 ± 3	39 ± 3	1.6 ± 0.1
673 K	0.14 ± 0.01	0.15 ± 0.01	0.07 ± 0.01	49 ± 2	51 ± 2	0.96 ± 0.04
773 K	0.12 ± 0.01	0.07 ± 0.01	0.07 ± 0.01	40 ± 2	60 ± 2	0.67 ± 0.02
873 K	0.10 ± 0.01	0.05 ± 0.01	0.09 ± 0.01	12 ± 1	88 ± 1	0.14 ± 0.02
973 K	0.05 ± 0.01	0.01 ± 0.01	0.05 ± 0.01	2 ± 2	98 ± 2	0.02 ± 0.01
1073 K	0.04 ± 0.01	0.00 ± 0.01	0.04 ± 0.01	0 ± 1	100 ± 1	0.00 ± 0.01

[a] not deconvolved due to presence of physisorbed water.

Table 3.1: Solid state ^{1}H NMR data for thermally treated silica.

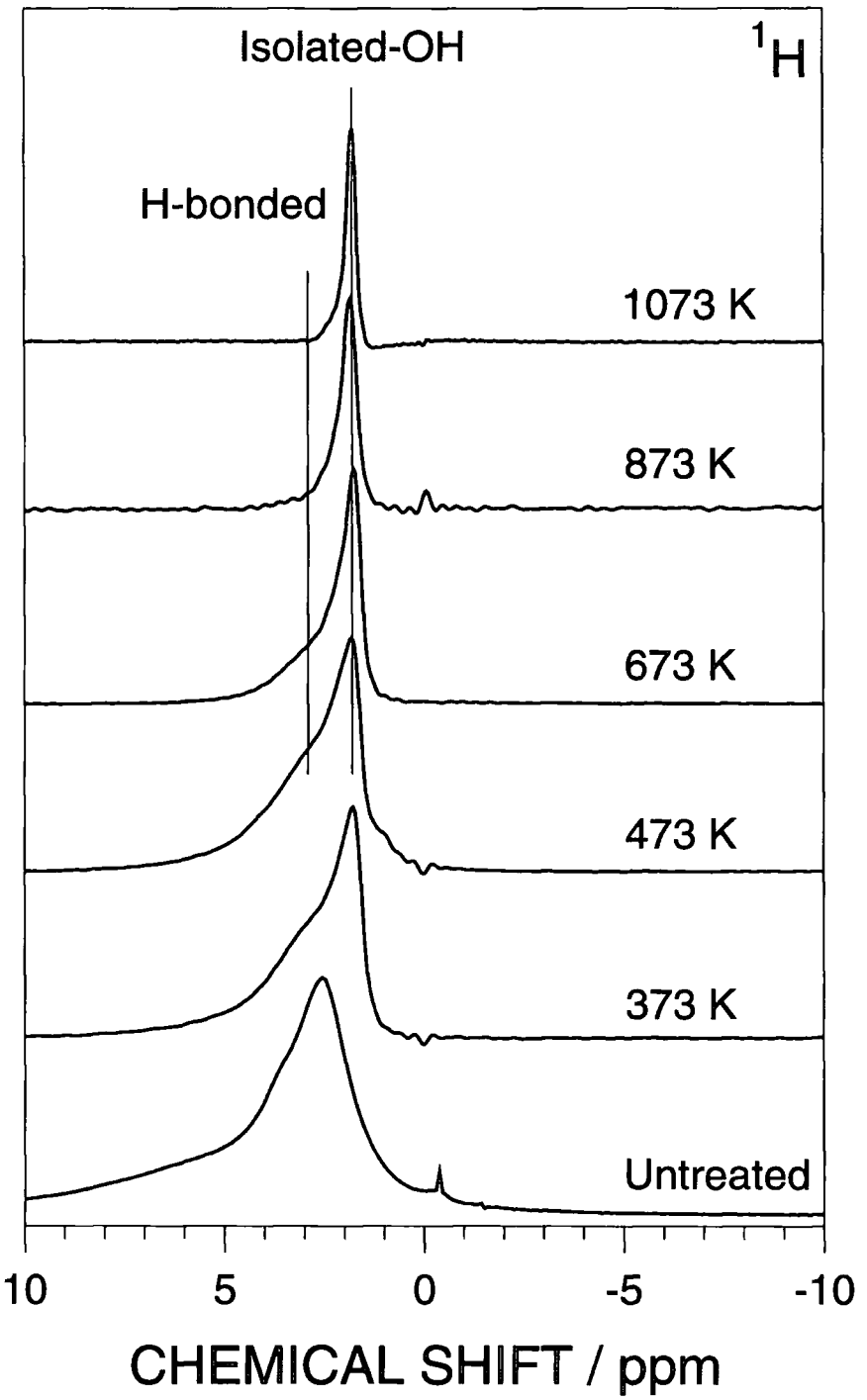

Figure 3.2: 299.945 MHz ^{1}H MAS NMR spectra (90° pulse, 5 s relaxation decay) of silica heated under nitrogen at different temperatures (all spectra have been normalised for intensity).

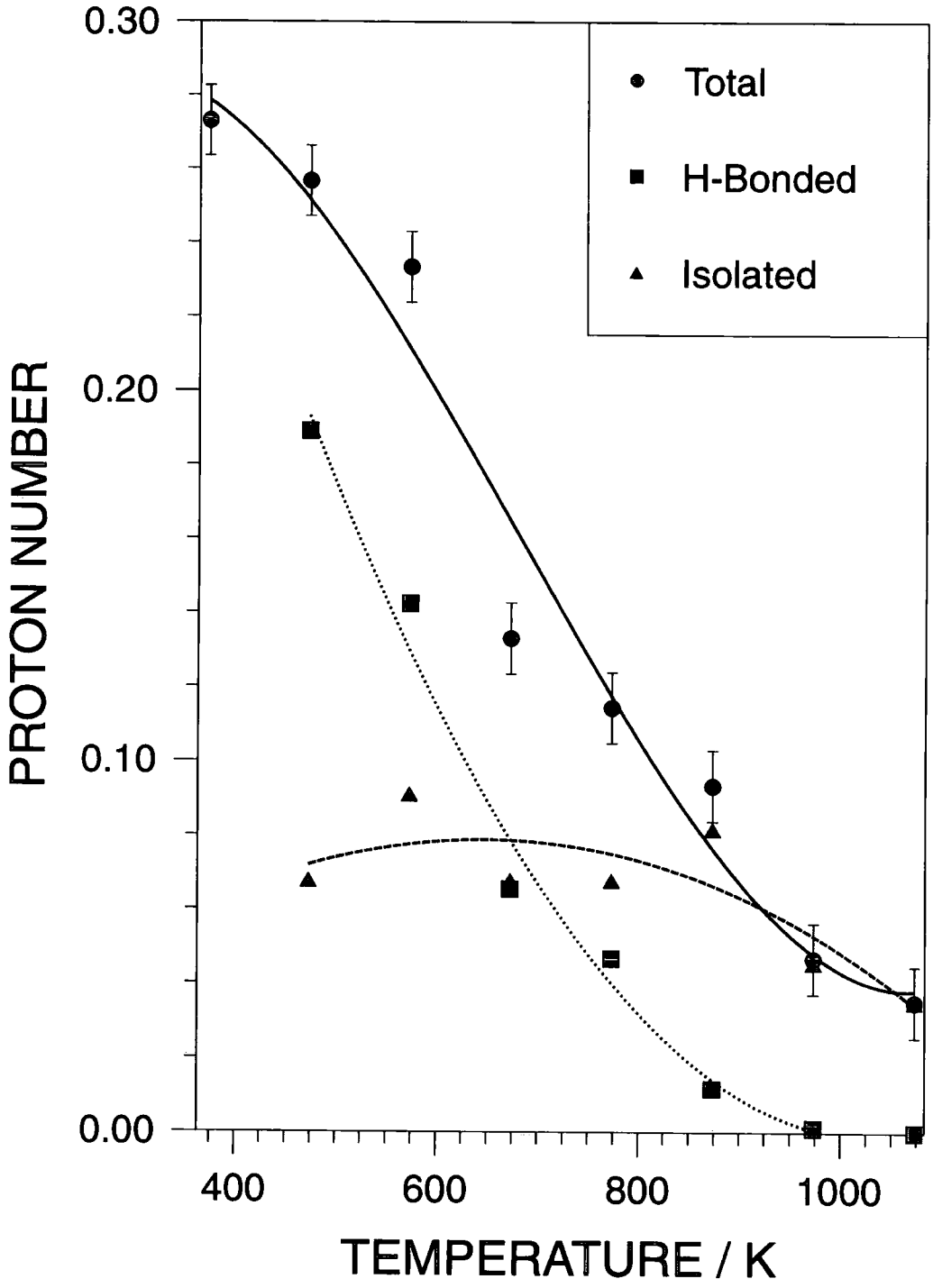

Figure 3.3: Effect of temperature upon hydroxyl distribution.

3.3.2 Plasma Dehydroxylation

Temperature programmed desorption showed that vacuum drying of silica removes physisorbed water, whereas the silanol condensation feature at higher temperatures is retained, Figure 3.1. Subsequent plasma treatment using various feed gases resulted in further dehydroxylation of the silica surface. This is evident from the observed attenuation of the high temperature TPD peak, and the rapid decline in intensity of the H_α 656.3 nm line observed by optical emission spectroscopy during plasma exposure, Figures 3.1 and 3.4 respectively.

Vacuum dried silica, and silica subjected to a variety of plasma treatments were also analysed by ^1H NMR, Table 3.2 and Figure 3.5. A 55% reduction in the total number of protons was found in the former case, i.e. the loss of physisorbed water without any disturbance of the surface hydroxyls.[20] Noble gas plasma treatment produced a small drop in the overall concentration of hydroxyl groups, whilst the relative proportion of isolated hydroxyls was slightly enhanced, Figure 3.6. Oxygen plasma treatment also resulted in surface dehydroxylation, but with a much greater loss of hydrogen bonded hydroxyls, accompanied by an increase in the absolute number of isolated hydroxyls. Carbon tetrafluoride plasmas were found to be the most effective at hydroxyl removal from the silica surface. In this case, the hydroxyl distribution was markedly different compared to the other plasma treatments: the ratio of hydrogen bonded to isolated hydroxyls remained similar to vacuum dried silica (although the concentrations were significantly less), Table 3.2.

Optimisation of the CF_4 glow discharge operating conditions was pursued using a 3-level-2-factor (power and pressure) experimental design, Table 3.3.[21] It was found that a combination of high power and pressure was the most effective at removing surface hydroxyls. Further improvement was achieved using Simplex optimisation.[22] CF_4 plasma treatment at 60 W power and 0.5 mbar pressure yielded a total hydroxyl number comparable to a conventional thermal activation at 773 K, Figure 3.6. However the hydroxyl distribution was different, with a higher proportion of hydrogen bonded

hydroxyls, and the remaining isolated hydroxyl density at the silica surface similar to that achievable by 1073 K thermal activation.

These optimum CF_4 plasma conditions were then combined with subsequent heating under dry nitrogen in order to see whether the hydroxyl distribution relaxes towards the expected thermodynamic equilibrium associated with conventional thermal treatment, Figure 3.7 and Table 3.4. It was found that annealing to 773 K reduced the total number of hydroxyls to that equivalent to a 1073 K thermal activation (the number of isolated hydroxyls was in fact 50% lower). Heating to higher temperatures did not produce any further drop in total hydroxyl population (within the detection limits of the ^1H NMR experiment); however some of the hydrogen bonded hydroxyls were converted to isolated hydroxyls, thereby shifting the overall distribution towards the expected 1073 K thermal equivalent, Figure 3.6.

BET surface area analysis indicated that no significant loss of porosity had occurred during any of the plasma treatments, Table 3.5.

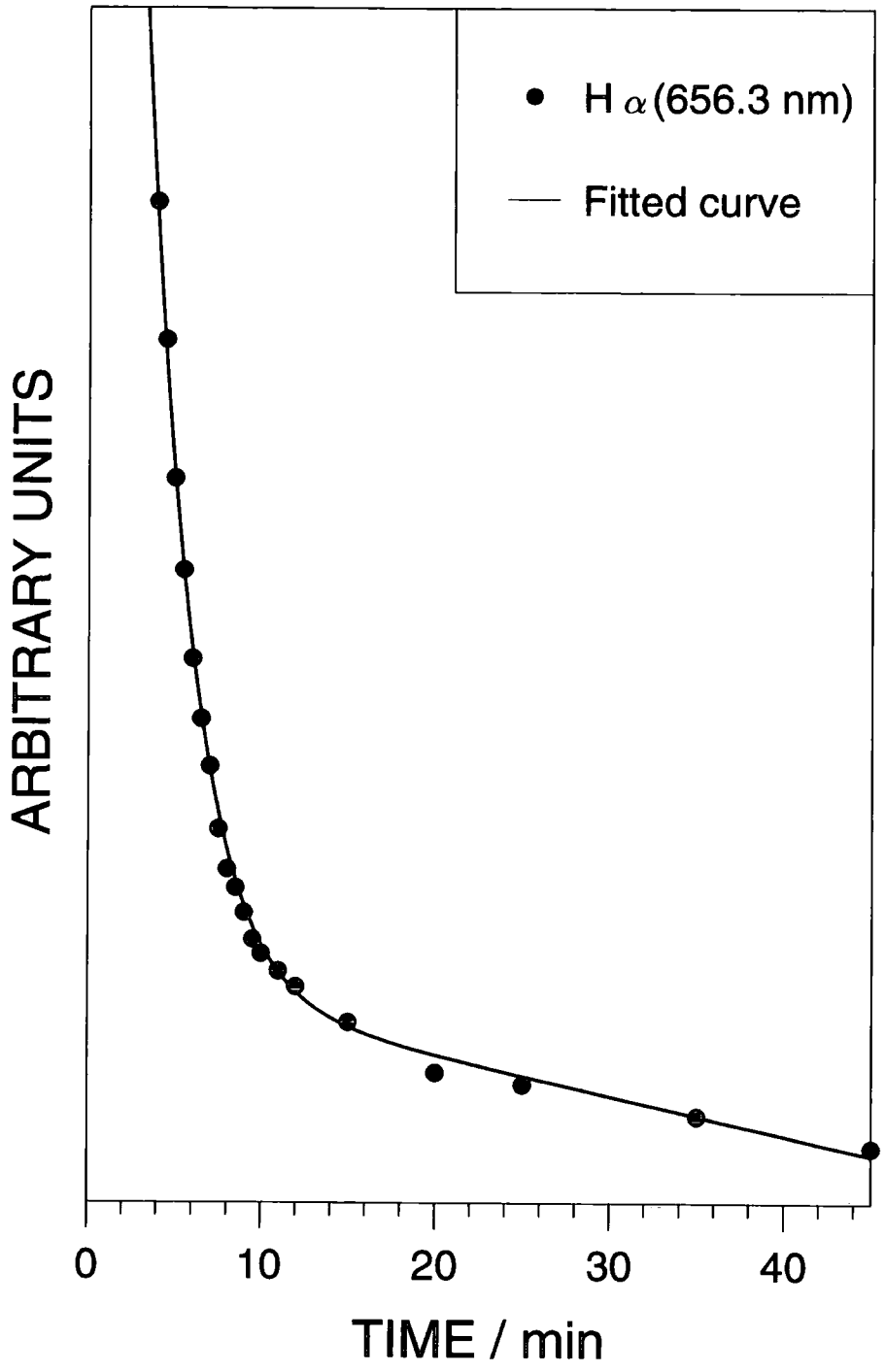

Figure 3.4: Optical emission spectroscopy of the 656.3 nm H_α line decay during oxygen plasma treatment of silica.

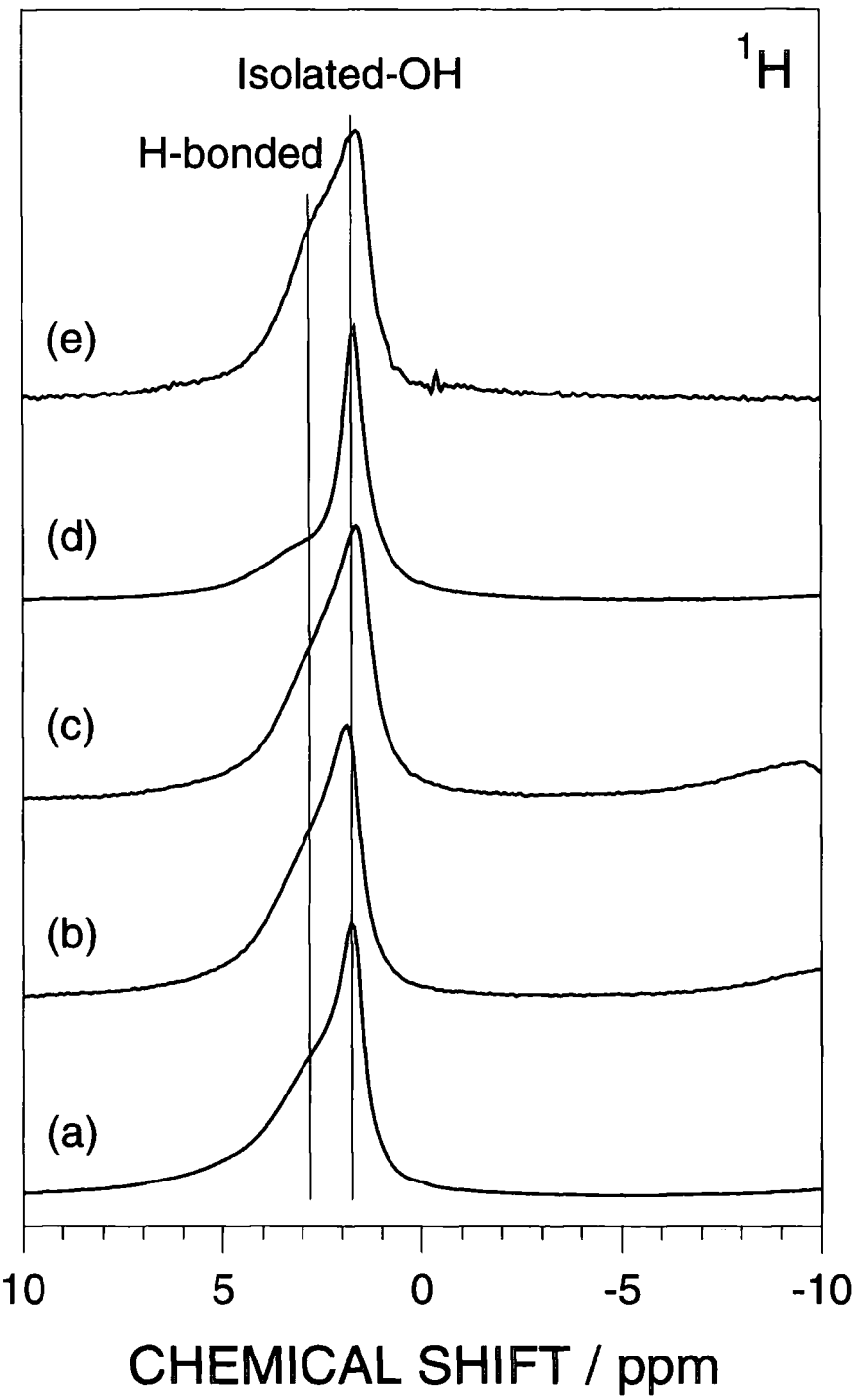

Figure 3.5: 299.945 MHz ^{1}H MAS NMR spectra (90° pulse, 5 s relaxation decay) of silica: (a) vacuum dried; (b) argon plasma treated; (c) helium plasma treated; (d) oxygen plasma treated; and (e) carbon tetrafluoride. (The minor variation in width of the ^{1}H resonances can be attributed to the slightly different magic angle spinning speeds employed during data acquisition.[23])

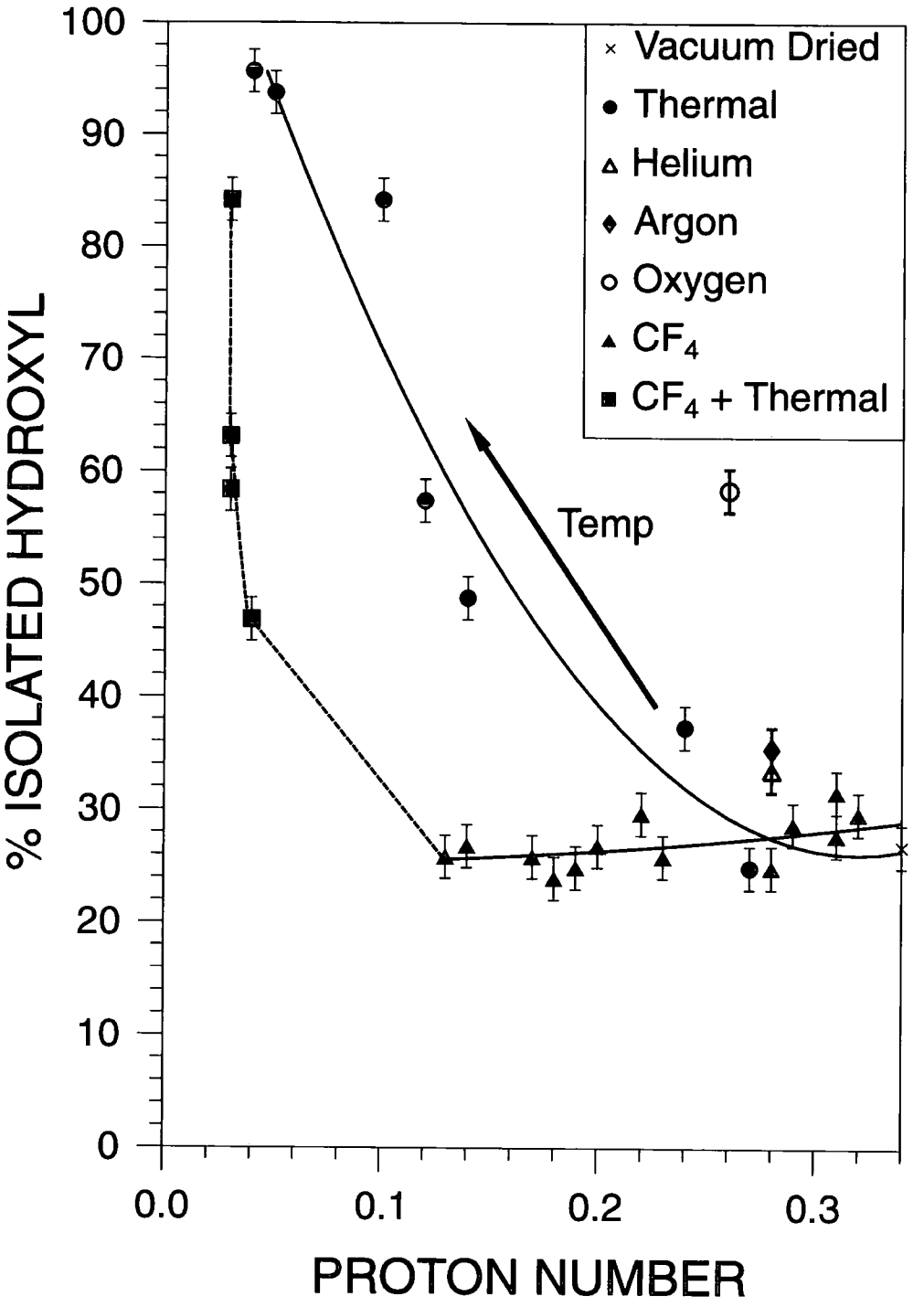

Figure 3.6: Comparison of the hydroxyl distribution between thermal, plasma, and combined plasma-thermal treatments of high surface area silica.

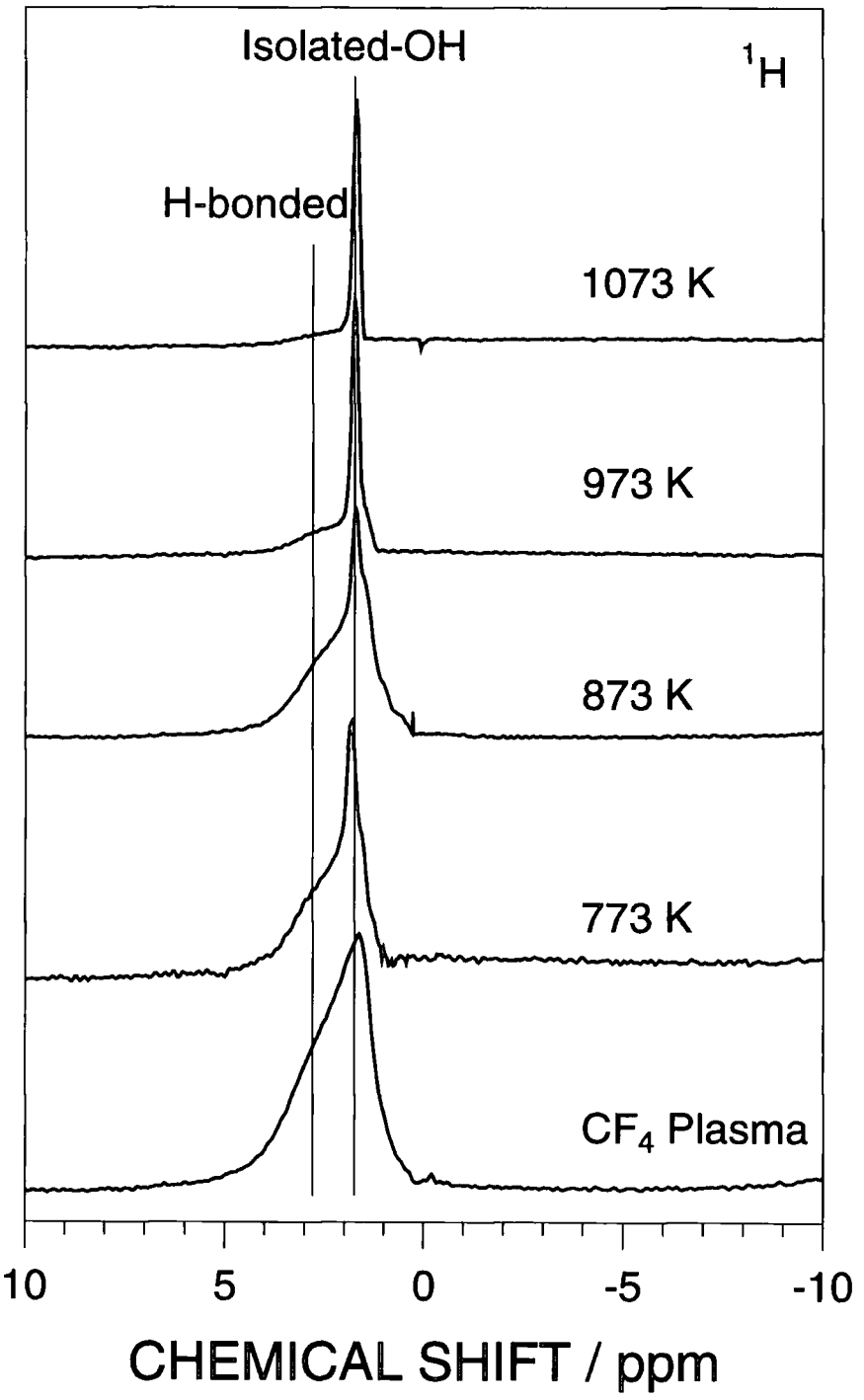

Figure 3.7: 299.945 MHz ^{1}H MAS NMR spectra (90° pulse, 5 s relaxation decay) of optimum carbon tetrafluoride plasma treatment of silica followed by annealing.

Silica treatment	"Proton Number"			Percentage		Ratio of hydrogen bonded to isolated hydroxyls
	Total	Hydrogen bonded	Isolated	Hydrogen bonded	Isolated	
Vacuum dried	0.34 ± 0.01	0.24 ± 0.01	0.10 ± 0.01	72 ± 2	28 ± 2	2.6 ± 0.1
Argon plasma	0.28 ± 0.01	0.18 ± 0.01	0.10 ± 0.01	63 ± 1	37 ± 1	1.8 ± 0.1
Helium plasma	0.28 ± 0.01	0.18 ± 0.01	0.10 ± 0.01	65 ± 1	35 ± 1	1.9 ± 0.1
Oxygen plasma	0.26 ± 0.01	0.10 ± 0.01	0.16 ± 0.01	39 ± 3	61 ± 3	0.64 ± 0.02
CF_4 plasma	0.19 ± 0.01	0.14 ± 0.01	0.05 ± 0.01	74 ± 2	26 ± 2	2.9 ± 0.2

Table 3.2: Solid state ^1H NMR data for vacuum dried and plasma treated silica (0.4 mbar, 60 W and 15 min).

Silica treatment	"Proton Number"			Percentage		Ratio of hydrogen bonded to isolated hydroxyls
	Total	Hydrogen bonded	Isolated	Hydrogen bonded	Isolated	
CF_4 20 W, 0.1 mbar	0.32 ± 0.02	0.23 ± 0.02	0.09 ± 0.02	71 ± 1	29 ± 1	2.4 ± 0.1
CF_4 20 W, 0.3 mbar	0.29 ± 0.03	0.20 ± 0.03	0.09 ± 0.03	70 ± 1	30 ± 1	2.3 ± 0.1
CF_4 20 W, 0.4 mbar	0.28 ± 0.01	0.21 ± 0.01	0.07 ± 0.01	74 ± 2	26 ± 2	2.9 ± 0.1
CF_4 40 W, 0.1 mbar	0.31 ± 0.01	0.21 ± 0.01	0.10 ± 0.01	67 ± 1	33 ± 1	2.0 ± 0.1
CF_4 40 W, 0.3 mbar	0.22 ± 0.01	0.15 ± 0.01	0.07 ± 0.01	69 ± 3	31 ± 3	2.2 ± 0.1
CF_4 40 W, 0.4 mbar	0.20 ± 0.01	0.14 ± 0.01	0.06 ± 0.01	72 ± 1	28 ± 1	2.6 ± 0.1
CF_4 60 W, 0.1 mbar	0.31 ± 0.02	0.22 ± 0.02	0.09 ± 0.02	71 ± 2	29 ± 2	2.4 ± 0.1
CF_4 60 W, 0.3 mbar	0.23 ± 0.01	0.17 ± 0.01	0.06 ± 0.01	73 ± 1	27 ± 1	2.8 ± 0.1
CF_4 60 W, 0.4 mbar	0.19 ± 0.01	0.14 ± 0.01	0.05 ± 0.01	74 ± 2	26 ± 2	2.9 ± 0.2
CF_4 60 W, 0.5 mbar	0.13 ± 0.01	0.09 ± 0.01	0.04 ± 0.01	73 ± 2	27 ± 2	2.7 ± 0.1
CF_4 60 W, 0.6 mbar	0.17 ± 0.02	0.12 ± 0.02	0.05 ± 0.02	73 ± 2	27 ± 2	2.7 ± 0.1
CF_4 80 W, 0.5 mbar	0.18 ± 0.02	0.13 ± 0.02	0.05 ± 0.02	75 ± 3	25 ± 3	3.0 ± 0.2
CF_4 80 W, 0.6 mbar	0.14 ± 0.01	0.10 ± 0.01	0.04 ± 0.01	72 ± 1	28 ± 1	2.6 ± 0.1

Table 3.3: Solid state ^1H NMR data for CF_4 plasma factorial experiments and Simplex optimisation (15 min treatment time).

Silica treatment	"Proton Number"			Percentage		Ratio of hydrogen bonded to isolated hydroxyls
	Total	Hydrogen bonded	Isolated	Hydrogen bonded	Isolated	
CF_4 + 773 K	0.04 ± 0.02	0.02 ± 0.02	0.02 ± 0.02	51 ± 4	49 ± 4	1.0 ± 0.1
CF_4 + 873 K	0.03 ± 0.02	0.01 ± 0.02	0.02 ± 0.02	39 ± 4	61 ± 4	0.64 ± 0.1
CF_4 + 973 K	0.03 ± 0.02	0.01 ± 0.02	0.02 ± 0.02	34 ± 3	66 ± 3	0.52 ± 0.07
CF_4 + 1073 K	0.03 ± 0.02	0.00 ± 0.02	0.03 ± 0.02	12 ± 4	88 ± 4	0.14 ± 0.05

Table 3.4: Solid state ^1H NMR data for optimum CF_4 plasma treatment (0.5 mbar, 60 W and 15 min) with subsequent thermal treatment.

Treatment	BET surface area / $m^2 g^{-1}$
Untreated	233 ± 3
Optimum CF_4 plasma	220 ± 4

Table 3.5: BET surface areas.

3.4 Discussion

It has been shown that bulk dehydroxylation of high surface area silica powder can be achieved by low temperature plasma exposure. This is consistent with previous investigations, where Phillips ethylene polymerisation catalyst precursors supported on silica were activated by plasma treatment.[24] It is of interest to note that depending upon the conditions employed, either the whole porous material,[24] or just the surface[25] can be modified.

It can be calculated using the perfect gas equation that at a typical operating plasma pressure of 0.4 mbar, on average, there will be less than one atom/molecule within each pore.[26] Furthermore the pores in mesoporous silica are much smaller in size (between 2 and 50 nm) compared to the plasma Debye length (2 μm < λ_D < 7 mm) under such conditions.[6,7] Therefore plasma ignition within the pores is unlikely. Rather penetration of excited species (electrons, ions and metastables) together with electromagnetic radiation is more probable. The negative charge associated with the plasma sheath potential adjacent to a particle surface will cause incident electrons to be retarded as they approach the silica surface.[7] Ions and short-lived metastables will predominately interact with the near surface region due to rapid loss of kinetic energy via collisions with the pore walls.[27,28] This leaves long-lived neutrals and photochemistry as potential candidates for bulk modification. In the case of noble gases, the intense M(I) emission lines of argon (106.7 and 104.8 nm) and helium (58.4 nm) superimposed on a weak, broad continuum between 105-155 nm and 58-110 nm respectively[29] are not able to penetrate throughout the whole particle, since silica attenuates wavelengths shorter than 160 nm.[30] Consequently the effect of noble gas plasma treatment must be confined to the surface region of the silica particles, and therefore accounts for the minor change in total hydroxyl population.

Oxygen plasmas contain additional chemically active species. These include neutral ground-state (e.g., O, O_2, O_3) and metastable (e.g., $O_2(a^1\Delta g)$) species, as well as positively charged (e.g., O^+, O_2^+, O_3^+, O_4^+) and negatively charged (e.g., O^-, O_2^-, O_3^-, O_4^-) ions.[31,32] Atomic oxygen is considered to be the predominant reactive constituent.[31] Again, electron, ion, and metastable bombardment will be localised to the particle surface. Permeation of some atomic oxygen species into the particle is likely,[33] although atomic oxygen will also undergo surface recombination processes:[32,34]

$$O + O \text{ (surface)} \rightarrow O_2$$

Direct photo-excitation of molecular oxygen within the pores is an alternative source of atomic species. Plasma UV radiation in the 240-250 nm range (O_2 $A^3\Sigma^+_u$ - $X^3\Pi_g$ transition)[9] is longer in wavelength compared to the silica absorption threshold at 160 nm, and therefore will penetrate throughout the particle to produce excited and ground state atomic oxygen within the pores:

$$O_2(X^3\Sigma_g^-) \rightarrow O_2(X^3\Sigma_u^+) \qquad 250 < \lambda < 300 \text{ nm}$$

$$O_2(X^3\Sigma_g^-) \rightarrow O(^3P) + O(^3P) \qquad \lambda < 242 \text{ nm}$$

This is supported by previous studies where vacuum ultraviolet (VUV) irradiation generated by excimer lamps (from plasma sources) is shown to be effective at removing hydroxyls from planar silica surfaces via a photo-assisted condensation mechanism.[35,36,37,38,39] Analogous reactions must be in operation during oxygen plasma treatment of high surface area silica.

CF_4 plasmas were found to be the most effective at bulk silica dehydroxylation. The predominant chemically reactive component of a CF_4 glow discharge is atomic fluorine together with a small concentration of CF, CF_2 and CF_3 radicals (there is no deposition[40,41]).[42] Therefore, the most likely reactive plasma species which could penetrate throughout the silica particles are UV radiation (CF ($A^2\Sigma$ - $X^2\Pi$, $B^2\Delta$ - $X^2\Pi$) and CF_2 (A^1B_1 -X^1A_1) in the range 220-270 nm)[9] and fluorine atoms either diffusing from the plasma into the particle, or being produced within the pores via CF_4 photodissociation:[43]

$$CF_4 \rightarrow CF_3 + F \qquad \lambda < 236 \text{ nm.}$$

The distribution of hydrogen bonded and isolated hydroxyls is similar to that of vacuum dried silica, Figure 3.7. Therefore hydroxyl loss must occur via an indiscriminate mechanism (unlike thermal dehydroxylation, Scheme 3.1), perhaps forming small quantities of HF,[44] as well as etching to produce volatile SiF_4 and O_2.[6,45,46] Any etching process must be slow,[47] since there is no

significant change in surface area, Table 3.5. The optimum CF_4 plasma treatment of silica yielded hydroxyl densities equivalent to a 773 K conventional thermal treatment with the benefit of less than 2% of the time and 1% of the energy. These high gas pressure and power conditions must be increasing atomic fluorine and VUV production within the discharge,[42,48] consequently greater dehydroxylation is observed.[49]

Subsequent thermal treatment at 773 K of CF_4 plasma treated silica further reduces the total hydroxyl population due to preferential surface condensation of the remaining hydrogen bonded hydroxyls, Scheme 3.1. Even higher temperatures (873 K → 1073 K) resulted in no further dehydroxylation of the silica (within the detection limits of the ^1H NMR experiment), rather the proportion of isolated hydroxyls increased towards thermodynamic equilibrium at this temperature. This indicates that hydrogen bonding breaks down at the silica surface to produce isolated hydroxyls. This probably involves the interaction of protons with oxygen atoms adjacent to siloxane bridges, to generate new surface hydroxyls, which are displaced relative to their initial position,[1] Scheme 3.3.

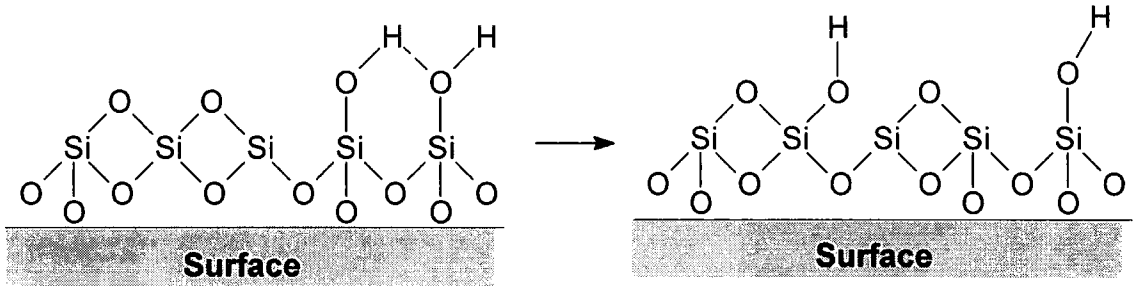

Scheme 3.3: Surface migration of hydroxyls.

3.5 Conclusions

Plasma treatment of high surface area silica provides a quick and energy efficient means for bulk dehydroxylation. It has been shown that room temperature CF_4 plasma treatment is equivalent to a 773 K thermal activation in terms of total hydroxyl population, whilst the number of isolated hydroxyls corresponds to a 1073 K conventional treatment. This is achieved in less than 2% of the time and 1% of the energy consumption.

3.6 References

[1] E.F. Vansant, P. van der Voort and K.C. Vrancken, *Stud. Surf. Sci. Catal.*, **1995**, *93*.

[2] R.K. Iler, *Chemistry of Silica*, Wiley, New York, 1979, Chapter 6.

[3] J.P. Gallas, J.C. Lavalley, A. Burneau and O. Berres, *Langmuir*, **1991**, *7*, 1235.

[4] M.P. McDaniel, *Adv. Catal.* **1985**, *33*, 47.

[5] S. Haukka and A. Root, *J. Phys. Chem.*, **1994**, *98*, 1695.

[6] B.N. Chapman, *Glow Discharge Processes*, John Wiley and Sons, New York, 1980.

[7] A. Grill, *Cold Plasmas in Materials Technology*, IEEE press, New Jersey, 1994.

[8] O. Sneh, S.M. George, *J. Phys. Chem.*, **1995**, *99*, 4639

[9] R.W.B. Pearse and A.G. Gaydon, *The Identification of Molecular Spectra*, 4th ed., John Wiley and Sons, New York, 1976.

[10] P. Mansfield, *Phys. Rev. A: At., Mol., Opt. Phys.*, **1965**, *137*, 961.

[11] C.E. Bronnimann, R.C. Ziegler and G.E. Maciel, *J. Am. Chem. Soc.*, **1988**, *110*, 2023.

[12] S. Haukka, E.L. Lakomaa and A. Root, *J. Phys. Chem.*, **1993**, *97*, 5085.

[13] C.H.C. Liu and G.E. Maciel, *J. Am. Chem. Soc.*, **1996**, *118*, 5103.

[14] S. Branauer, P.H. Emmett and E. Teller, *J. Am. Chem. Soc.*, **1938**, *60*, 309.

[15] V.J. Ruddick, P.W. Dyer, G. Bell, V.C. Gibson and J.P.S. Badyal, *J. Phys. Chem.*, **1996**, *100*, 11062.

[16] I.S. Chaung and G.E. Maciel, *J. Am. Chem. Soc.*, **1996**, *118*, 401.

[17] P. van der Voort, I. Gillis-D'Hammers and E.F. Vansant, *J. Chem. Soc., Faraday Trans.*, **1990**, *86*, 3751.

[18] L.T. Zhuralev and A.V. Kiselev, *Russ. J. Phys. Chem. (Eng. Transl.)*, **1965**, *39*, 236.

[19] L.T. Zhuralev, *Langmuir*, **1987**, *3*, 316.

[20] G. Ghiotti, E. Garrone, C. Morterra and F. Boccuzzi, *J. Phys. Chem.*, **1979**, *83*, 2863.

[21] E. Morgan, *Chemometrics: Experimental Design*, John Wiley and Sons, Chichester, 1991, 81-150.

[22] S.J. Haswell, *Practical Guide to Chemometrics*, Dekker, New York, 1992, 201.

[23] S.F. Dec, C.E. Bronnimann, R.A. Wind and G.E. Maciel, *J. Magn. Reson.*, **1989**, *82*, 454.

[24] V.J. Ruddick and J.P.S. Badyal, *J. Phys. Chem. B*, **1997**, *101*, 9240.

[25] Y. Takahata and R. Miyagawa, U.S. Patent 4,694,092, 1987.

[26] P.W. Atkins, *Physical Chemistry*, 4th ed., Oxford University Press, Oxford, 1990, Chapter 1.

[27] T. Yasuda, T. Okuno, M. Miyama and H. Yasuda, *J. Polym. Sci., Polym. Chem. Ed.*, **1994**, *32*, 1829.

[28] E.V. Karoulina and Y.A. Lebedev, *J. Phys. D: Appl. Phys.*, **1992**, *25*, 401.

[29] D.T. Clark and A. Dilks, *J. Polym. Sci., Polym. Chem. Ed.*, **1980**, *18*, 1233.

[30] A. Hollander, J.E. Klemberg-Sapieha and M.R. Wertheimer, *J. Polym. Sci., Polym. Chem. Ed.*, **1995**, *33*, 2013.

[31] Y. Ichikawa, R.L.C. Wu and T. Kaneda, *J. Appl. Phys.*, **1990**, *67*, 108.

[32] M. Shibata, N. Nakano and T. Makabe, *J. Appl. Phys.*, **1995**, *77*, 6181.

[33] S.L. Koontz, U.S. Patent 5,798,261, 1998.

[34] G.A. Melin and R.J. Maddix, *Trans. Faraday Soc.*, **1971**, *67*, 198.

[35] C. Debauche, C. Licoppe, J. Flicstein, O. Dulac and R.A.B. Devine, *Appl. Phys. Lett.* **1992**, *61*, 306.,

[36] V.Y. Fominski, A.M. Markeev, O.I Naumenko, V.N. Nevolin, A.P. Alyokhin and L.A. Vyukov, *Appl. Surf. Sci.*, **1994**, *78*, 437.

[37] E.G. Parada, P. Gonzalez, J. Serra, B. Leon, M. Perez-Amor, J. Flicstein and R.A.B. Devine, *Appl. Surf. Sci.*, **1995**, *86*, 294.

[38] J. Flicstein, Y. Vitel, O. Dulac, C. Debauche, Y.I. Nissim and C. Licoppe, *Appl. Surf. Sci.*, **1995**, *86*, 286.

[39] R.E. Van de Leest, *Appl. Surf.Sci.*, **1995**, *86*, 278.

[40] J.Q. Wang, D.M. Feng, H.Z. Wang, M. Rembold and F. Thommen, *J. Appl. Polym. Sci.*, **1993**, *50*, 585.

[41] M. Strobel, S. Corn, C.S. Lyons and G.A. Korba, *J. Polym. Sci., Polym. Chem. Ed.*, **1985**, *23*, 1125.

[42] D. Edelson and D.L. Flamm, *J. Appl. Phys.*, **1984**, *56*, 1522.

[43] L.C. Lee, X.Y. Wang and M. Suto. *J. Chem. Phys.*, **1986**, *85*, 6294.

[44] C.J. Mogas, A.C. Adams and D.L. Flamm, *J. Appl. Phys.*, **1978**, *49*, 3796.

[45] D.L. Flamm. In *Plasma Etching, An Introduction*, D.M. Manos and D.L. Flamm, Eds., Academic Press, London, 1989, Chapter 2.

[46] D.L. Flamm, C.J. Mogas and E.R. Skalaver, *J. Appl. Phys.*, **1979**, *50*, 6211.

[47] H.F. Winters and J.W. Coburn, *Surf. Sci, Rep.*, **1992**, *14*, 161.

[48] J.W. Coburn and M. Chen, *J. Vac. Sci. Technol.*, **1981**, *18*, 353.

[49] J. Ding, J.-S. Jenq, G.-H. Kim, H.L. Maynard, J.S. Hamers, N. Hershkowitz and J.W. Taylor, *J. Vac. Sci. Technol., A*, **1993**, *11*, 1283.

CHAPTER 4

PLASMA ACTIVATION OF THE PHILLIPS Cr(ACETATE)/SiO_2 POLYMERISATION CATALYST PRECURSOR. PART 2: COMBINED PLASMA ACTIVATION AND PLASMA DEHYDROXYLATION.

4.1 Introduction

Non-equilibrium oxygen plasma treatment of the Cr(acetate)/SiO_2 Phillips catalyst precursor produces an active catalyst.[1,2] However, the resulting polymerisation activity is low due to the support's high hydroxyl population and low chromium dispersion.[2] An improvement in activity can be achieved by using a high temperature thermal treatment after plasma activation. This decreases the hydroxyl population, and produces a polymer with a narrow molecular weight distribution.[2] Carbon tetrafluoride non-equilibrium plasmas are capable of decreasing the hydroxyl population on silica to a level comparable with a conventional 773 K thermal activation.[3] The use of non-equilibrium plasmas to both dehydroxylate and activate the catalyst is highly desirable, due to the rapid activation and the low energy consumption required compared to thermal calcination.

In this study, an investigation is made into whether a combined plasma process, using the CF_4 and O_2 plasma conditions described earlier in Chapters 2 and 3, can dehydroxylate and activate the catalyst precursor.

4.2 Experimental

The catalyst precursor was prepared by impregnating silica (EP10X, Crosfield Ltd, particle size $\approx$ 100 μm) with an aqueous solution of basic chromium(III) acetate (EP30X, Crosfield Ltd, Cr 1 wt.% after calcination).

Plasma activation was carried out in a 13.56 MHz rotating plasma reactor designed to treat powder samples, as described earlier in Chapter 2.

Prior to each experiment the reactor was cleaned with detergent, rinsed with isopropyl alcohol, oven dried, and then cleaned *in situ* using a 0.3 mbar air plasma at 30 W. 1 g of catalyst precursor was then loaded into the reactor and evacuated to base pressure before CF_4 gas (Air Products 99.7%) was introduced at a pressure of 0.5 mbar via a fine leak valve. At this stage rotation of the reactor commenced and a 60 W plasma was ignited. After 15 min the rf power supply was switched off and the reactor evacuated to base pressure. Oxygen (Air Products 99.995%, dried through an activated 3A molecular sieve (Aldrich) column to less than 1.0 ppm_v H_2O) was then introduced to the reactor at a pressure of 0.3 mbar and a 70 W plasma ignited for 45 min. Upon completion of plasma treatment, agitation of the catalyst particles was stopped, the rf power supply was switched off, and the chamber evacuated back to its original base pressure, prior to bringing up to an atmosphere of oxygen. Alternatively, the reverse procedure was used whereby the catalyst was activated using an O_2 plasma for 45 min and then dehydroxylated with a CF_4 discharge for 15 min. All samples were transferred under a dry nitrogen atmosphere (H_2O < 1.0 ppm_v), prior to analysis.

Inductively coupled plasma mass spectrometry (ICP-MS) was used to quantify the catalyst chromium loading after activation. Sample preparation and analysis were carried out as described in Chapter 2.

UV/vis Diffuse reflectance was performed on a PYE UNICAM SP8-150 UV/vis spectrophotometer fitted with an integrating spheroid accessory. Spectra were obtained using a 2 nm bandwidth and a scan speed of 1 nm s^{-1}. The output was collected on a chart recorder and then manually digitised.

Carbon monoxide reduction isotherms were obtained in a catalytic microreactor. The catalyst transfer and CO_2 quantification were performed as described in Chapter 2.

Quantification of the proton signal intensity and the relative proportion of isolated and hydrogen bonded hydroxyls was obtained using solid state ^1H NMR performed on a Varian Unity Plus 300 MHz spectrometer. The static echo and magic angle spinning experimental parameters were the same as described earlier in Chapter 2. Catalyst samples were transferred into 5 mm o.d. silicon nitride rotors with push-on caps in a nitrogen atmosphere glove box.

Ethylene polymerisation activity was tested by reducing the plasma activated catalyst at 623 K, with a 15 min exposure of carbon monoxide (at a

flow rate of 1.5 dm^3 h^{-1}). The catalyst was then cooled to 383 K and exposed to ethylene (Scott Speciality Gases 99.8%, dried as before). The resultant material was characterised by attenuated total reflectance Fourier transform infrared spectroscopy (ATR-FTIR). Absorption spectra were acquired using a Mattson Polaris spectrometer fitted with a Graseby Specac Golden Gate ATR accessory. The scan range was 600-4000 cm^{-1} at a resolution of 4 cm^{-1}, averaged over 32 scans, in conjunction with background subtraction.

4.3 Results

The chromium loading of the activated catalysts varied according to the sequence of plasma treatment, Table 4.1. When an initial CF_4 plasma dehydroxylation was performed, the loading was comparable to after thermal or plasma activation.[2] In contrast, when CF_4 treatment was carried out after O_2 plasma activation, the chromium loading was reduced by 13%. A lemon-yellow substance was observed to collect in the cold trap, which sublimed on warming. This was attributed to CrF_6.[4] There was no evidence of CrF_6 in the cold trap when the plasma treatments were performed in the reverse order.

UV/vis diffuse reflectance spectra taken after each of the combined plasma treatments (CF_4/O_2 and O_2/CF_4) showed a broad chromate band at approximately 470 nm,[5,6] Figure 4.1. There was no peak at 600 nm which could be attributed to the chromium acetate precursor, indicating that complete oxidation occurred throughout the catalyst particle.[6]

The dispersion of the Cr(VI) species on the support was investigated by measuring the evolution of CO_2 during CO reduction of the catalyst using quadrupole mass spectrometry. When CF_4 dehydroxylation was carried out prior to O_2 activation, the amount of CO_2 evolved was the same as for the solely O_2 plasma activated catalyst,[2] Table 4.2. A 13% decrease in CO_2 evolution was observed when O_2 activation was carried out prior to CF_4 dehydroxylation. This decrease was explained by the loss of chromium from the support during CF_4 plasma treatment.

In comparison to the solely O_2 plasma activated catalyst, an additional CF_4 plasma dehydroxylation lowered the total hydroxyl population by a further 25% (from the equivalent of a 373 K to a 573 K thermal treatment), Table 4.3.

A mixture of isolated and hydrogen bonded hydroxyls were observed in the ^1H MAS NMR spectra (at 1.7 and 3.0 ppm respectively[7,8,9]), Figure 4.2. This reduction was less than that observed during CF_4 plasma dehydroxylation of the silica support.[3]

For both of these combined treatments, catalyst activity was confirmed by the formation of white granules after polymerisation. These were identified by ATR-FTIR analysis as polyethylene by C-H stretches at 2920 cm^{-1} and 2850 cm^{-1}, and methylene bending and rocking modes at 1469 cm^{-1} and 719 cm^{-1} respectively (all remaining peaks were assigned to the silica support),[10,11] Figure 4.3.

Activation	Cr / wt.%	CO_2 area
Thermal[2]	0.84 ± 0.02	109 ± 3
O_2 plasma[2]	0.87 ± 0.02	91 ± 3
CF_4 then O_2 plasma	0.81 ± 0.02	94 ± 4
O_2 then CF_4 plasma	0.73 ± 0.02	82 ± 3

Table 4.1: Chromium elemental analysis and CO reduction areas.

			Percentage	
Sample	**Activation**	**"Proton Number"**	**Hydrogen bonded**	**Isolated**
Silica	**Thermal[3]**	0.04 ± 0.02	0 ± 1	100 ± 1
	O_2 plasma[3]	0.26 ± 0.02	39 ± 3	61 ± 2
	CF_4 plasma[3]	0.13 ± 0.02	73 ± 2	27 ± 2
Catalyst	**Thermal[2]**	0.03 ± 0.02	2 ± 2	98 ± 2
	O_2 plasma[2]	0.28 ± 0.02	62 ± 3	38 ± 3
	CF_4 then O_2 plasma	0.21 ± 0.02	65 ± 3	35 ± 3
	O_2 then CF_4 plasma	0.21 ± 0.02	62 ± 2	38 ± 2

Table 4.2: Solid state ^1H NMR data for activated silica and catalyst.

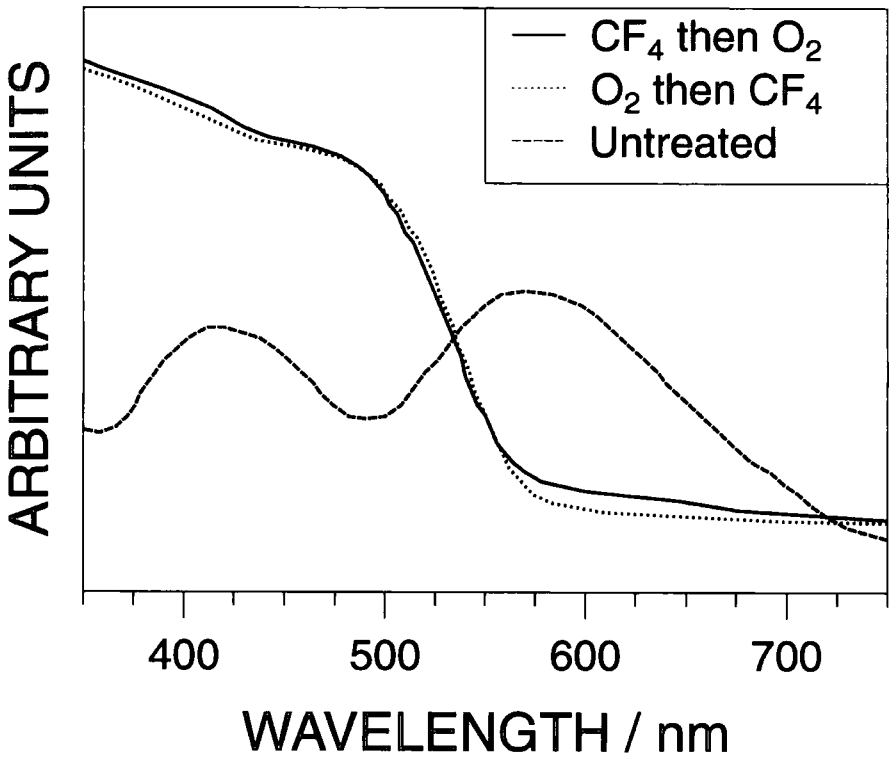

Figure 4.1: UV/vis diffuse reflectance spectra of the catalysts.

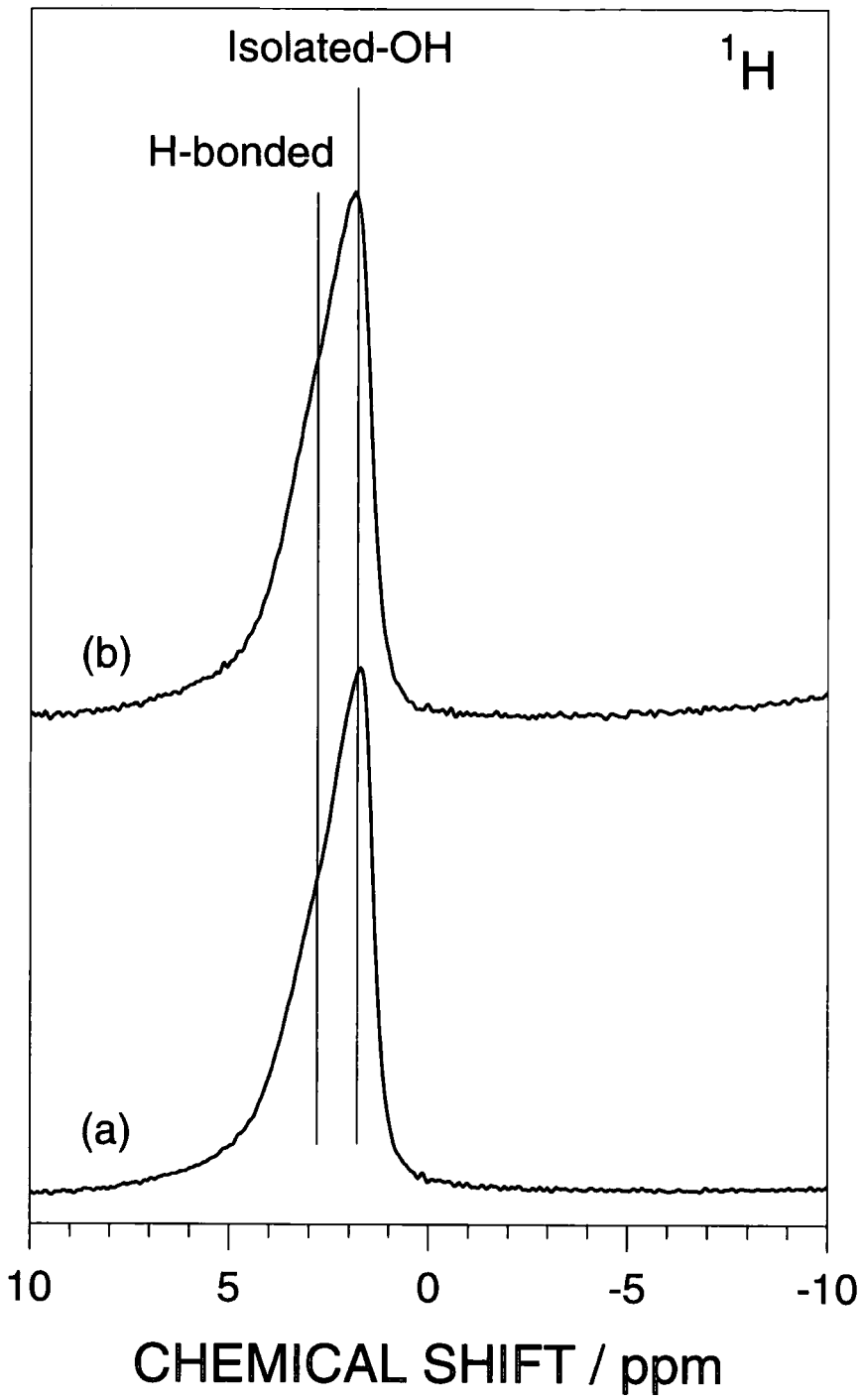

Figure 4.2: 299.945 MHz ^{1}H MAS NMR spectra (90° pulse, 5 s relaxation decay) of catalyst activated; (a) CF_4 then O_2 plasma and (b) O_2 then CF_4 plasma.

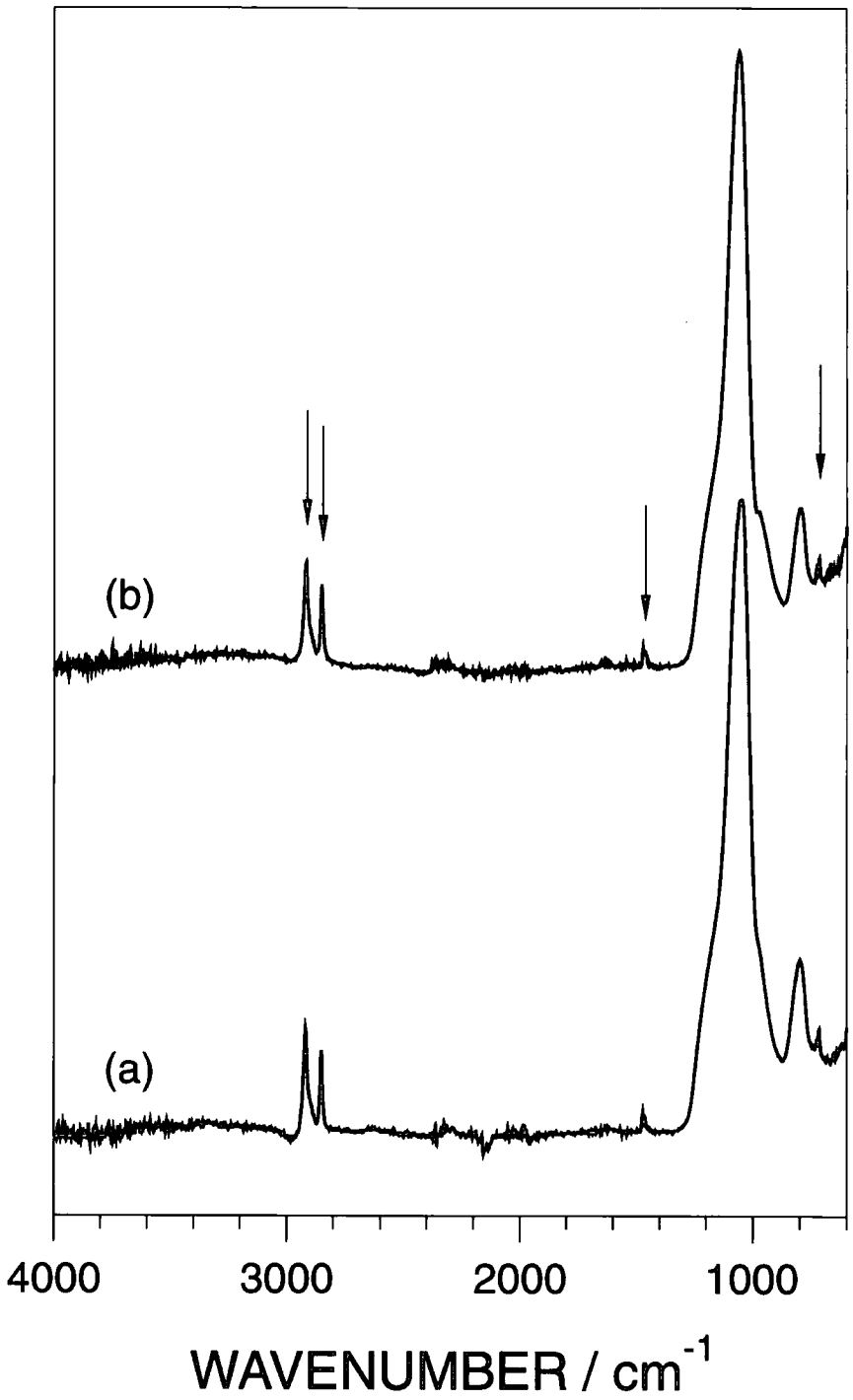

Figure 4.3: ATR-FTIR spectra of the polymerisation products of the catalyst activated; (a) CF_4 then O_2 plasma and (b) O_2 then CF_4 plasma.

4.4 Discussion

Chromium hexafluoride can only be synthesised conventionally under harsh conditions. For example, chromium powder requires reaction with fluorine at 200 bar and 673 K, and produces a mixture of CrF_5 and CrF_6.[4] Less severe conditions are required when CrO_3 is used as the precursor, typically reacting with fluorine at 25 bar and 443 K.[12] CrF_6 is lemon-yellow and highly volatile, subliming between 173 and 193 K.[12]

Non-equilibrium plasmas are partially ionised gases consisting of ions, electrons, metastables, neutrals, and electromagnetic radiation, where the electron temperature ($T_e \approx$ 10,000 K) is much greater than the bulk gas temperature ($T_g \approx$ 300 K).[13] Therefore although the overall temperature of the system is close to ambient, the electrons possess sufficient energy to cause rupture and excitation of chemical bonds. A CF_4 plasma provides a source of fluorine atoms (with relatively low concentrations of CF_x species) and does not lead to polymer deposition.[14,15,16] The depth of fluorine penetration is limited to only approximately 1 μm[17,18] in the case of impermeable substrates, but this can be much greater for porous materials.[19] As described in Chapters 2 and 3, plasma ignition within the subsurface is unlikely due to there being on average less than one atom/molecule within each pore,[20] and the Debye length (2 μm < λ_D < 7 mm) of the plasma being much greater than the pore size (2-50 nm).[21] Penetration of excited plasma species (electrons, ions and metastables) together with electromagnetic radiation is more probable. The negative charge associated with the plasma sheath region adjacent to a particle surface will cause incident electrons to be retarded as they approach the silica surface;[21] hence electron bombardment is unlikely to be important. Ion and short-lived metastables will predominantly interact with the near surface region due to rapid loss of kinetic energy via collisions with pore walls.[19,22] The most likely reactive CF_4 plasma species which could penetrate throughout the whole silica particle are therefore UV radiation (CF ($A^2\Sigma$ - $X^2\Pi$, $B^2\Delta$ - $X^2\Pi$) and CF_2 (A^1B_1 - X^1A_1) in the range 220-270 nm)[23] and fluorine atoms, either diffusing into the particle from the plasma, or undergoing CF_4 photodissociation within the pores.[24]

$$CF_4 \rightarrow CF_3 + F \qquad \lambda < 236 \text{ nm}$$

Atomic fluorine is therefore thought to fluorinate some of the CrO_3 formed after O_2 plasma oxidation of the precursor. The product, CrF_6, is then removed under vacuum to the cold trap, thereby explaining the reduction in the catalyst chromium loading after activation. This shows the enhanced chemical reactivity of a CF_4 plasma, allowing a reaction to occur at room temperature which requires harsh conventional conditions. The absence of chromium removal after CF_4 plasma treatment of Cr(acetate)/SiO_2 can be explained on the basis of thermodynamically favoured fluorination of the acetate ligand over the chromium centre. C-H bond strengths are in the range 3-4 eV, compared to 6 eV for H-F and 5 eV for C-F, whereas Cr-O bonds are 5 eV, similar in value to Cr-F bonds at 5 eV.[25,26]

The smaller reduction in the catalyst precursor hydroxyl population compared to silica can be explained in terms of atomic fluorine participating in the ongoing chemistry at the chromium centre, thereby reducing the rate of dehydroxylation.

Both of the catalysts produced less CO_2 than a thermally calcined catalyst, indicating that chromium clusters are present on the support after activation.[5]

Using combined treatments produced active polymerisation catalysts. Quantitative information was not obtained, so a comparison with the solely oxygen plasma activated catalyst cannot be made.

4.5 Conclusions

Using a combined plasma dehydroxylation and activation has the advantage of reducing the hydroxyl population on the support. The order of treatment is important; CF_4 plasma treatment of the oxygen plasma activated CrO_3/SiO_2 catalyst removes some chromium from the support.

Both activations are shown to produce active ethylene polymerisation catalysts.

4.6 References

[1] V.J. Ruddick and J.P.S. Badyal, *J. Phys. Chem., B*, **1997**, *101*, 9240.

[2] S.P. Godfrey, Ph.D. Thesis, University of Durham, England, 1999, Chapter 2.

[3] S.P. Godfrey, Ph.D. Thesis, University of Durham, England, 1999, Chapter 3.

[4] O. Glemser, H. Roesky, K.-H. Hellberg, *Angew. Chem., Int. Ed. Engl.*, **1963**, *2*, 266.

[5] C. Groeneveld, P.P.M.M. Wittgen, A.M. van Kesbergen, P.L.M. Miestron, C.E. Nuijten and G.C.A. Schuit, *J. Catal.*, **1979**, *59*, 153.

[6] M.P. McDaniel, *J. Catal.*, **1982**, *76*, 37.

[7] C.E. Bronnimann, R.C. Ziegler and G.E. Maciel, *J. Am. Chem. Soc.*, **1988**, *110*, 2023.

[8] S. Haukka, E.L. Lakomaa and A. Root, *J. Phys. Chem.*, **1993**, *97*, 5085.

[9] C.H.C. Liu and G.E. Maciel, *J. Am. Chem. Soc.*, **1996**, *118*, 5103.

[10] P.C. Painter, M.M. Coleman and J.L. Koenig, *The Theory of Vibrational Spectroscopy and its Application to Polymeric Materials*, John Wiley and Sons, Chichester, 1982.

[11] J.G. Grasselli, M.K. Snavely and B.J. Bulkin, *Chemical Applications of Raman Spectroscopy*, John Wiley and Sons, Chichester, 1981.

[12] E.G. Hope, P.J. Jones, W. Levason, J.S. Ogden, M. Tajik and J.W. Turff, *J. Chem. Soc. Dalton Trans.*, **1985**, 1443.

[13] B.N. Chapman, *Glow Discharge Processes*, John Wiley and Sons, New York, 1980.

[14] J.Q. Wang, D.M. Feng, H.Z. Wang, M. Rembold and F. Thommen, *J. Appl. Polym. Sci.*, **1993**, *50*, 585.

[15] M. Strobel, S. Corn, C.S. Lyons and G.A. Korba, *J. Polym. Sci., Polym. Chem. Ed.*, **1985**, *23*, 1125.

[16] D. Edelson and D.L. Flamm, *J. Appl. Phys.*, **1984**, *56*, 1522.

[17] E.A. Wildi, G.J. Scilla and A. DeLuca, *Mater. Res. Soc. Symp. Proc.*, **1985**, *48*, 79.

[18] I.-H. Loh, E. Cohent and R.F. Baddour, *J. Appl. Polym. Sci.*, **1986**, *31*, 901.

[19] T. Yasuda, T. Okuno, M. Miyama and H. Yasuda, *J. Polym. Sci., Polym. Chem. Ed.*, **1994**, *32*, 1829.

[20] P.W. Atkins, *Physical Chemistry*, 4th ed., Oxford University Press, Oxford, 1990, Chapter 1.

[21] A. Grill, *Cold Plasmas in Materials Technology*, IEEE press, New Jersey, 1994.

[22] E.V. Karoulina and Y.A. Lebedev, *J. Phys. D: Appl. Phys.*, **1992**, *25*, 401.

[23] R.W.B. Pearse and A.G. Gaydon, *The Identification of Molecular Spectra*, 4th ed., John Wiley and Sons, New York, 1976.

[24] L.C. Lee, X.Y. Wang and M. Suto. *J. Chem. Phys.*, **1986**, *85*, 6294.

[25] F.D. Egitto, L.J. Matienzo and H.B. Schreyer, *J. Vac. Sci. Technol., A.*, **1992**, *10*, 3060.

[26] D.M. Golden and S.W. Benson, *Chem. Rev.*, **1969**, *69*, 125.

CHAPTER 5

NON-EQUILIBRIUM PLASMA CHLORINATION OF A SUPPORTED DIABUTYLMAGNESIUM PRECURSOR

5.1 Introduction

Phillips polymerisation catalysts are typically supported on high surface area silicas.[1] The support has two important roles: to chemically bond with the chromium, and to fragment during polymerisation. Unlike Phillips catalysts, which typically produce polymers with a broad molecular weight distribution (M_w/M_n values of 8-30),[2] Ziegler-Natta catalysts produce polyethylene with a narrower distribution (M_w/M_n values of 3-7).[3] Such Ziegler-Natta catalysts are a mixture of a group IA to IIIA base metal alkyl co-catalyst and a group IVB to VIIIB metal salt, although not all possible combinations are active for polymerisation.[4,5]

Ziegler-Natta catalysts were originally supported on ball-milled magnesium chloride.[5] Magnesium chloride acts as a good support for titanium chloride based Ziegler-Natta catalysts, due to the similarities between the ionic radii of magnesium and chlorine.[5] The ball-milling process introduces surface defects upon which the titanium tetrachloride is able to bind.[6] However, supporting these catalysts on a carrier such as silica has several advantages. The amount of co-catalyst required is reduced, the polymerisation rate is more uniform, and the polymer produced contains less chlorine.[7]

Supporting titanium tetrachloride directly on to silica produces a catalyst with low activity;[7] this activity is increased by first reacting the high surface area silica with a magnesium compound.[7,8] Various approaches have been used to anchor magnesium compounds on to the silica surface: these include the use of Grignard reagents (Scheme 5.1),[9,10] dialkylmagnesiums (Scheme 5.2)[11] and magnesium chloride.[12,13]

$$O_3SiOH + RMgCl \longrightarrow O_3SiOMgCl + RH$$

Scheme 5.1: Reaction of a Grignard reagent with surface silanol.

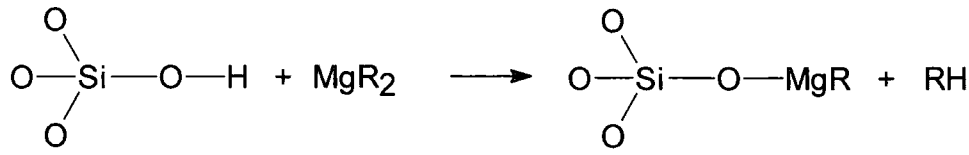

Scheme 5.2: Reaction of a dialkylmagnesium with surface silanol.

The silica supported magnesium alkyl compound can subsequently be chlorinated using silicon or tin chlorides, or HCl.[9,10] The active catalyst is then produced by adding titanium tetrachloride together with the co-catalyst.[9,10] Titanium tetrachloride reacts with the magnesium halide layer via a bridged chlorine atoms.[5] The cocatalyst creates the active species, thought to be a cationic metal salt, by alkylation, ligand abstraction and counter-ion complexation.[14]

In this study, a preliminary investigation is made into the use of a non-equilibrium CCl_4 plasma as a chlorinating agent to produce a magnesium halide from a dialkylmagnesium precursor supported on high surface area silica. The extent of removal of butyl groups is studied using ^1H MAS NMR, and the composition of the resulting surface investigated with elemental analysis.

5.2 Experimental

High surface area silica (EP10X, Crosfield Ltd, particle size $\approx$ 100 μm) was used as a control sample for elemental analysis. The dialkylmagnesium precursor was prepared by impregnating silica (ES70, Crosfield Ltd, previously calcined at 973 K for 5 h) with di-n-butylmagnesium (DBM) (Aldrich n-butyl) in a hexane slurry.

Plasma modification was carried out in a 13.56 MHz rotating plasma reactor designed to treat powder samples, as described in Chapter 2. Prior to each experiment the plasma chamber was cleaned with detergent, rinsed with

isopropyl alcohol, dried, and then cleaned further *in situ* using a 0.3 mbar air plasma at 30 W. After evacuation to base pressure, nitrogen (BOC 99.998%, dried through an activated 3A molecular sieve (Aldrich) column to less than 1.0 ppm_v H_2O) was admitted, the reactor was then sealed and removed from the experimental arrangement. 1 g of dibutylmagnesium/silica (DBM/SiO_2) was transferred across to the reactor, the plasma chamber reassembled and evacuated to base pressure. CCl_4 (Aldrich 99+% previously subjected to several freeze-thaw cycles) was leaked into the reactor at 0.2 mbar using a Young's tap. At this stage, rotation of the reactor commenced and a 40 W glow discharge was ignited. Upon completion of the plasma treatment, agitation of the particles ceased, the rf power supply was switched off, and the chamber evacuated back to its original base pressure, prior to bringing up to an atmosphere of nitrogen. All samples were transferred under a dry nitrogen atmosphere (H_2O < 1.0 ppm_v), prior to analysis.

^1H MAS NMR was performed on a Varian Unity Plus 300 MHz spectrometer. Samples were transferred into 5 mm o.d. silicon nitride rotors with push-on caps in a nitrogen atmosphere glove box. 32 transients were acquired using a 90° pulse, 5 s recycle delay, 100 kHz spectral width, and a magic angle spinning speed of 4-8 kHz. The background signal from an empty rotor was subtracted from each spectrum.

Magnesium analysis was performed by reaction with nitric acid / perchloric acid mixture, whereas chlorine analysis required sample combustion in oxygen. Analysis was then performed using a Dionex DX500 ion chromatogram calibrated using appropriate standard solutions.

5.3 Results

Before treatment of the DBM/SiO_2 precursor, ^1H MAS NMR detected three chemical environments, associated with isolated hydroxyl (1.7 ppm)[15,16] and butyl groups (CH_2 and CH_3 at 1.2 and 0.7 ppm respectively),[17] Figure 5.1. CCl_4 plasma treatment decreased the intensities of the CH_2 and CH_3 functionalities after 4 minutes and almost removed the peaks completely after 10 minutes, to leave a feature associated with isolated hydroxyls. The broad background between 10 and 0 ppm was attributed to background subtraction, and is visible in all three spectra.

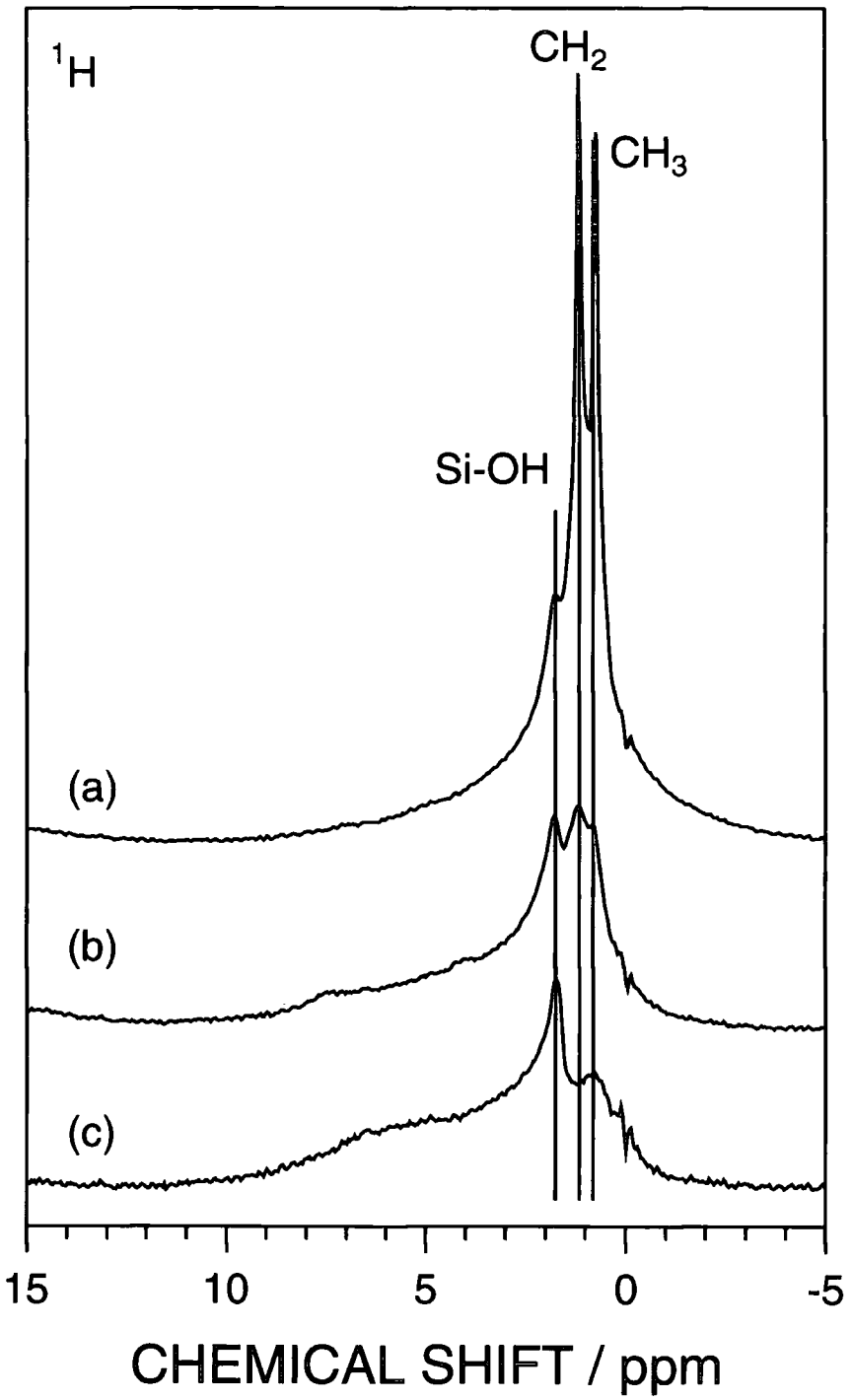

Figure 5.1: 299.945 MHz ^{1}H MAS NMR spectra (90° pulse, 5 s relaxation decay) of the precursor: (a) untreated; (b) CCl_4 plasma treated for 4 minutes; and (c) CCl_4 plasma treated for 10 minutes.

Elemental analysis of the high surface area silica control sample showed no incorporation of chlorine after CCl_4 plasma treatment (within the experimental error of the elemental analysis), Table 5.1. In contrast, after plasma treatment, DBM/SiO_2 showed the presence of chlorine. No loss of magnesium was observed after CCl_4 plasma treatment.

		mmol g^{-1}		
Sample	**Activation**	**Cl**	**Mg**	**Cl : Mg**
Silica	**Untreated**	0.2 ± 0.2	-	-
	CCl_4 plasma 4 min	0.1 ± 0.2	-	-
	CCl_4 plasma 10 min	0.1 ± 0.2	-	-
DBM/Silica	**Untreated**	0.2 ± 0.2	1.2 ± 0.2	0.2 ± 0.2
	CCl_4 plasma 4 min	2.2 ± 0.2	1.3 ± 0.2	1.6 ± 0.2
	CCl_4 plasma 10 min	3.1 ± 0.2	1.2 ± 0.2	2.6 ± 0.3

Table 5.1: Elemental analysis.

5.4 Discussion

CCl_4 plasmas are a source of atomic chlorine,[18] and are used to etch silicon,[19,20] and chlorinate polymer films.[21] Atomic chlorine producing plasmas have previously been used to produce $CuCl_x$ layers from thin copper films.[22]

As described in Chapters 2 and 3, plasma ignition within the subsurface is unlikely due to there being on average less than one atom/molecule within each pore,[23] and the Debye length (2 μm < λ_D < 7 mm) of the plasma being much greater than the pore size (2-50 nm).[24] Penetration of excited species (electrons, ions and metastables) together with electromagnetic radiation is more probable. Ion and electron bombardment is likely to be restricted to the surface region due to rapid loss of kinetic energy in collisions with the pore walls.[25,26] The chemical modification within the subsurface will therefore occur due to the presence of long-lived excited plasma species produced by the CCl_4 plasma and UV (≈ 280 nm $A^2\Delta$-$X^2\Pi$ and ≈ 230 nm $B^2\Sigma^+$-$X^2\Pi$)[27] above the absorption threshold for silica.[28]

The decrease in signal from the butyl groups in ^1H MAS NMR spectra after 10 min CCl_4 plasma treatment is due either to their removal, or chlorination to CCl_2 and CCl_3 groups. The low Cl : Mg ratio detected with elemental analysis favours the plasma chlorination of the surface magnesium. If perchlorination of the butyl groups occurred a Cl : Mg ratio of approximately 9 would have been obtained. Attempts to further characterise the material using powder X-Ray diffraction yielded no additional information. This was due to the low loading on the support and the experimental difficulty of analysing an air sensitive sample.

5.5 Conclusions

A CCl_4 non-equilibrium plasma has been shown to be a chlorinating agent for DBM/SiO_2. After plasma treatment a large reduction in the contribution of the butyl groups in the ^1H MAS NMR spectra is observed and chlorine is incorporated on to the surface.

5.6 References

[1] M.P. McDaniel, *Ind. Eng. Chem. Res.*, **1988**, *27*, 1559.

[2] M.P. McDaniel, C.H. Leigh and S.M. Wharry, *J. Catal.*, **1989**, *120*, 170.

[3] M. Shida, T.J. Pullukat and R.E. Hoff, U.S. Patent 4,263,171, 1981.

[4] J. Boor, *Ziegler-Natta Catalysts and Polymerizations*, Academic Press, London, 1979.

[5] P.J.T. Tait. In *Comprehensive Polymer Science*, G. Allen and J.C. Bevington, Eds., Pergaman Press, Oxford, 1989, Vol. 4, Chapter 1.

[6] R. Gerbasi, A. Marigo, A. Martorana, R. Zannetti, G.P. Guidetti and G. Baruzzi, *Eur. Polym. J.*, **1984**, *20*, 967.

[7] T.J. Pullukat and R.E. Hoff, *Silica - Based Zeigler-Natta Catalysts - A Patent Review*, The PQ Corporation, 1998.

[8] M. Shida, T.J. Pullukat and R.E. Hoff, U.S. Patent 4,263,171, 1981.

[9] B.H. Johnson, U.S. Patent 4,707,530, 1987.

[10] F. Milani, L. Luciani and A. Labianio, U.S. Patent 5,348,925, 1994.

[11] L. Luciani, F. Milani, R. Invernizzi, I. Borghi and A. Labianio, U.S. Patent 5,310,716, 1994.

[12] A. Kostiainen, B. Gustafsson and P. Sormunen, U.S. Patent 5,413,979, 1993.

[13] L. Luciani, M. Pondrelli, R. Invernizzi and I. Borghi, U.S. Patent 5,227,439, 1993.

[14] J.P. Candin. In *Catalysis and Chemical Processes*, R.E. Pearce and W.R. Patterson, Eds., Blackie, Glasogow, 1981, Chapter 10.

[15] C.E. Bronnimann, R.C. Ziegler and G.E. Maciel, *J. Am. Chem. Soc.*, **1988**, *110*, 2023.

[16] C.H.C. Liu and G.E. Maciel, *J. Am. Chem. Soc.*, **1996**, *118*, 5103.

[17] D.H. Williams and I. Flemming, *Spectroscopic Methods in Organic Chemistry*, 5th ed., McGraw-Hill, London, 1995.

[18] T.J. Sommerer and M.J. Kushner, *J. Vac. Sci. Technol., B*, **1992**, *10*, 2179.

[19] D.L. Flamm. In *Plasma Etching, An Introduction*, D.M. Manos and D.L. Flamm, Eds., Academic Press Inc. London, 1989, Chapter 2.

[20] H.F. Winters and J.W. Coburn, *Surf. Sci. Rep.*, **1992**, *14*, 161.

[21] N. Inagaki, S. Tasaka and M. Imai, *J. Appl. Polym. Sci.*, **1993**, *48*, 1963.

[22] M.S. Kwon, J.Y. Leer, K.C. Choi and C.H. Han, *Jap. J. Appl. Phys. A*, **1998**, *37*, 4103.

[23] P.W. Atkins, *Physical Chemistry*, 4th ed., Oxford University Press, Oxford, 1990, Chapter 1.

[24] A. Grill, *Cold Plasmas in Materials Technology*, IEEE press, New Jersey, 1994.

[25] T. Yasuda, T. Okuno, M. Miyama and H. Yasuda, *J. Polym. Sci., Polym. Chem. Ed.*, **1994**, *32*, 1829.

[26] E.V. Karoulina and Y.A. Lebedev, *J. Phys. D: Appl. Phys.*, **1992**, *25*, 401.

[27] R.W.B. Pearse and A.G. Gaydon, *The Identification of Molecular Spectra*, 4th ed., John Wiley and Sons, New York, 1976.

[28] A. Hollander, J.E. Klemberg-Sapieha and M.R. Wertheimer, *J. Polym. Sci., Polym. Chem. Ed.*, **1995**, *33*, 2013.

CHAPTER 6

PLASMA FLUORINATION OF POROUS POLYSTYRENE BEADS

6.1 Introduction

There is a growing interest in the use of polymers as supports for heterogeneous catalysts.[1,2,3,4,5] They offer several advantages over conventional metal oxide materials, including control of pore architecture and inertness.[5] High surface area polystyrene supports and modified variants are of particular interest because of the wide range of physical properties and different functionalities with which they can be synthesised.[6] For instance, polystyrene resins are used to overcome the destructive interaction between highly reactive metallocene polymerisation catalysts and conventional silica supports.[1,2,3,4] In this context, fluorinated polystyrene derivatives are widely sought after since they offer enhanced thermal stability and hydrophobicity, thereby being capable of supporting highly sensitive catalysts under harsh reactor conditions.[5] The chemical nature of the internal pore walls of such supports is considered to be a key factor in determining the dispersion and anchoring of catalytic moieties. A number of different ways have been explored in the past to make such materials, these include copolymerisation with a functionalised styrene[7] followed by tethering of the catalyst[1,2,3,4] and direct fluorination of porous polystyrene beads[8,9] by exposure to a mixture of fluorine and a diluent gas.[10] Cost is a major limiting factor in the former case, whereas polymer degradation, safety, and poor selectivity are major drawbacks for the latter.[9,11]

A potentially safer, cheaper, and faster alternative to direct gaseous fluorination is to employ a low temperature plasma. Chemical modification by this type of medium comprises reaction of the substrate with ions, free radicals, excited species, electrons and electromagnetic radiation.[12] In the case of plasma fluorination, electrical excitation of CF_4 gas provides a source of

fluorine atoms (and relatively low concentrations of CF_x species) which have been shown to be effective at chemically modifying polymer surfaces.[13,14,15] In the case of impermeable substrates the depth of penetration is limited to the outermost 1 μm,[16,17] whereas this can be significantly greater for porous materials.[18]

A systematic investigation into how polystyrene beads with differing scales of porosity are affected by CF_4 plasma fluorination is described in this study. The depth and nature of chemical modification has been determined using a combination of elemental analysis, XPS, ATR-FTIR, ^{19}F MAS NMR and imaging TOF-SIMS.

6.2 Experimental

Three types of poly(styrene-*co*-divinylbenzene) beads were used to investigate how depth of fluorination varies with substrate porosity: non-porous beads (40 μm size, ≈2% divinylbenzene (DVB), Polyscience Inc.), mesoporous beads (30 μm particle size, pore size less than 50 nm, pore volume 65%, ≈36% DVB, Dyno Particles AS) and microporous beads (300-800 μm particle size, pore size less than 2 nm, pore volume 0.75 $cm^3\ g^{-1}$, ≈20% DVB, Aldrich). In the case of XPS and ATR-FTIR surface analysis, the microporous beads were ground to a fine powder (≈10 μm) prior to plasma fluorination, whereas they were treated as a whole for bulk elemental analysis, ^{19}F magic angle spinning NMR, TOF-SIMS and gas sorption analysis.

Plasma fluorination experiments were carried out in a capacitively coupled 13.56 MHz Bio-Rad E2000 system, which had been fitted with a revolving powder holder controlled by a stepper motor. The reactor was continuously pumped by a 33 $dm^3\ h^{-1}$ Edwards E2M2 rotary pump via a liquid nitrogen cold trap to yield a base pressure of 4×10^{-2} mbar (with a leak rate better than 1×10^{-8} mol s^{-1}).[19] Prior to each experiment, the plasma chamber was scrubbed with detergent, rinsed with isopropyl alcohol, oven dried, and then cleaned further *in situ* using a 0.3 mbar air plasma at 30 W. 0.5 g of polymer was then loaded into the reactor and evacuated down to base pressure. Next, CF_4 gas (Air Products, 99.7% purity) was introduced into the plasma chamber at a pressure of 0.4 mbar (equivalent to a flow rate of $8 \pm 1 \times$

10^{-7} mol s^{-1}) via a fine needle valve. At this stage rotation of the reactor commenced and the gas discharge was ignited at 40 W. Upon completion of plasma treatment, the rf power supply was switched off, and CF_4 gas allowed to continue to pass through the reactor for a further two minutes, prior to evacuation back to its original base pressure.

Nitrogen gas sorption measurements at liquid nitrogen temperature were carried out using a PMI sorptometer. Only the mesoporous beads were found to obey the BET relationship by showing a constant BET gradient over the range $0.04 < p/p_o < 0.25$.[20]

Bulk carbon and hydrogen concentrations were determined using an Exeter Analytical, Inc, CE 440 elemental analyser, employing oxygen as the combustion gas and helium as the carrier gas. The amount of fluorine incorporated was measured by combusting each sample in an oxygen bomb, and then using a Dionex DX500 ion chromatogram to analyse an aqueous solution of the remains.

The outer 2-5 nm of the polymer beads was characterised by X-ray photoelectron spectroscopy (XPS).[21] A VG ESCALAB MKII spectrometer fitted with an unmonochromatised Mg Kα X-ray source (1253.6 eV) and a hemispherical analyser operating in the CAE mode (20 eV pass energy) was used for surface analysis. The photo-emitted core level electrons were collected at a take-off angle of 30° from the substrate normal. Instrumentally determined sensitivity factors for unit stoichiometry were taken as C(1s) : F(1s) = 1.00 : 0.23. For this technique, the polystyrene beads were embedded into indium foil (Aldrich, 99.99%), mounted on to the sample probe.

Attenuated total reflectance (ATR) FT-IR was used to probe down to $\approx$ 4.5 μm.[22] Absorption spectra of the polystyrene beads were acquired using a Mattson Polaris spectrometer fitted with a Greasby Specac Golden Gate ATR accessory. The scan range was 600-4000 cm^{-1} at a resolution of 4 cm^{-1}, this was averaged over 32 scans, in conjunction with background subtraction.

The overall chemical nature of the fluorinated beads was obtained by ^{19}F magic angle spinning NMR. This was performed on a Varian Unity Plus 300 MHz spectrometer (^{19}F resonance 282.2 MHz). 260 transients were acquired using a 90° pulse, 5 s recycle delay, 200 kHz spectral width, and a magic angle spinning speed of approximately 16 kHz.

Preparation of the beads for microtoming was performed in one of two ways: Non-porous and microporous beads were embedded into a thermoplastic adhesive (Tempfix, Agar scientific) at 383 K. Mesoporous beads were fixed between a double layer of adhesive tape. The samples were sliced at 243 K using a cryogenic microtoming apparatus (Leica RM 2165).

Images of the cleaved and uncut mesoporous beads were collected on a CamScan Series 2 scanning electron microscope after the samples were sputtered with gold in an argon discharge.

TOF-SIMS analysis was carried out with a Physical Electronics 7200 instrument. The primary ion beam (25 keV Ga^+) was rastered over the required area, with the total dose less than 10^{13} ions cm^{-2} (static conditions).

6.3 Results

BET surface area analysis showed that no loss of porosity occurred during CF_4 plasma treatment of the mesoporous beads, Table 6.1.

Sample	Untreated / $m^2 g^{-1}$	Fluorinated / $m^2 g^{-1}$
Non-porous [a]	-	-
Mesoporous	271.3 ± 2	268.2 ± 2
Microporous [b]	-	-

[a] Below nitrogen adsorption detection limit

[b] Microporous substrates do not fit to BET equation due to micropore filling.[23]

Table 6.1: BET surface area of the polymer beads.

Bulk elemental analysis of the untreated polystyrene beads yielded hydrogen to carbon ratios approximately equal to the expected theoretical value of 1.0, Table 6.2. CF_4 plasma fluorination was found to increase along the series: non-porous < microporous < mesoporous polystyrene beads. Elemental composition calculated from the XPS peak areas gave similar F:C ratios for all three types of bead (no other elements were detected by this technique), Table 6.2. Therefore it appears that the degree of fluorination is greater in the

surface region compared to the bulk in each case. C(1s) XPS spectra of the untreated polystyrene beads showed the presence of only $\underline{C}_xH_y$ groups at 285.0 eV, together with a weak π - π^* shake-up satellite at 291.6 eV,[24] Figure 6.1. CF_4 plasma fluorination produced a broadening of the C(1s) envelope towards higher binding energies corresponding to the formation of $\underline{C}$-CF_n (286.6 eV), $\underline{C}F$ (287.6 eV), $\underline{C}F$-CF_n (289.3 eV), $\underline{C}F_2$ (291.2 eV) and $\underline{C}F_3$ (293.3 eV) environments (additional Mg $K\alpha_{3,4}$ satellite peaks at $\approx$ 9 eV lower binding energy were taken into consideration),[25] Figure 6.2.

	Bulk Analysis		XPS
Substrate	**H:C**	**F:C**	**F:C**
Non-porous	1.0	-	-
Non-porous CF_4 treated	1.0	0.002 ± 0.001	0.78 ± 0.03
Mesoporous	1.1	-	-
Mesoporous CF_4 treated	1.1	0.061 ± 0.006	0.84 ± .04
Microporous	1.0	-	-
Microporous CF_4 treated	1.0	0.014 ± 0.001	0.76 ± .05

Table 6.2: Bulk versus surface elemental analysis.

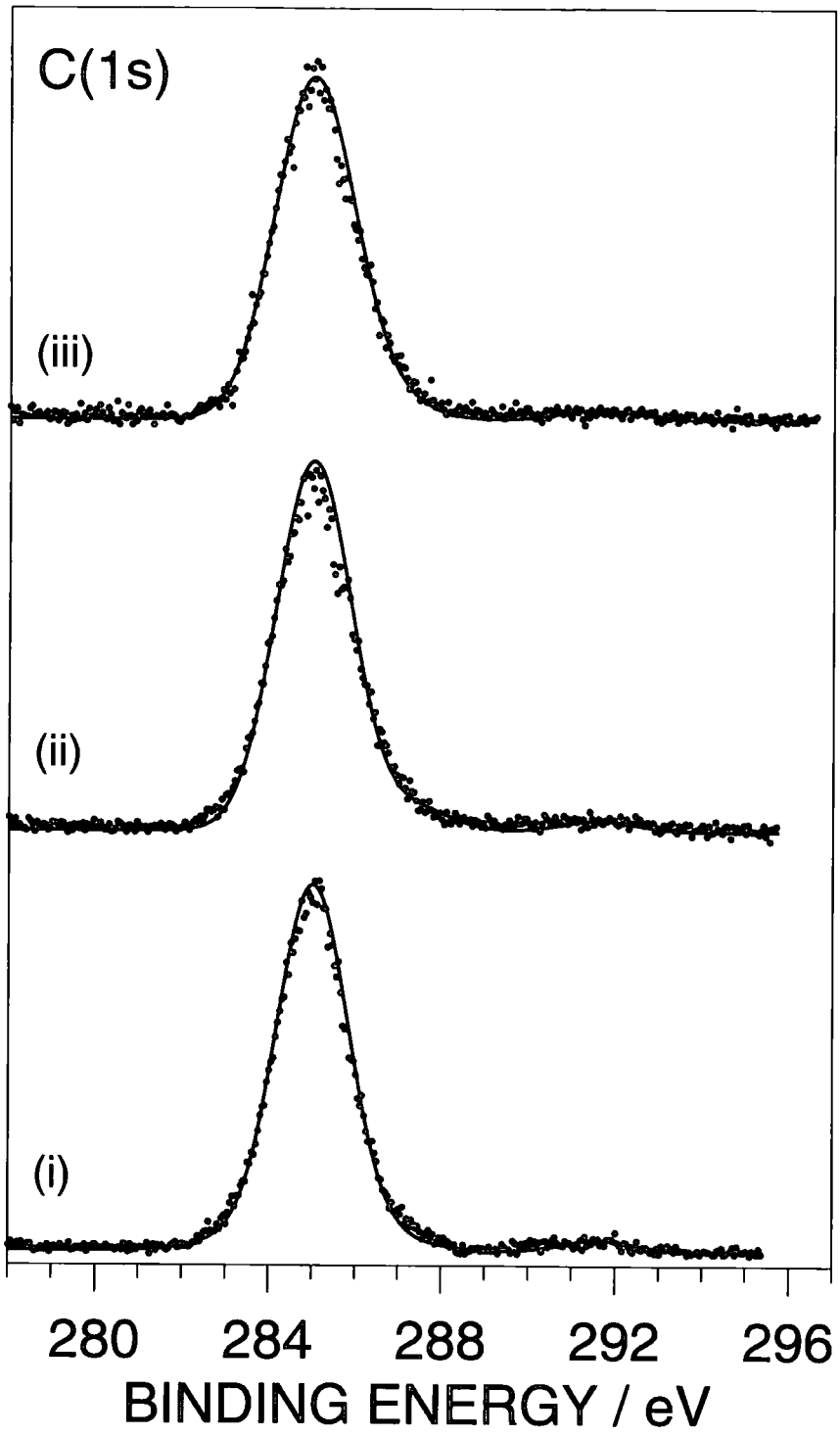

Figure 6.1: C(1s) XPS spectra of the untreated polystyrene beads: (i) non-porous; (ii) mesoporous; and (iii) microporous.

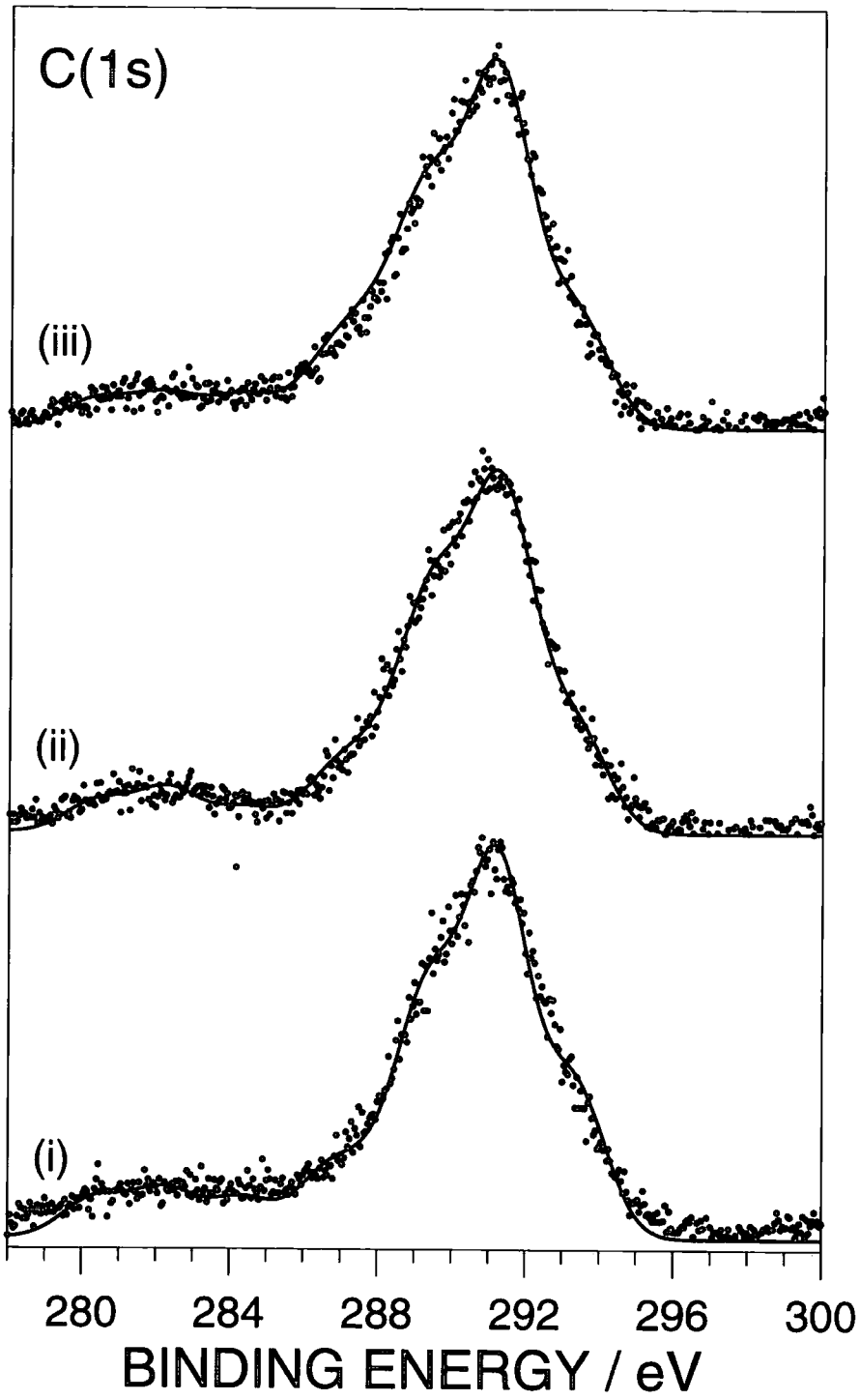

Figure 6.2: C(1s) XPS spectra of the CF_4 plasma treated polystyrene beads: (i) non-porous; (ii) mesoporous; and (iii) microporous.

Contrary to XPS, no change after fluorination could be detected by ATR-FTIR for the non-porous beads, Figures 6.3 and 6.4, whereas, the mesoporous and ground microporous beads displayed a new absorption feature in the 1200-1400 cm^{-1} range associated with ($C-F_x$) functionalities,[26] Table 6.3. However, it was difficult to distinguish between the CF, CF_2 and CF_3 groups because of band overlap.[27] On this basis, it is clear that fluorination occurs at least down to the sampling depth of ATR-FTIR (4.5 μm)[22] for the mesoporous and microporous beads.

Vibrational mode	**Wavenumber / cm^{-1}**
Phenyl ring C-H stretching modes	3029, 3138
Symmetric CH_2 stretching mode	2923
Antisymmetric CH_2 stretching mode	2851
Ring skeleton in-plane bend or stretch	1606, 1493, 1450
Symmetric C-F stretching mode	1400 - 1200
Ring in-plane C-C-H bending	1154, 1070, 1027
Ring out of plane deformation	906, 842, 760, 700

Table 6.3: Assignment of the IR spectra.[28]

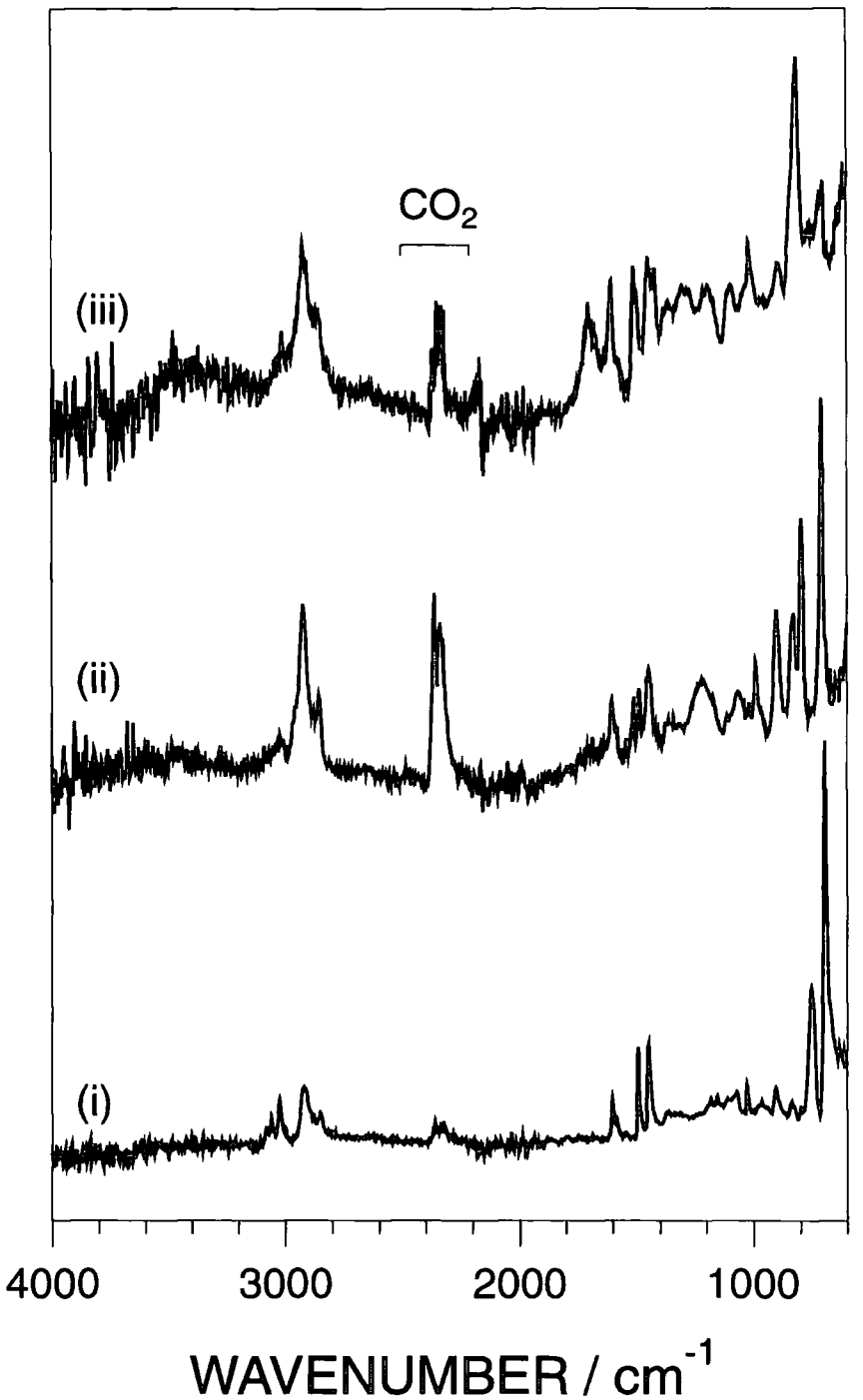

Figure 6.3: ATR-FTIR spectra of the untreated polystyrene beads: (i) non-porous; (ii) mesoporous; and (iii) microporous. (The CO_2 absorption is attributed to CO_2 gas contained within the pores.)

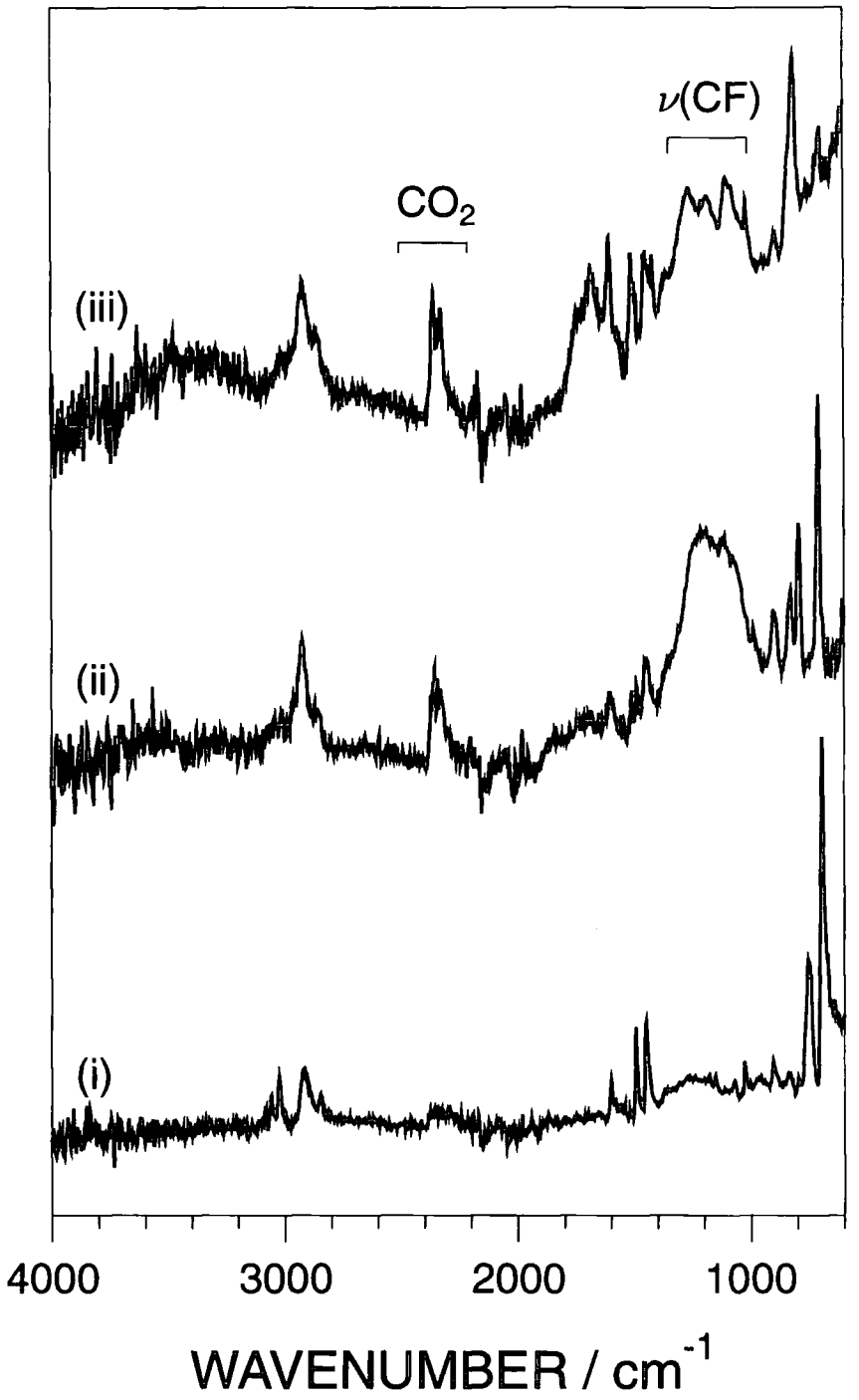

Figure 6.4: ATR-FTIR spectra of the CF_4 plasma treated polystyrene beads: (i) non-porous; (ii) mesoporous; and (iii) microporous. (The CO_2 absorption is attributed to CO_2 gas contained within the pores.)

The low level of bulk fluorination associated with the non-porous beads was confirmed by the absence of any signal during solid state ^{19}F magic angle spinning NMR analysis. Whereas both the mesoporous and microporous beads displayed three distinct regions: a broad feature between -30 to -90 ppm associated with $C\underline{F}_3$ groups,[29,30,31] a band between -100 to -130 ppm due to $C\underline{F}_2$ groups,[29,32] and a resonance around -150 ppm associated with aromatic $C\underline{F}$ groups,[33,34] Figure 6.5. The $C\underline{F}_3$ and $C\underline{F}_2$ regions are more intense for the mesoporous beads compared to the microporous beads, and can be explained on the basis that the smaller mesoporous beads give rise to a plasma-solid interface which is approximately 20 times greater in size compared to the larger microporous beads. Therefore the relative volume accessible to all the plasma species is greater for the mesoporous beads.

Optical microscopy was used to verify that the larger microporous beads could be fractured open by cryogenic microtoming. Scanning electron microscopy confirmed that this was also the case for the smaller mesoporous particles, Figure 6.6. Preliminary $^{19}F^-$ TOF-SIMS images of the untreated polystyrene beads taken after microtoming confirmed the absence of any fluorine within the bulk. In the case of the microporous beads, fluorination was evident down to a depth of 5 μm, Figure 6.7. The $^{19}F^-$ TOF-SIMS image of the fractured mesoporous beads shows that chemical modification is discernible on all the fragmented pieces.

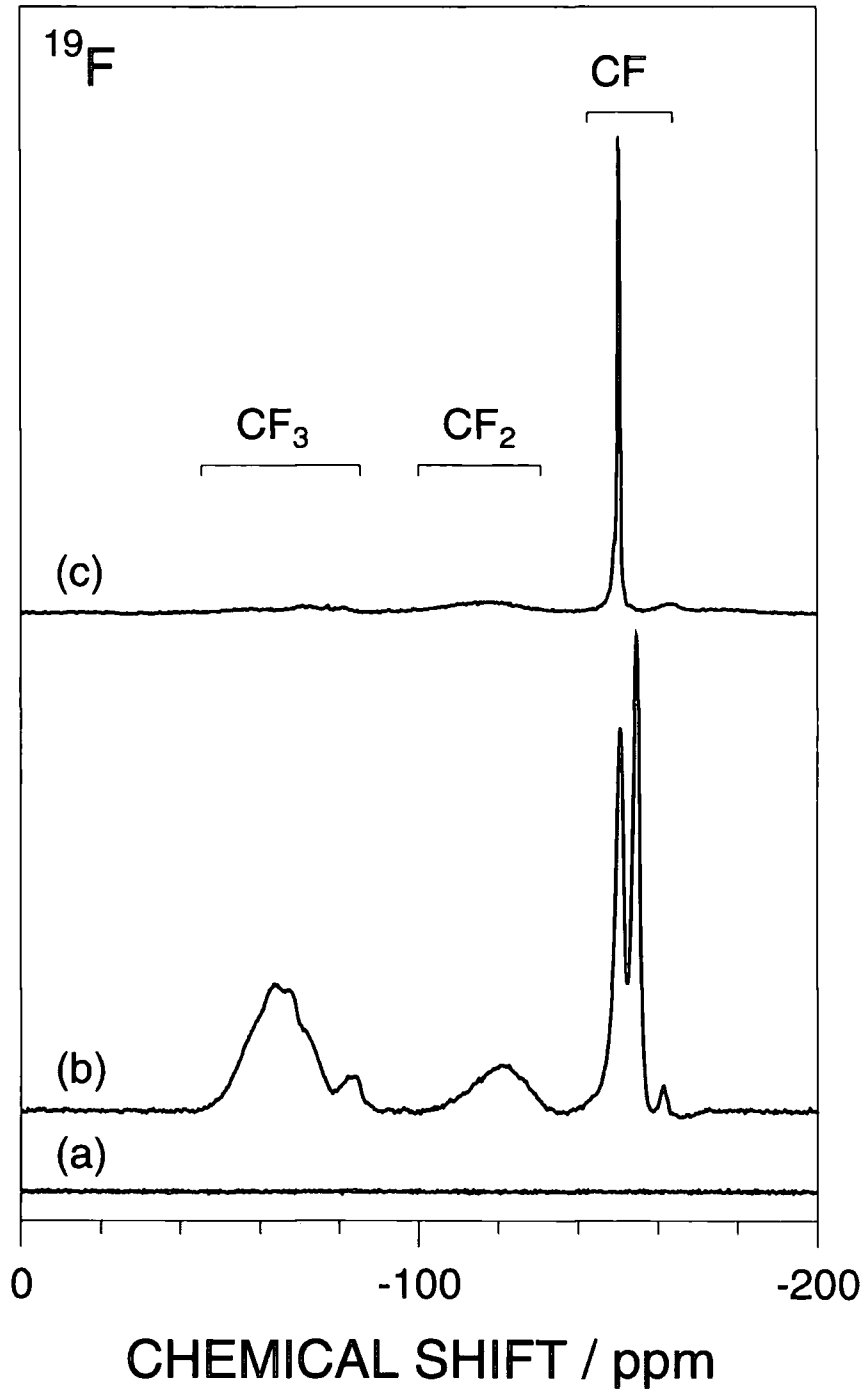

Figure 6.5: ^{19}F MAS NMR spectra of the fluorinated beads: (a) non-porous; (b) mesoporous; and (c) microporous.

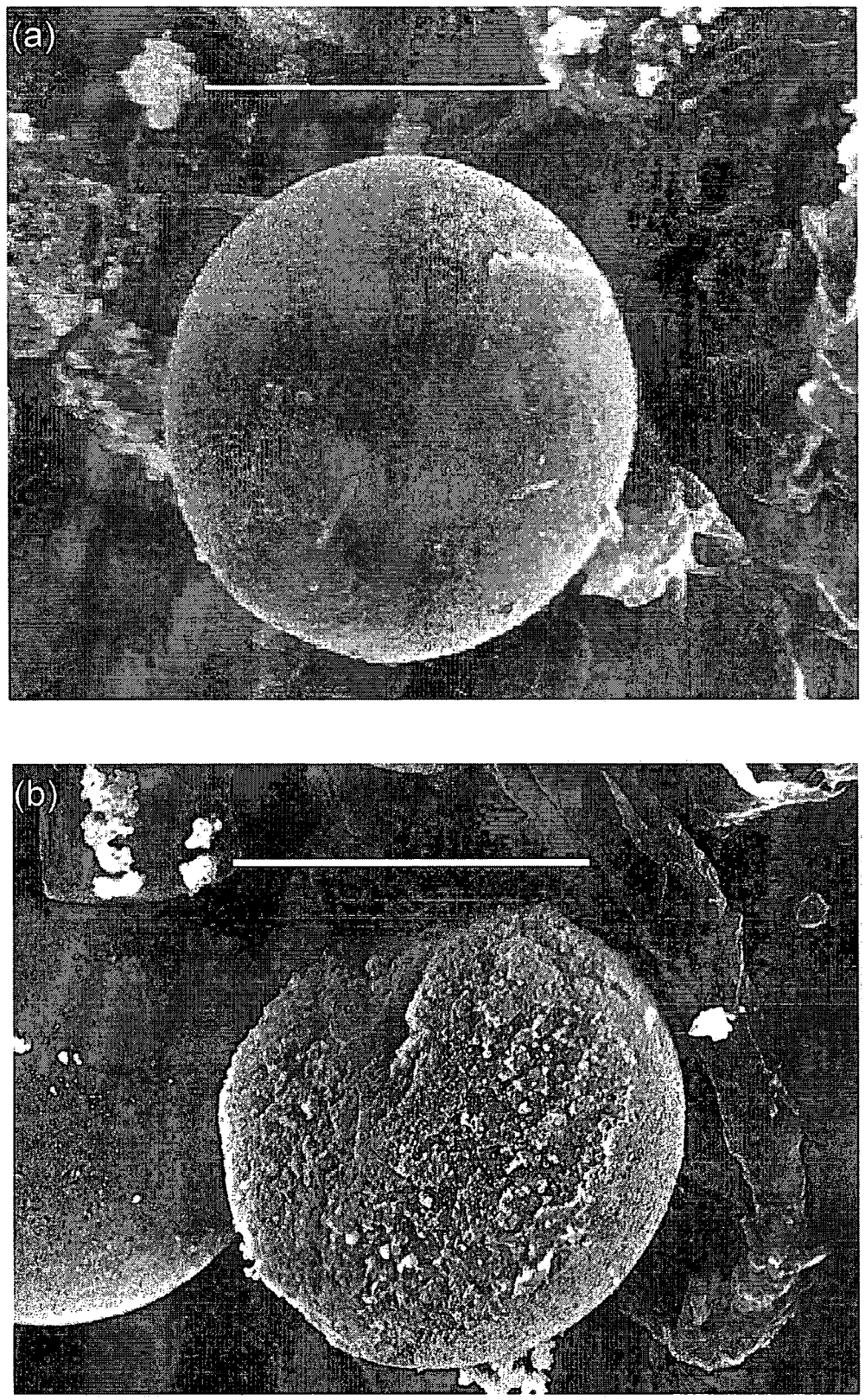

Figure 6.6: SEM images of 30 μm mesoporous polystyrene beads : (a) whole; and (b) microtomed.

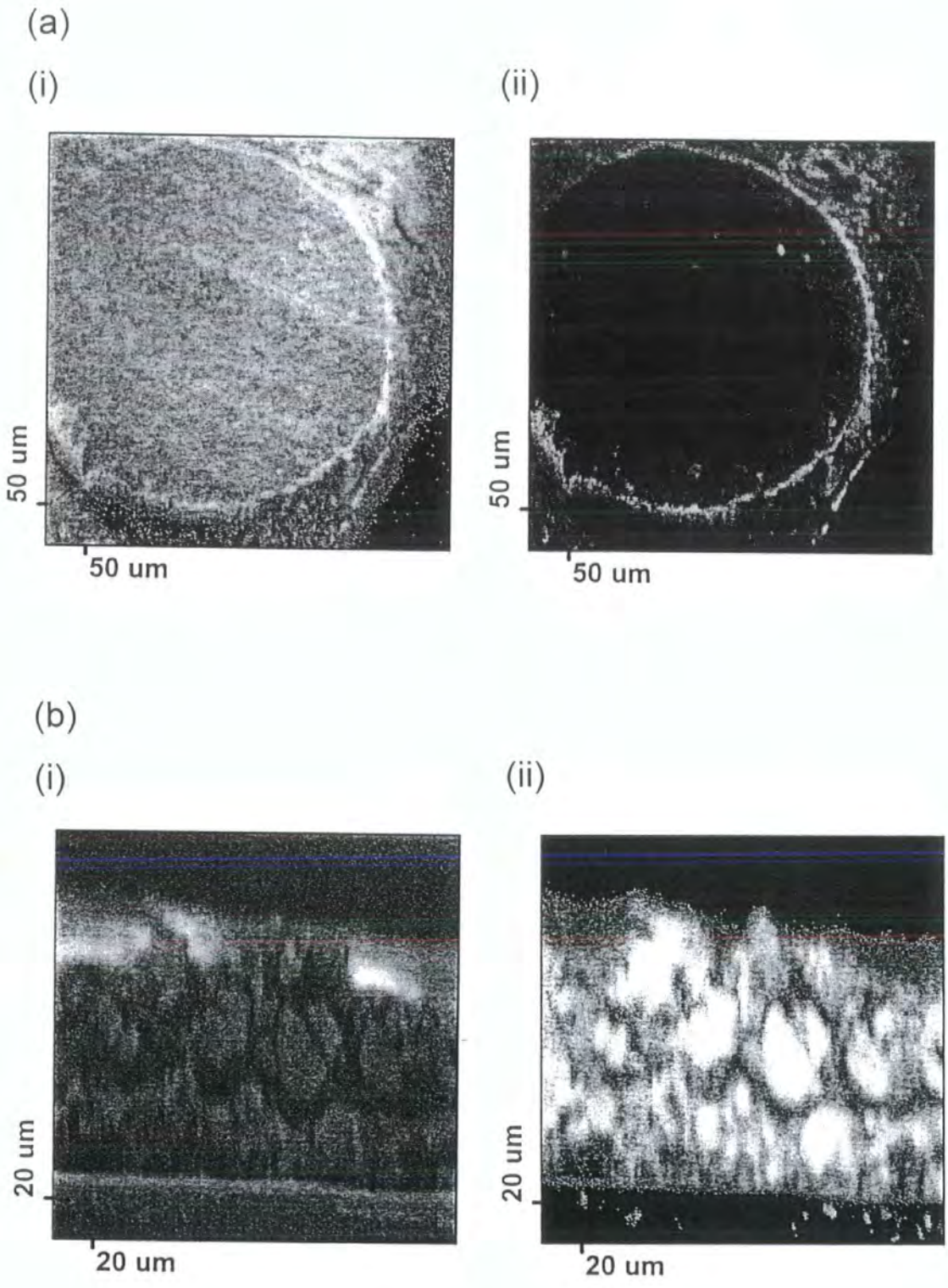

Figure 6.7: $^{19}F^-$ TOF imaging SIMS of polystyrene beads: (a) microtomed microporous (plasma fluorination occurs down to a depth of 5 μm) and (b) mesoporous (fluorination is observable on all the fragmented pieces), where (i) is the total ion and (ii) the $^{19}F^-$ image.

6.4 Discussion

The high concentration of fluorine atoms contained within a CF_4 electrical discharge (together with a small concentration of CF, CF_2 and CF_3 radicals)[35] can readily react with a polymer surface to yield CF, CF_2 and CF_3 functionalities.[36] Deposition is not a complication under these circumstances.[14,37] Previous studies using fluidized bed plasma reactors, have shown that just the surface is fluorinated in the case of non-porous polyethylene and polystyrene beads.[17,38,39] This is consistent with the present study with non-porous polystyrene beads where no changes are detectable in the ATR-FTIR and ^{19}F MAS NMR spectra (fluorination occurs to a depth of less than 1 μm).[16,17] However, it has been shown that fluorination into the subsurface can be achieved for the porous polystyrene beads.

Plasma ignition within the polymer pores is unlikely since their dimensions (micoporous < 2 nm, and mesoporous < 50 nm) are much smaller compared to the Debye length (2 μm < λ_D < 7 mm) for this type of electrical discharge.[12,40] Reaction with the pore wall surfaces must therefore be occurring via diffusion of reactive species across the plasma-solid interface. Ion penetration will be restricted to the surface region due to rapid loss of kinetic energy in collisions with pore walls. Previous studies have shown that penetration of atomic fluorine through multiple layers of fabric can occur,[18] and therefore it is likely that the predominant mechanism for subsurface fluorination of the porous beads is via atomic fluorine attack. The divinylbenzene linkages can effectively be considered to form part of the polystyrene chain network, Structure 6.1. On this basis there will be the thermodynamically favoured substitution of C-H bonds to form C-F linkages, and fluorine addition to the unsaturated phenyl groups can be expected to occur.[16,41,42]

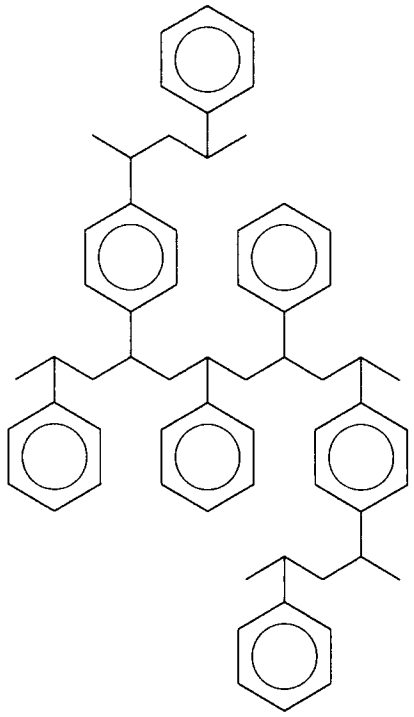

Structure 6.1: Divinylbenzene crosslinkages in the polystyrene beads.

A quantitative comparison between the bulk and surface $\underline{C}F_x$ environments can be made by examining the XPS and ^{19}F magic angle spinning NMR data, Table 6.4. The outermost 2-5 nm sampling depth of XPS consists mostly of $\underline{C}F_2$ functionalities whereas the bulk contains predominantly $\underline{C}F$ groups (with a significant number of $\underline{C}F_3$ groups in the mesoporous material due to the smaller bead sizes and greater porosity). The greater level of fluorination in the surface region can be accounted for in terms of additional reactions at the plasma-solid interface associated with ions, electrons, and VUV photons.

		% Fluorinated carbon		
Substrate	**Technique**	(C̲F + C̲F-CF_n)	C̲F_2	C̲F_3
Mesoporous	**^{19}F MAS NMR**	67 ± 2	10 ± 3	23 ± 3
	XPS	37 ± 2	50 ± 3	13 ± 2
Microporous	**^{19}F MAS NMR**	85 ± 2	12 ± 2	3 ± 1
	XPS	38 ± 3	47 ± 5	15 ± 3

Table 6.4: Comparison between ^{19}F MAS NMR and XPS C(1s) spectra of CF_4 plasma fluorinated mesoporous and microporous beads.

The diffusion of plasma species into the subsurface is expected to occur via Knudsen flow since pore sizes are smaller than the mean free path of the gas (≈ 100 μm).[43,44] The greater penetration into the bulk observed by TOF-SIMS for the mesoporous compared to the microporous beads can be attributable to the pore size of the former being approximately 25 times greater.

6.5 Conclusions

The depth of fluorination of polystyrene beads is shown to depend on the substrate porosity. In the region directly in contact with the plasma there is a high degree of modification, whereas in the subsurface the absence of ion and electron bombardment allows a highly selective mode of fluorination to occur.

6.6 References

[1] S.B. Roscoe, J.M.J. Frechet, J.F. Walker and A.J. Dias, *Science*, **1998**, *280*, 270.

[2] A.G.M. Barrett and Y.R. de Miguel, *Chem. Commun.*, **1998**, 2079.

[3] M.C.W. Chan, K.C. Chew, C.I. Dalby, V.C. Gibson, A. Kohlmann, I.R. Little and W. Reed, *Chem. Commun.*, **1998**, 1673.

[4] T. Kitagawa, T. Uozuni, K. Soga and T. Takata, *Polymer*, **1997**, *38*, 615.

[5] J.J. Wu, L. Fu and K.T. Chung, *Appl. Catal.*, **1991**, *72*, 71.

[6] J. Leito, D. Milstein, R.L. Albright, J.V. Minkiwicz and B.C. Gates, *CHEMTECH*, **1983**, *13*, 46.

[7] G.D. Darling and J.M.J. Frechet, *J. Org. Chem.*, **1986**, *85*, 2270.

[8] J.J. Wu, L. Fu and K.T. Chung, *Appl. Catal.*, **1991**, *72*, 71.

[9] J.D. Hewes, S. Curren and E.A. Leone, *J. Appl. Polym. Sci.*, **1994**, *53*, 291.

[10] R.J. Lagow and J.L. Margrave, *Prog. Inorg. Chem.*, **1979**, *26*, 161.

[11] A.P. Kharitonov and Y.L. Moskvin, *J. Fluorine Chem.*, **1998**, *91*, 87.

[12] A. Grill, *Cold Plasmas in Materials Technology*, IEEE press, New Jersey, 1994.

[13] E.A. Truesdale and G. Smolinsky, *J. Appl. Phys.*, **1979**, *50*, 6594.

[14] M. Strobel, S. Corn, C.S. Lyon and G.A. Korba, *J. Polym. Sci. Polym. Chem. Ed.*, **1985**, *23,* 1225.

[15] J.A. McCaulley and H.A. Goldberg, *J. Appl. Polym. Sci.*, **1994**, *53*, 543.

[16] E.A. Wildi, G.J. Scilla and A. DeLuca, *Mater. Res. Soc. Symp. Proc.*, **1985**, *48*, 79.

[17] I.-H. Loh, E. Cohent and R.F. Baddour, *J. Appl. Polym. Sci.*, **1986**, *31*, 901.

[18] T. Yasuda, T. Okuno, M. Miyama and H. Yasuda, *J. Polym. Sci., Polym. Chem. Ed.*, **1994**, *32*, 1829.

[19] C.D. Ehrlich and J.A. Basford, *J. Vac. Sci. Technol., A*, **1992**, *10*, 1.

[20] S. Branauer, P.H. Emmett and E. Teller, *J. Am. Chem. Soc.*, **1938**, *60*, 309.

[21] D. Briggs and M.P. Seah, *Practical Surface Analysis, Volume 1- Auger and X-ray Photoelectron Spectroscopy*, 2nd ed., John Wiley and Sons, Chichester, 1983.

[22] Graseby Specac Ltd, *Sampling Techniques for Infrared Analysis*, p 14, 1997.

[23] S.J. Gregg and K.S.W. Sing, *Adsorption, Surface Area and Porosity*, Academic Press, London, 1967, Ch. 4.

[24] D.T. Clark, H.R. Thomas, *J. Polym. Sci., Polym. Chem. Ed.*, **1978**, *16,* 791.

[25] G. Beamson and D. Briggs, *High Resolution XPS of Organic Polymers: The Scienta ESCA 300 Database*, John Wiley and Sons, Chichester, **1992**.

[26] P.C. Painter, M.M. Coleman and J.L. Koenig, *The Theory of Vibrational Spectroscopy and its Application to Polymeric Materials*, John Wiley and Sons, New York, 1982.

[27] D. Lin-Vien, N.B. Colthup, W.G. Fateley and J.G. Grasselli, *The Handbook of Infrared and Raman Characteristic Frequencies of Organic Materials*, Academic Press, London, 1991.

[28] D.I. Bower and W.F. Maddans, *The Vibrational Spectroscopy of Polymers*, Cambridge University Press, Cambridge, 1989.

[29] R.K. Harris and P. Jackson, *Chem. Rev.*, **1991**, *91*, 1427.

[30] C. Tonelli and V. Tortelli, *J. Fluorine Chem.*, **1994**, *67*, 125.

[31] V. Tortelli, C. Tonelli and C. Corvaja, *J. Fluorine Chem.*, **1993**, *60*, 165.

[32] A.D. English and O.T. Garza, *Macromolecules*, **1979**, *12*, 351.

[33] P.J. Toscano, J. Waechter and E.J. Schermerhorn, P. Zhoue and H.J. Frish. *J. Polym. Sci., Polym. Chem. Ed.*, **1993**, *31*, 859.

[34] M.A. Carvalho de Mederios, S. Cosnier, A. Devonzier and J.-C. Moutet, *Inorg. Chem.*, **1996**, *35*, 2659.

[35] D. Edelson and D.L. Flamm, *J. Appl. Phys.*, **1984**, *56*, 1522.

[36] E. Occhiello, M. Morra, F. Garbassi and J.F. Bargon, *Appl. Surf Sci.*, **1989**, *36*, 285.

[37] J.Q. Wang, D.M. Feng, H.Z. Wang, M. Rembold and F. Thommen, *J. Appl. Polym. Sci.*, **1993**, *50*, 585.

[38] M. Arand, R.E. Cohen and R.F. Baddour, *Polymer*, **1981**, *22*, 361.

[39] S.H. Park and S.D. Kim, *Polym. Bulletin.*, **1998**, *41*, 479.

[40] B.N. Chapman, *Glow Discharge Processes*, John Wiley and Sons, New York, 1980.

[41] J. Hopkins and J.P.S. Badyal, *J. Phys. Chem.*, **1995**, *99*, 4261.

[42] M. Strobel, P.A. Thomas and C.S. Lyons, *J. Phys. Chem.*, **1987**, 25, 3343.

[43] J.M. Thomas and W.J. Thomas, *Introduction to the Principles of Heterogeneous Catalysis*, Academic Press, London, 1967.

[44] P.W. Atkins, *Physical Chemistry*, 4th ed., Oxford University Press, Oxford, 1990, Ch. 24.

CHAPTER 7

CONCLUSIONS

In this thesis various aspects of the application of non-equilibrium plasmas to tailor supported olefin polymerisation catalysts have been investigated. These were primarily the activation of the Phillips catalyst and the modification of Ziegler-Natta and metallocene supports. To achieve this, it was necessary to construct a plasma reactor which could homogeneously treat air sensitive powders.

Phillips catalysts are conventionally activated by heating the chromium/silica precursor to 573-1073 K under either dry air or oxygen. High temperature heating causes extensive silanol condensation, removing hydroxyls which interfere with the chromium centres. During oxygen plasma activation, the Cr(acetate)/silica precursor is oxidised to Cr(VI) by the penetration of long-lived excited plasma species (probably atomic oxygen) throughout the catalyst particles. The dispersion of the chromium centres is lower than after thermal activation and a large population of hydroxyls (9 times more than after thermal calcination at 1053 K) remains on the support. This high hydroxyl population, combined with the low dispersion of Cr(VI) centres, leads to low polymerisation activity. In order to enhance the polymerisation activity, different discharge gases were used to dehydroxylate high surface area silica. Noble gas discharges only caused a small reduction in the hydroxyl population due to the absorbance, by the silica support, of the intense plasma VUV emission lines. Oxygen plasmas produced a similar reduction in hydroxyl population, through preferential loss of hydrogen bonded hydroxyls. This hydroxyl loss and the increase in proportion of isolated hydroxyls is due to UV assisted silanol condensation. Non-isothermal CF_4 plasmas caused the greatest decrease in total hydroxyl population (equivalent to a 773 K thermal treatment). The distribution of silanols after treatment was similar to the starting distribution and contained isolated and hydrogen bonded hydroxyls. This was attributed to diffusion of atomic fluorine throughout the particles,

reacting indiscriminately with surface hydroxyls. Subsequent thermal activation removed hydrogen bonded hydroxyls at low temperatures. Further heating (higher than 773 K) caused the remaining silanols to relax to the equivalent thermal distribution owing to the onset of hydroxyl migration. When CF_4 dehydroxylation was applied to the Phillips catalyst, in conjunction with oxygen plasma activation, an active catalyst was produced, with a reduced total hydroxyl population compared to that when solely oxygen plasma activated. The sequence of plasma treatment affected the catalyst chromium loading. CF_4 dehydroxylation was able to remove chromium after oxygen plasma oxidation to CrO_3. It has also been shown that combined thermal and plasma activations produce catalysts with a low hydroxyl population and increased activity, compared to solely plasma treated catalysts. Despite being of lower activity than when only thermally calcined, such catalysts are of interest because of the reduction in polymer molecular weight distribution.

Next, the potential use of a plasma as a chlorinating agent was demonstrated by CCl_4 glow discharge treatment of a dibutylmagnesium/silica precursor. After CCl_4 plasma treatment, almost complete loss of butyl groups from the precursor was observed in the ^1H MAS NMR spectrum. No loss of magnesium was detected but chlorine was incorporated on to the surface.

Finally, plasma fluorination of polystyrene beads suitable for use as supports for metallocene catalysts was studied. It was shown that plasma fluorination was localised at the surface of non-porous beads. However, when the beads were porous, the depth of modification could reach at least 15 μm, with greater porosity increasing the extent of penetration. The degree of fluorination also varied between the surface and subsurface. A higher degree of fluorination occurred at the plasma-surface interface due to the bombardment by energetic plasma species, whereas a highly selective modification occurred in the subsurface.

In conclusion, this thesis has shown that plasmas not only chemically modify the surface of porous media, but also the subsurface. This is due to long-lived excited species diffusing into the bulk and causing chemical modification within the pores.

APPENDIX

University of Durham - Board of Studies in Chemistry
Colloquia, Lectures and Seminars from Invited Speakers

1996

October 22nd	*Polymers for Biomedical Applications* Prof. B.J. Tighe, Aston University
October 23rd	*Function Based on Organisation* Prof. H. Ringsdorf, Johannes Gutenberg-Universitat
November 6th	*Probing Dynamic Processes with Photoelectrons* Dr. K.L. Reid, Nottingham University
November 18th	*Crossing Conventional Lines in my Chemistry of the Elements* Prof. G.A. Olah, University of Southern California
November 20th	*Surface Light Scattering: Ripples and Relaxations* Prof. J.C. Earnshaw, Belfast University
December 4th	*Very High Resolution ZEKE Spectroscopy* Prof. K. Muller-Dethlefs, York University

1997

February 6th	*Integrated Chemical Synthesis* Prof. P. Bartlet, Southampton University

March 3rd — *Siloxanes at Surfaces*
Dr. M. Owen and Dr. D. Gravier, Dow Corning

October 15th — *Studying Catalysis in Action*
Dr. R.M. Ormerod, Keele University

October 22nd — *Organoplatinum Chemistry and Catalysis*
Prof. R.J. Puddephatt, University of Western Ontario

October 29th — *Probing Chirality with Circular Dichroism*
Prof. R.D. Peacock, Glasgow University

November 12th — *Spectroscopy of Liquid Interfaces: From Bio-orgainc Chemistry to Atmospheric Chemistry*
Dr. J. Frey, Southampton University

November 26th — *A Random Walk in Polymer Science*
Prof. R.W. Richards, Durham University

1998

January 14th — *Energy Transfer and Optical Harmonics in Molecular Systems*
Prof. D.L. Andrews, University of East Anglia

February 18th	*Surprises in the Photochemistry of Tropospheric Ozone* Prof. G. Hancock, Oxford University
March 11th	*How to make Phthalocyanine Films and what to do with them* Prof. M.J. Cook, University of East Anglia
October 20th	*Dynamic Electrochemistry: Small is Beautiful* Prof. P. Unwin, Warwick University
October 23rd	*In Search of Hypervalent Free Radicals* Prof. J.C. Scaiano, University of Ottawa
October 26th	*Reactions of the Highly Electrophilc Boranes $HB(C_6F_5)_2$ and $B(C_6F_5)_3$ with Zirconium and Tantalum Based Metallocenes* Dr W.E. Piers, University of Calgary
October 28th	*Tailoring Solid Surfaces* Prof. J.P.S. Badyal, Durham University
November 18th	*Biodegradable Polymers* Dr. R.E. Cameron, Cambridge University
December 9th	*Multinuclear Solid-State Magnetic Resonance Studies of Noncrystalline Oxides and Glasses* Dr. M.E. Smith, Warwick University

1999

January 27th — *Foresight or Hindsight? Some Borane Lessons and Loose Ends*
Prof. K. Wade, Durham University

February 10th — *Surfactant Adsorption and Marangoni Flow at Expanding Liquid Surfaces*
Dr. C.D. Bain, Oxford University

February 17th — *Microelectrode Techniques for the Study of Enzymes and Nucleic Acids at Interfaces*
Dr. B.R. Horrocks, Newcastle University

Conference Attended

1997

September 14 - 18th — Leverhulme Summer School in Catalysis, *Catalysis: Fundamentals and Practice*, University of York

Examined Lecture Courses

Spectroscopies (Dr. Halliday)
Electron Microscopy (Dr. Durose)
Synthetic Methodology in Organometallic and Coordination Chemistry (Prof. Parker)
Experimental Design (Prof. Badyal)